Investigation of Biological and Technical Components for the Development of a 3D-Bioprinting Process for Vascularized Organs-on-a-Chip

Zur Erlangung des akademischen Grades Doktor-Ingenieur (Dr.-Ing.)
genehmigte Dissertation von Anna Moritz-Fritschen aus Berlin

Tag der Einreichung: 24.04.2024, Tag der Prüfung: 17.07.2024

1. Gutachten: Prof. Dr.-Ing. Andreas Blaeser
2. Gutachten: Prof. Dr. rer. nat. Robert Stark

Darmstadt, Technische Universität Darmstadt, Fachbereich Maschinenbau

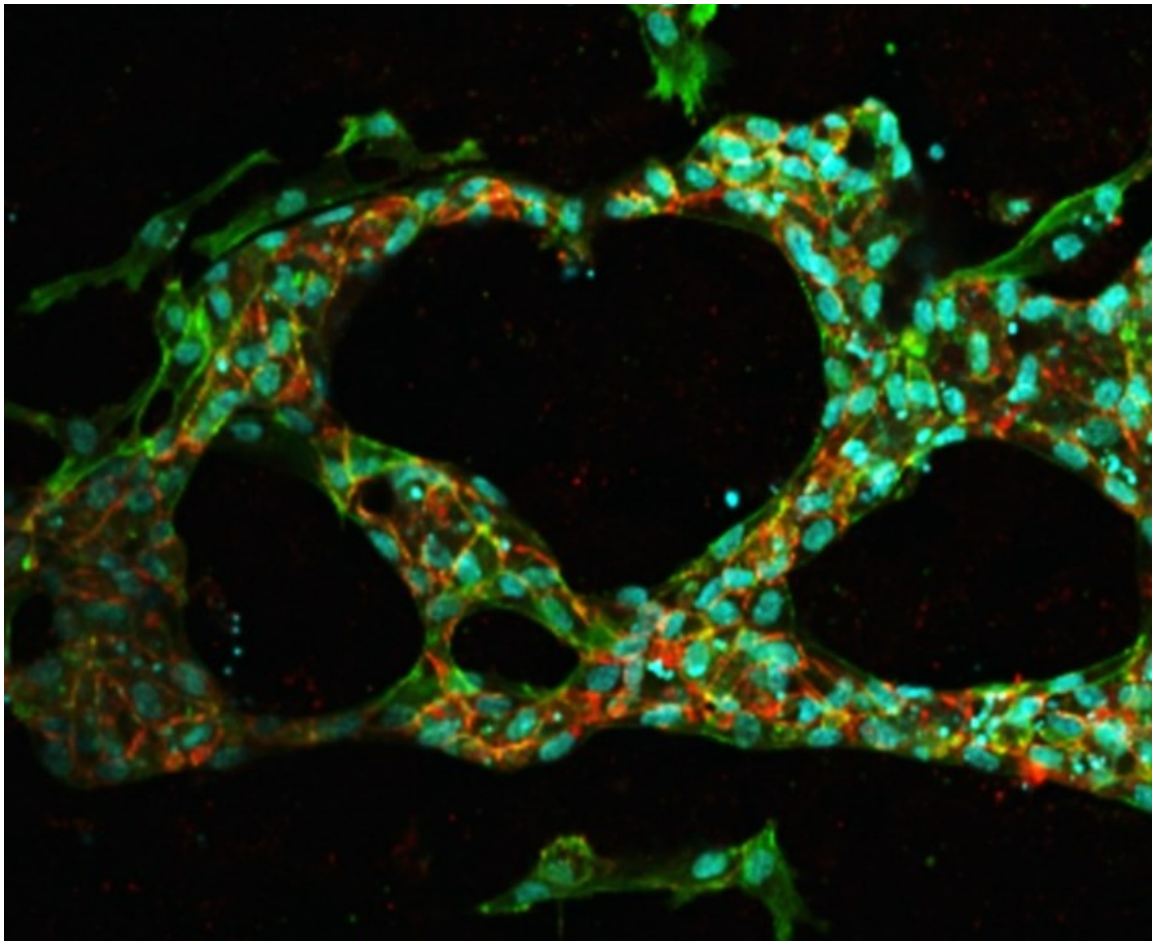

Anna Moritz-Fritschen

Investigation of Biological and Technical Components for the Development of a 3D-Bioprinting Process for Vascularized Organs-on-a-Chip

Jahr der Veröffentlichung der Dissertation auf TUprints: 2024

Tag der mündlichen Prüfung: 17.07.2024

Erklärungen laut Promotionsordnung

§8 Abs. 1 lit. c PromO
Ich versichere hiermit, dass die elektronische Version meiner Dissertation mit der schriftlichen Version übereinstimmt.

§8 Abs. 1 lit. d PromO
Ich versichere hiermit, dass zu einem vorherigen Zeitpunkt noch keine Promotion versucht wurde. In diesem Fall sind nähere Angaben über Zeitpunkt, Hochschule, Dissertationsthema und Ergebnis dieses Versuchs mitzuteilen.

§9 Abs. 1 PromO
Ich versichere hiermit, dass die vorliegende Dissertation selbstständig und nur unter Verwendung der angegebenen Quellen verfasst wurde.

§9 Abs. 2 PromO
Die Arbeit hat bisher noch nicht zu Prüfungszwecken gedient.

Darmstadt, den 24.04.2024

Anna Moritz-Fritschen

Preface

This thesis is a synopsis of the following publications in peer-reviewed journals:

I. Fritschen, A., and Blaeser, A. (2021). **Biosynthetic, biomimetic, and self-assembled vascularized Organ-on-a-Chip systems**. *Biomaterials*, 268, 120556.[1]

II. Fritschen, A., Bell, A. K., Königstein, I., Stühn, L., Stark, R. W. & Blaeser, A. (2022). **Investigation and comparison of resin materials in transparent DLP-printing for application in cell culture and Organs-on-a-Chip**. *Biomaterials Science*, 10(8), 1981-1994.[2]

III. Fritschen, A., Acedo Mestre, M., Scholpp, S. & Blaeser, A. (2023). **Influence of the physico-chemical bioink composition on the printability and cell biological properties in 3D-bioprinting of a liver tumor cell line**. *Frontiers in Bioengineering and Biotechnology,* 11, 1093101.[3]

IV. Fritschen, A., Lindner, N., Scholpp, S., Richthof, P., Dietz, J., Linke, P., Guttenberg, Z. & Blaeser, A. (2024). **High-scale 3D-bioprinting platform for the automated production of vascularized Organs-on-a-Chip**. *Advanced Healthcare Materials*, 2304028.[4]

Kurzfassung

Aktuell dienen Zellkulturen und Tierversuche in der pharmazeutischen Forschung der Bewertung von Wirksamkeit und Sicherheit neuer Substanzen. Dabei beruht die Beliebtheit zweidimensionaler Zellkultursysteme auf ihrer kostengünstigen Herstellung und Wartung, der Skalierbarkeit und den bereits etablierten Analysemethoden. Trotz ihrer Vorteile führen diese Systeme oft zur Fehleinschätzung von Substanzen, die in späteren Studien an Menschen aufgrund von unerkannten Nebenwirkungen oder verminderter Wirksamkeit zu Fehlschlägen führen. Um kostspielige Misserfolge zu vermeiden, sind deutlich genauere und zuverlässigere Gewebemodelle notwendig. Solche Modelle erfordern die gezielte Platzierung verschiedener Zelltypen in einem Matrixmaterial, das der extrazellulären Matrix des menschlichen Körpers ähnelt. Dies kann am effektivsten durch hochauflösende 3D-Biodrucker umgesetzt werden. Um eine angemessene Nährstoffversorgung und die Nachahmung der nativen Nährstoff- sowie Medikamentenaufnahme zu imitieren, ist die Integration eines Blutgefäßnetzes in das Gewebemodell entscheidend. Die Perfusion dieser Gefäße lässt sich am besten mittels eines mikrofluidischen Chips realisieren, der den Flüssigkeitsfluss und die Medikamentenzufuhr reguliert. Solche perfundierten Gewebemodelle auf einem Mikrofluidikchip werden als Organs-on-a-Chip bezeichnet. Obwohl Organs-on-a-Chip gegenüber zweidimensionalen Zellkulturen Vorteile bieten, werden sie in der pharmazeutischen Forschung nur begrenzt eingesetzt, da Herausforderungen wie die Skalierbarkeit und die Automatisierung der Herstellung und Handhabung bestehen bleiben.

Diese Arbeit befasst sich daher mit den Forschungsaspekten, die für die automatisierte Herstellung vaskularisierter Organs-on-a-Chip notwendig sind und ihre Anwendung in der präklinischen Arzneimittelforschung ermöglichen. Sie konzentriert sich auf die Herstellung eines dreidimensionalen, vaskularisierten und multizellulären Leberkarzinom-on-a-Chip mittels mikroventilbasiertem 3D-Biodruck. Ziel ist es festzustellen, ob der 3D-Biodruck die Herstellung von Organs-on-a-Chip automatisieren und ein höheres Maß an Komplexität sowie biomimetische Gefäßstrukturen hinzufügen kann. Zuerst werden in der Literatur vorgestellte Ansätze zur Vaskularisierung in Organs-on-a-Chip gesichtet, nach ihrem Grad der Biomimetik klassifiziert und ihre Eignung für das geplante Modell bewertet. Anhand dieser Analyse wird ein geeigneter und mit dem verfügbaren Biodrucker kompatibler Ansatz ausgewählt und in der Arbeit angewendet. Die Entwicklung komplexer Gewebemodelle erfordert oft mehrere Iterationen im Zusammenhang mit dem Design des eingesetzten Mikrofluidikchips, welche durch konventionellen 3D-Druck verbessert und beschleunigt werden könnten. Daher werden mögliche Anpassungen des Druckverfahrens und der Materialauswahl eines konventionellen 3D-Druckers untersucht, die nötig sind, um transparente und zytokompatible Bauteile zu erhalten. Dieser angepasste Prozess wird daraufhin hinsichtlich Druckauflösung und allgemeinem Druckprozess auf seine Eignung für die Prototypenherstellung untersucht.
Als nächstes erfolgt die Auswahl eines Matrixmaterials für die Leberkrebszellen, das präzise und mit hoher Auflösung vom Biodrucker platziert werden kann. Verschiedene Hydrogel-Kombinationen werden untersucht, um ein Material zu identifizieren, welches die Vitalität und Proliferation der Zellen bewahrt ohne die Druckauflösung zu beeinträchtigen. Schließlich wird der Biodrucker mit einer Robotereinheit kombiniert, um die manuelle Handhabung bei der Herstellung des Organ-on-a-Chip zu automatisieren. Dieses Verfahren wird an einem multizellulären, vaskularisierten Leberkarzinom-on-a-Chip getestet und bewertet. Das resultierende Modell wird anhand der Druckauflösung, der Morphologie des Gefäßnetzes und der Proliferation der Leberkarzinomzellen über 14 Tage beurteilt.

Abstract

In today's pharmaceutical research, conventional cell culture and animal testing are used to quantify the efficacy and safety of new pharmaceutical substances and drugs. The popularity of two-dimensional cell culture systems is based on their low costs in production and maintenance, high scalability, well-established testing and automated analysis methods. Despite these advantages, these methods often misjudge substances, resulting in late failures later on in human studies due to undetected side effects or reduced efficacy. In order to prevent these costly late failures, it is necessary to develop tissue models that more accurately and reliably represent human tissues in research. Such models require the targeted placement of multiple cell types in a matrix material that is similar to the human body, which can best be realized using high-resolution additive manufacturing such as microvalve-based 3D-bioprinting. To ensure nutrient supply and to mimic both the native nutrient and drug uptake, the integration of a blood vessel network into the tissue model is essential. The perfusion of these vascular networks can most reliably be realized on a microfluidic chip, which regulates liquid flow and drug administration. When tissue models are cultured under perfusion on such a microfluidic chip, they are called Organs-on-a-Chip. Despite the advantages of Organs-on-a-Chip over two-dimensional cell cultures, their use in pharmaceutical research remains limited as aspects such as their scaled-up fabrication and automatization in handling remain challenging.

This work addresses the mentioned research aspects required for the automated fabrication of vascularized Organs-on-a-Chip for a translation of these models into preclinical pharmaceutical research. It focuses on the fabrication of a three-dimensional, vascularized and multicellular liver carcinoma Organ-on-a-Chip model via microvalve-based 3D-bioprinting. The objective is to determine if 3D-bioprinting can enhance automation in the fabrication of Organs-on-a-Chip and add a higher level of complexity as well as biomimetic vascular structures. In the first step, approaches to vascularization in Organs-on-a-Chip presented in the literature are reviewed, classified according to their degree of biomimicry and assessed for their suitability regarding the planned multi-cellular Organ-on-a-Chip. Based on this analysis, an approach compatible with the available bioprinting system and suitable for the envisioned tissue model is selected and employed in this work. Since the development of complex tissue models often requires multiple iterative steps concerning the microfluidic chip, conventional 3D-printing could enhance and accelerate the prototyping of these chips. Possible adaptations to the print process and a material selection of a conventional 3D-printer required to obtain transparent and cytocompatible components are therefore studied. This adapted process is then tested to examine if the print resolution as well as the general print process is capable of prototyping various microfluidic chip designs required for the tissue model and bioprint process.
Next, a matrix material has to be selected that contains the liver carcinoma cells and that can be placed by the bioprinter with high precision and in small volumes. For this purpose, different hydrogel combinations are studied to identify a material that can retain and stimulate cell viability and growth without compromising the print resolution within the microfluidic chip. In the final step, the bioprinter is combined with a robotic handling unit to replace manual handling in the assembly of the Organ-on-a-Chip. This process is tested and assessed on the multi-cellular and vascularized liver carcinoma Organ-on-a-Chip. The resulting model is evaluated by the print resolution, the morphology of the vascular network and the proliferation of the liver carcinoma cells over a culture time of 14 days.

Acknowledgements

An dieser Stelle möchte ich mich bei all jenen bedanken, die mich während der Zeit der Promotion und auf dem Weg dahin unterstützt und motiviert haben.

Zuerst gebührt mein Dank Prof. Andreas Blaeser, der mich auf dem Weg zu dieser Arbeit immer unterstützt und gefördert hat. Die Unterstützung, konstruktive Kritik und das Feedback zu meiner Forschung haben zu dieser Arbeit maßgeblich beigetragen. Ich hatte viel Spaß an unseren Diskussionen über das Schreiben von Publikationen und von dieser Arbeit und konnte sehr viel dabei lernen. Außerdem habe ich so die einmalige Chance erhalten, die Entstehung und den Aufbau einer neuen Arbeitsgruppe zu begleiten.
Ein besonderer Dank geht an Prof. Edgar Dörsam für den Stoß in Richtung Promotion – denn „ich bin eher praktisch talentiert“. Ohne Sie wäre ich nicht am IDD gelandet und hätte so viele schöne Momente und gute Zeiten verpasst.

Ganz wichtig sind und waren natürlich meine Kolleg:innen am IDD. Ein besseres Umfeld – sowohl sozial als auch wissenschaftlich – hätte ich mir nicht wünschen können. Besonderer Dank geht an Pauline als mein großes Vorbild, die als beste Büronachbarin überhaupt immer alle Infos hat. Ohne Evas humorvolle Begleitung von Anfang an, unsere Kletterabende und geteilten Essen wäre das Abenteuer BMT auch nur halb so unterhaltsam gewesen. Außerdem muss ich mich bei all den tollen Studierenden bedanken, die meine Forschung vorangetrieben haben. Besonderer betonen möchte ich dabei Jamina für den mutigen Start der Zellkultur, Sebastian, ohne den ich niemals den Drucker ans laufen bekommen hätte, Inga für die tolle Ausarbeitung beim 3D-Druck, Mariana für die unendlichen Stunden mit zu vielen HepG2s, Johanna für die unzähligen Drucke für mich und Philipp für die Hilfe bei meinen viel zu komplexen Chipversuchen. Ich finde es großartig, inzwischen so viele von euch als Kolleg:innen weiterhin täglich dabei zu haben.

Auch möchte ich meinen Projektpartnern bei der Firma ibidi, insbesondere Philipp Linke und Zeno von Guttenberg, für die exzellente Zusammenarbeit in der Entwicklung des DynaVasc Chips danken. Ohne Philipp, der unzählige Mikrofluidikchips für mich zusammengesetzt hat, wären die Experimente nicht so erfolgreich gewesen. Die Diskussionen und die gemeinsame Forschung haben mir sehr geholfen.

Ein großes Dankeschön gilt zudem der Arbeitsgruppe Physics of Surfaces für die Einführung in die Forschung und den Zugang zur für mich neuen Welt der Zellkultur. Insbesondere gilt mein Dank Dr. Christian Dietz für seine inspirierende Vorlesung und das spannende Thema meiner ersten wissenschaftlichen Arbeit. Außerdem möchte ich Alena Bell für die (auch noch am Anfang dieser Promotion) unglaublich warmherzige und großartige Betreuung danken. Prof. Robert Stark möchte ich besonders für die Möglichkeit der Arbeit in seiner Gruppe, für seine Arbeit als Gutachter und für das Verständnis für die Klettertouren danken.

Ebenfalls möchte ich mich bei der Spaßtruppe bedanken – ohne euch hätte ich das Studium nicht ansatzweise so erfolgreich und mit so viel Spaß absolviert und wäre heute nicht mehr in Darmstadt. Eure Unterstützung und eure Freundschaft haben diese akademische Zeit zu einer unvergesslichen Reise gemacht.

Abschließend möchte ich mich bei meinem Mann Dominik und meiner gesamten Familie bedanken, die mich in dieser spannenden Zeit stets unterstützt und begleitet haben, und die immer ein offenes Ohr für mich haben.

…Und die andere Anna, bei der ich immer den Kopf frei bekommen und meine nötige Portion Sauerstoff und Vitamin D tanken konnte.

Table of Contents

List of Publications

This list gives an overview over all publications by Anna Moritz-Fritschen. The publications that comprise the synopsis are marked in blue as well as with numbers I – IV.

Bachelor thesis - Fritschen (2017). **Untersuchung von Endothelzellen mittels statischer und dynamischer Rasterkraftmikroskopie.** *Technical University of Darmstadt.*

Master thesis - Fritschen (2019). **Stereolithographic 3D printing of transparent and biocompatible devices**. *Technical University of Darmstadt.*

Article - Stühn et al. (2019). **Nanomechanical sub-surface mapping of living biological cells by force microscopy.** *Nanoscale*, 11 (27), 13089-13097.

Article I - Fritschen and Blaeser (2021). **Biomimetic, biosynthetic, and self-assembled vascularized Organ-on-a-Chip Systems**. *Biomaterials*, 268, 120556.

Article II - Fritschen et al. (2022). **Investigation and comparison of resin materials in transparent DLP-printing for application in cell culture and organs-on-a-chip**. *Biomaterials Science*, 10, 19981 – 1994.

Patent - Brumm, Fritschen, Dörsam and Blaeser (2021). **Verfahren zur Erzeugung von dendritischen und/oder biomimetischen Netzwerk-Strukturen, Gewebe und deren Anwendungen**. *Deutsches Patent- und Markenamt*, DE10 2021 118 900.4.

Article – Brumm*, Fritschen* et al. (2022**). Fabrication of biomimetic networks using viscous fingering in flexographic printing**. *Biomedical Materials*, 17 (4), 045012.

Patent - Guttenberg, Fritschen and Blaeser (2022). **Zellkulturträger**. *European Patent Office,* EP22 177 581.0.

Article III - Fritschen et al. (2023**). Influence of the physico-chemical bioink composition on the printability and cell biological properties in 3D-bioprinting of a liver tumor cell line**. *Frontiers in Bioengineering and Biotechnology*, 11(2023): 1093101.

Article IV – Fritschen et al. (2024). **High-scale 3D-bioprinting platform for the automated production of vascularized Organs-on-a-Chip**. *Advanced Healthcare Materials*, 2304028.

*Both authors contributed equally to this work.

Author Contributions

The following author contributions are displayed following the CRediT (Contributer Roles Taxonomy) system.

1st - Biosynthetic, biomimetic, and self-assembled vascularized Organ-on-a-Chip systems

Biomaterials, 268 (2021): 120556, DOI: 10.1016/j.biomaterials.2020.120556

Anna Fritschen: Conceptualization, Methodology, Validation, Investigation, Writing – Original draft, Writing – Review & Editing, Visualization

Andreas Blaeser: Conceptualization, Resources, Writing – Review & Editing, Supervision, Project administration

2nd - Investigation and comparison of resin materials in transparent DLP-printing for application in cell culture and Organs-on-a-Chip

Biomaterials Science, 10.8 (2022): 1981-1994; DOI: 10.1039/D1BM01794B

Anna Fritschen: Conceptualization, Methodology, Validation, Formal analysis, Investigation, Writing – Original draft, Writing – Review & Editing, Visualization

Alena Bell: Writing – Review & Editing, Investigation (Raman spectroscopy)

Inga Königstein: Writing – Review & Editing, Investigation, Visualization, Formal analysis

Lukas Stühn: Supervision, Methodology

Robert Stark: Funding acquisition, Resources

Andreas Blaeser: Conceptualization, Resources, Writing – Review & Editing, Supervision, Project administration

3rd - Influence of the physico-chemical bioink composition on the printability and cell biological properties in 3D-bioprinting of a liver tumor cell line

Frontiers in Bioengineering and Biotechnology, 11 (2023): 1093101; DOI:10.3389/fbioe.2023.1093101

Anna Fritschen: Conceptualization, Methodology, Validation, Formal analysis, Investigation, Writing – Original draft, Writing – Review & Editing, Visualization

Mariana Acedo Mestre: Methodology, Investigation (cell culture, imaging), Formal analysis, Data curation (fluorescence microscopy), Writing – Review & Editing, Visualization

Sebastian Scholpp: Investigation (DoD printing), Writing – Review & Editing

Andreas Blaeser: Conceptualization, Resources, Writing – Review & Editing, Supervision, Funding acquisition, Project administration

4th - High-scale 3D-bioprinting platform for the automated production of vascularized Organs-on-a-Chip

Advances Healthcare Materials, 2304028 (2024): 1 – 11; DOI: 10.1002/adhm.202304028

Anna Fritschen: Conceptualization, Methodology, Validation, Formal analysis, Investigation, Writing – Original draft, Writing – Review & Editing, Visualization

Nils Lindner: Methodology, Investigation (robotics), Software, Writing – Review & Editing, Visualization

Sebastian Scholpp: Investigation (DoD printing), Writing – Review & Editing

Philipp Richthof: Investigation (3D printed microfluidic chips), Writing – Review & Editing

Jonas Dietz: Software, Writing – Review & Editing

Philipp Linke: Investigation (COP chip fabrication), Writing – Review & Editing

Zeno Guttenberg: Investigation (COP chip fabrication), Funding acquisition, Resources, Writing – Review & Editing

Andreas Blaeser: Conceptualization, Visualization, Resources, Writing – Review & Editing, Supervision, Funding acquisition, Project administration

Abbreviations

Abbreviation	Description
Ag	Agarose
BAPO	Phenylbis(acyl) phosphine oxide
BSA	Bovine serum albumin
CD31	Cluster of differentiation 31
CLSM	Confocal laser scanning microscopy
Col	Collagen I
COP	Cyclic olefin polymer
DAPI	4′,6-diamidino-2-phenylindole
DLP	Digital Light Processing
DoD	Drop-on-Demand
EC	Endothelial cell
ELISA	Enzyme-linked immunosorbent assay
FDA	Fluorescein diacetate
FFF	Fused Filament Fabrication
Fib	Fibrinogen
FITC	Fluorescein isothiocyanate
Gel	Gelatin
HDF	Human dermal fibroblasts
HepG2	Human liver carcinoma cell line
HUVEC	Human umbilical vein endothelial cell
IPA	Isopropanol
μVN	Microvascular networks
OOC	Organ-on-a-Chip
PDMS	Polydimethylsiloxane
PEG-1	Polyethylene glycol diacrylate mixed with photoinitiator
PEG-2	Polyethylene glycol diacrylate mixed with photoinitiator and a photosensitizer
PI	Propidium iodide
SL	Stereolithography

List of Symbols

Symbol	Description	Unit
γ	Surface tension	N/m
$\dot{\gamma}$	Shear rate	1/s
δ	Phase angle	°
η	Shear viscosity	Pa s
k	Consistency factor	mPa s
n	Power-law constant	-
ρ	Density	g/cm^3
r	Nozzle radius	μm
τ	Shear stress	Pa
T	Temperature	°C
t_{valve}	Valve opening time	s
V_{drop}	Drop volume	nl

1. Introduction and Objectives of this Work

Pharmaceutical research is crucial for improving human health, for fighting diseases such as cancer, diabetes and novel respiratory infections and also aims to find treatment options for rare diseases[5–7]. Today's pharmaceutical research encompasses multiple stages in the development of new drugs and medication, starting from initial compound testing in laboratory settings, progressing to animal testing and later on to human trials[8,9]. However, this line of development is often faced with challenges and setbacks, including a high incidence of late-stage clinical trial failures, which results in tremendously high costs for new drugs[10,11].

One reason for these late failures is that typical 2D cell culture methods have a low resemblance to physiological conditions and that differences in metabolism between animals and humans exist[12–14]. To change this, innovative approaches such as organoids and Organ-on-a-Chip (OOC) technologies have emerged as compelling and promising alternatives to conventional 2D cell cultures[15–17]. These alternatives are especially noteworthy in the preclinical phase of drug development, offering opportunities for both fundamental research and disease modeling, but might also serve as valuable tools in substance testing[12,18,19]. OOCs, which are microfluidic devices that culture an arrangement of cells under perfusion[16,20], have already performed with great success in modeling pharmacokinetics and pharmacodynamics, the evaluation of drug efficacy and in the assessment of organ-specific toxicity[10,21,22]. First OOC designs have already been transferred into commercial products[23,24] and have been used by the pharmaceutical industry for in-house decisions in drug development[25]. Their recent successes in these domains emphasize their potential to transform and advance pharmaceutical research, ultimately leading to safer and more effective medical interventions. In acknowledgement of these advances, the American Food and Drug Association has recently permitted OOCs to replace animal testing in preclinical studies[26]. To establish OOC technology as an accepted and transformative platform within pharmaceutical research, a fast and reliable fabrication of these tissue models, coupled with automation and a simple design is crucial to ensure high repeatability and low-cost production[27–29]. A part of the solution to the automated fabrication of small tissue units on-chip could be 3D-bioprinting, which is an additive manufacturing technique that processes human cells and tissue components. These printers allow the targeted and spatially defined placement of multiple cell types on-chip[30–32], as has been shown for the liver[33–35], heart[36], brain tumors[37,38] and breast cancer[39].

In the process of creating even more relevant OOCs, the inclusion of vasculature in these models has become a focus of research[40,41]. To ensure a sufficient nutrient supply and to mimic both the native nutrient and drug uptake, the integration of a network of blood vessels into the tissue model is essential. The vasculature also enables the long-term cultivation of these tissue models, as the limited diffusion distance of nutrients of only $100 - 200\,\mu$m in native tissue[42,43] would otherwise lead to necrosis. Furthermore, the inclusion of an endothelial barrier into OOCs is crucial for predictive disease modeling and studies on pharmacokinetics, as the permeability of biomolecules through an endothelium is different from the administration through a biomaterial alone[44–47].

The work of this cumulative dissertation addresses some of the mentioned research aspects required for the automated fabrication of vascularized Organs-on-a-Chip for a translation of these models into pre-clinical pharmaceutical research. It focuses on the fabrication of a three-dimensional, vascularized and multi-cellular liver carcinoma Organ-on-a-Chip model that is

produced using a fully automated microvalve-based 3D-bioprinting process. On the way to such a tissue model, four scientific problems have to be solved:

1. How is vascularization of Organs-on-a-Chip addressed in literature and how can the presented approaches be classified according to their degree of biomimicry? Is the selection and application of these approaches to vascularization limited and governed by the design requirements of the chosen tissue model?

2. Fabrication of microfluidic chips would benefit from conventional 3D-printing technology for rapid prototyping. Which adaptations to the print process and materials are needed to fulfill the requirements regarding transparency and cytocompatibility for cell culture? Is the modified print process precise enough to fabricate all components of a microfluidic chip?

3. Which bioink formulations can solve the trade-off between cell biology and print process requirements? Which bioink compositions can retain and stimulate tissue-specific cell functions of parenchymal and stromal cells without compromising print resolution on chip?

4. Can the combination of robotic handling and 3D-bioprinting replace the manual handling of microfluidic chips in the assembly of Organs-on-a-Chip? And does this process yield a functional, multi-cellular and vascularized Organ-on-a-Chip?

These four scientific questions will be addressed in four publications focusing on each individual problem[1–4] and will result in a 3D-bioprinted, multicellular and vascularized liver carcinoma Organ-on-a-Chip (**Figure 1**).

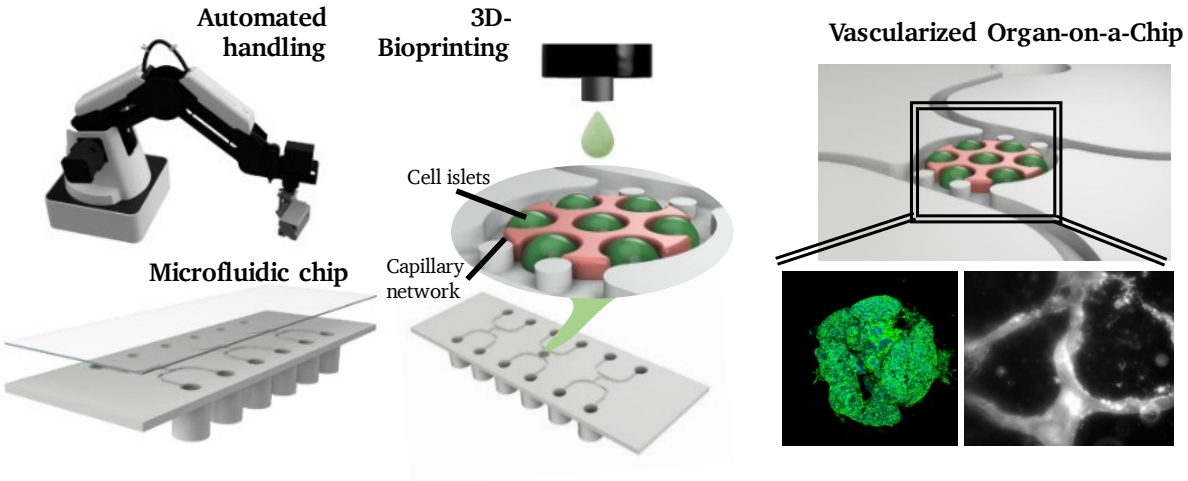

Figure 1: Sketch of the 3D-bioprint process and the design of the tissue model of a liver carcinoma Organ-on-a-Chip model.

At the beginning of this work, a detailed review of the existing approaches to vascularization in OOCs was conducted. The methods to include vasculature are classified according to their degree in biomimicry and evaluated regarding their suitability for the envisioned tissue model comprising liver carcinoma cell islands surrounded by a vascular network (→ **Section 4.1**).

Next, a microfluidic chip compatible with a 3D-bioprinter and adapted to the tissue model design has to be developed. For the tissue model planned in this project, the chip design is a key aspect that requires many iterations to reach a final and suitable design for the envisioned

process. As the commonly used soft-lithography, but also alternatives such as hot embossing and injection molding either require expensive equipment, are time-consuming or not fitted for prototyping, a suitable 3D-print process has to be developed that can fabricate transparent and cytocompatible microfluidic chips accessible for a 3D-bioprinter (→ **Section 4.2**).

To advance automatization in the fabrication of OOCs, a microvalve-based Drop-on-Demand (DoD) bioprint process has to be developed that can place the liver carcinoma islands on chip without harming the cells during this process. This requires the selection of a bioink that can combine the requirements for printability regarding rheological and gelation properties, mechanical stability and nutrient diffusivity with cell biological considerations such as cell proliferation and functionality (→ **Section 4.3**). In a similar manner, a second bioink containing endothelial cells and fibroblasts is selected that can fill the space between the liver carcinoma islets and support the tissue model with nutrients and oxygen by self-assembling into microvascular networks (→ **Section 4.4**).

Finally, the bioprint process is combined with a robotic system to remove any manual steps and its suitability is shown for a complex and vascularized OOC. To enable robotic handling and chip filling, the microfluidic chip design is adapted to the robotic unit to enable placement and especially closure of the chip. The fabrication of the microfluidic chip is translated from prototyping into injection molding of larger piece numbers, increasing the reproducibility and availability of the chips. To complete this work, the suitability and capabilities of the developed automated process in combination with complex biological processes such as microvascular self-assembly are shown for a vascularized liver carcinoma Organ-on-a-Chip (→ **Section 4.4**).

2. State of Research

2.1. Organs-on-a-Chip

Organs-on-a-Chip are microfluidic devices that simulate human or animal biology *in vitro* at the smallest biologically acceptable scale. They consist of a microfluidic chip connected to a perfusion system and cells that are cultured in this chip[25,48]. The microfluidic chip enables the control over small volumes of fluid in the microliter range within channel systems at low flow rates under laminar flow conditions. The microfluidic chip advances typical tissue models from a static to a dynamic state while offering a circulating supply of fresh culture medium, better waste removal and the possibility for in-line nutrient read-outs[49]. The design and set-up of OOCs vary greatly and always depend on the application and scientific question. Thile the simplest OOCs are made of a 2D cell layer on a surface within the microfluidic chip, more complex designs include membranes, cells seeded within a scaffold material in 3D or scaffold-free 3D agglomerates[19,23,50].

When designing an OOC, the scientific question to be studied is critical as it determines the required components (**Figure 2**). This process begins with the sub-organ functional unit to be studied, specifically the cell-biological architecture or interface of interest. The size and complexity of this area of interest then govern the required cell types and possible combinations of these. Once the functional unit has been decided on, the tissue model has to be designed. In this step, the sourcing of cells is an important step, as biopsies of certain tissue samples such as the human brain or liver are hard to come by, while cell lines, the same cell species from a different location within the body or animal cells, are more available alternatives (→ **Section 3.2**). Next, the complexity of the model has to be decided on. While simple 2D layer or membrane-based approaches are a possibility, more complex models embed multiple cell types in a matrix material or spatially defined place different cell types and materials within a small volume. If a three-dimensional model is planned, the choice of the cell-surrounding biomaterial is of great importance (→ **Section 3.4**). With the biological questions solved, topics such as the microfluidic chip design (→ **Section 2.3**), perfusion and filling strategies, in- and off-line measurement planning and the inclusion of read-out possibilities directly on the chip have to be considered and planned.[23,51,52]

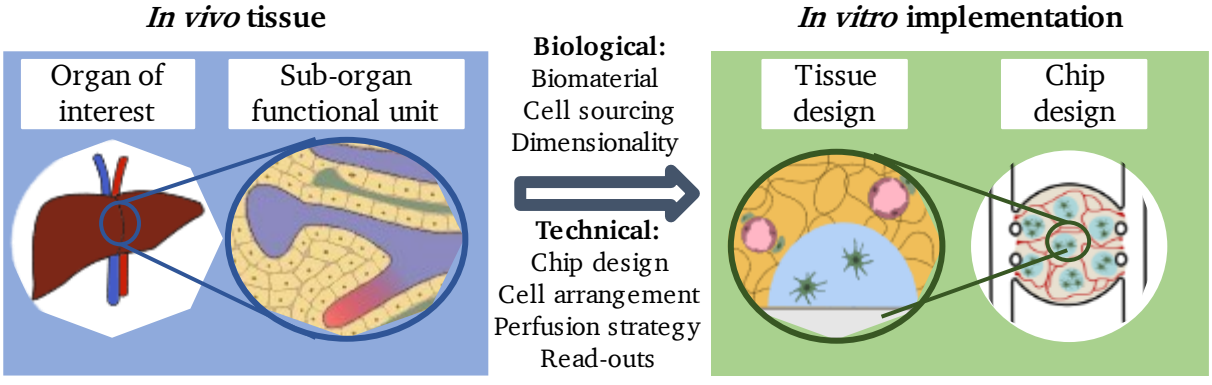

Figure 2: Design considerations in Organs-on-a-Chip. In the first step, the *in vivo* tissue is studied. From the organ of interest, the sub-organ functional unit that is to be represented is selected, including the required complexity and cell types of the following tissue model. The *in vitro* implementation covers the biological components such as the dimensionality (2D or 3D), the sourcing of cells and possible biomaterials. Finally, the technical components such as chip design, cellular arrangement, perfusion strategies and possible read-outs are considered.

2.2. Vascularization for Biomimetic Organs-on-a-Chip

While tissue models consisting of only parenchymal cells have already proven their use and are popular in research, today's focus has turned to the inclusion of vasculature into the models. Vascularization of tissue models is required to achieve larger tissue samples to prevent cell death by necrosis, as the typical diffusion limit of oxygen and nutrients in the human body is around 100 – 200 μm. However, the inclusion of vasculature is not only important for larger tissues, but also for OOCs to enable a biomimetic drug and nutrient uptake in the designed models. In the body, no direct contact exists between parenchymal cells and the blood flow, but the supply of nutrients and oxygen, waste removal as well as exposure to fluid shear are all mediated through the vasculature. The permeability of the endothelium, which is the inner layer of blood vessels formed by endothelial cells, varies from organ to organ and plays a critical role in drug uptake and tissue response.[30,43,45,53–55]

Vascular networks in the human body range in size from various centimeters for larger arteries down to a few micrometers for capillaries. The general transport of blood to and from the organs is conducted by arteries and veins, which split into smaller arterioles and venules until they form a fine capillary bed that is everywhere in the body (**Figure 3** A)[53,56]. Capillaries are the smallest of blood vessels with a diameter of around 8 – 15 μm and they consist of a single layer of endothelial cells (ECs) that wrap around each other and are stabilized by pericytes (**Figure 3** B, C)[53,56]. The larger arterioles have an additional layer of smooth muscle cells that enable the dilation and contraction of the blood vessels, while arteries are additionally embedded in fibroblasts[53,57]. In humans, blood vessels are formed in two ways. The formation of new blood vessels takes place during embryonic development and is referred to as vasculogenesis, while angiogenesis describes the formation of blood vessels from already existing vessels, as occurs in wound healing[53,58].

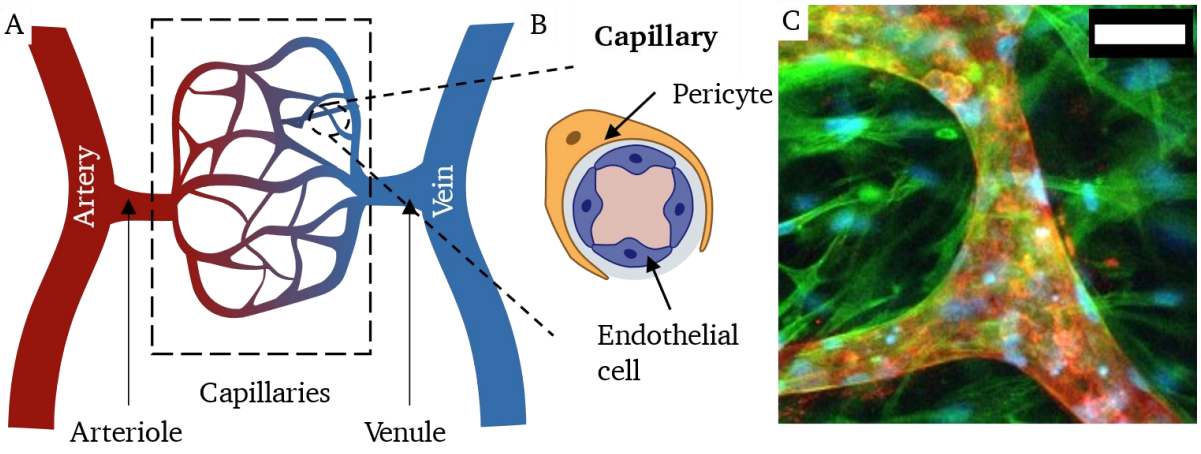

Figure 3: In the human body, the vasculature ranges in size from larger arteries down to arterioles and capillaries (A), which are built from endothelial cells (EC) and pericytes (B). Fluorescence microscopy image of an *in vitro* microvascular structure formed by HUVEC (stained red) surrounded by fibroblasts, with actin filaments stained green and cell nuclei in blue (C). Scale bar showing 50 µm.

In tissue models and OOCs, different options and approaches to the inclusion of vascular structures exist. There are many publications on this topic that range from highly engineered, synthetic approaches in 2.5D designs to printed 3D channels and models using solely the self-organization capabilities of cells to form vessels.

Derived research motivation:

To get an overview of available approaches to vascularization on-chip and to be able to evaluate an option suitable for this work, the existing publications on this topic are collected, classified and discussed in detail as part of this cumulative dissertation review paper[1] (→ Publication I) and in **Section 4.1**.

2.3. Microfluidic Chip Design and Fabrication

All Organs-on-a-Chip require a microfluidic chip tailored to the specific needs of a certain tissue type that is to be modeled. This begins with the dimensions of the tissue-containing chamber(s) and their geometry. For tissue models based on synthetic membranes and interfaces, these interfaces have to be included. For 3D matrix-based models, the tissue chamber has to be separated from the microfluidic channels, which can happen either through pillars or small openings. The number and geometry of the microfluidic channels govern the flow characteristic and possible perfusion strategies. For perfusion, connections via Luer connectors, hose fittings or needle insertions have to be planned as well (**Figure 4** A). In addition, the tissue chamber has to be accessible either to manual filling via loading ports, or open at the top to enable 3D-bioprinting into the tissue chamber. After filling, the chip has to be completely tight and leakage-free under perfusion.[12,23,59,60]

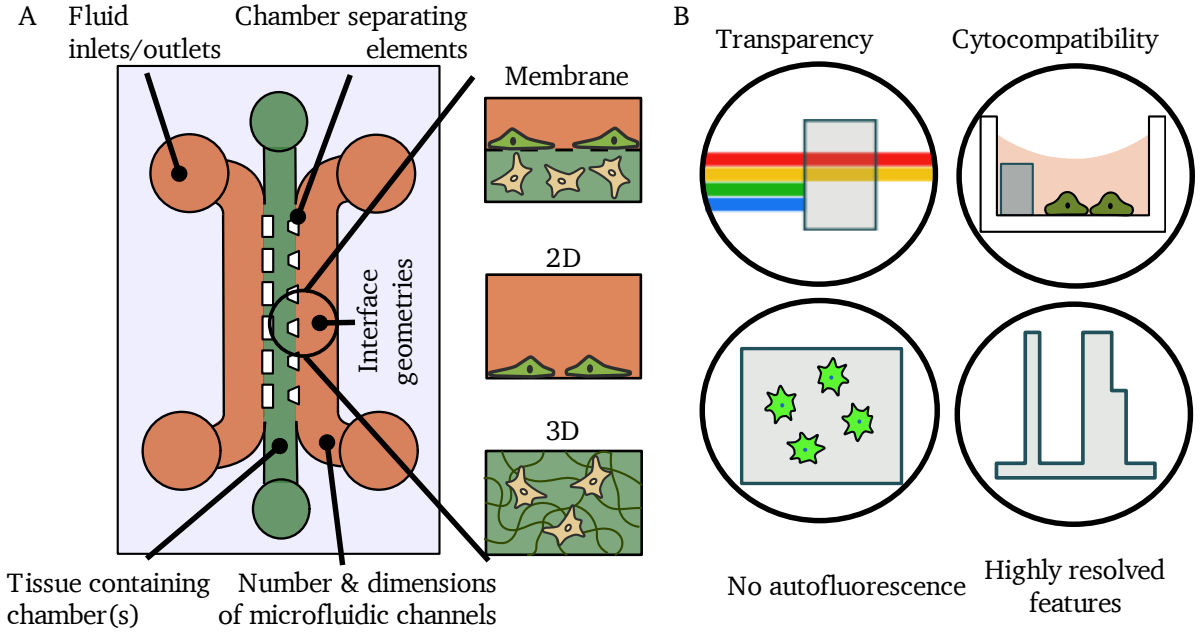

Figure 4: Microfluidic chip designs for OOCs are highly diverse depending on the type of tissue model that is to be achieved. Factors to consider include the number of tissue-containing chambers, the number and dimension of the microfluidic channels, possible interface geometries or elements that separate the tissue chamber from the channels as well as fluid inlets and outlets (A). Requirements on microfluidic chips for OOCs include high transparency, cytocompatibility, no or low autofluorescence as well as highly resolved features (B).

Apart from the design aspects, the materials and the final chip have to fulfill certain requirements to ensure correct culture conditions and tissue analysis (**Figure 4** B). Naturally, the chip has to be highly cytocompatible, neither harming the contained cells nor affecting their behavior by leakage of certain chemical or biological compounds. As (fluorescence) microscopy

is a key analysis method always required in tissue models and cell cultures, the chip has to be transparent for light in the range of 350 – 800 nm wavelength to allow the excitation of common fluorescence dyes and imaging of their emission. At the same time, the chip material should not contain autofluorescent components to not interfere with the sample's signal. Microfluidic chips are per definition of small dimensions, so the fabrication technology has to be capable and the material to be processable in such a way that features of around 100 μm can be resolved. As very thin bottom layers are needed for high-resolution microscopy, the material also has to be stiff enough to be handled. Furthermore, low absorbance of molecules that are of interest in read-outs by the chip material should occur.[59,61,62]

The most commonly used approach to microfluidic chip fabrication is replica molding of lithography-structured surfaces with polydimethylsiloxane (PDMS). Soft-lithography enables the fabrication of chips with highly resolved features down to a few micrometers with high aspect ratios and high control over the geometry. However, the lithography process only allows for rectangular channels and requires expensive equipment and materials for photolithography, wafers and photoresists. Due to the casting process, closed channel systems cannot be fabricated, but a minimum of two layers are cast that have to be sealed later on via plasma bonding or screws. Though being highly transparent and with a high oxygen permeability, PDMS has the great disadvantage that it absorbs small hydrophobic molecules, which can interfere with quantitative assays.[12,18,49,61–63]

Alternatives to PDMS soft lithography include thermoplastics or other polymers that are fabricated via laser structuring[64,65], injection molding[66–70], hot embossing[35,65,71] or 3D-printing[59,62,72–74]. From these methods, 3D-printing is a promising tool for rapid chip fabrication as it offers great flexibility in prototyping, comes at a reduced acquisition cost and offers such a high geometrical freedom that microfluidic chips can be fabricated in a single-step process[75,76].

A variety of 3D-printing technologies exist (→ **Section 3.1**), but only a few of them are suitable to print transparent and cytocompatible microfluidic chips. Of these, Fused Filament Fabrication (FFF) and Stereolithography (SL) printing are the most popular and promising approaches for Organs-on-a-Chip[77,78]. FFF printers can handle cytocompatible thermoplastics such as PLA and PCL and have already been used for the fabrication of microfluidic chips[33,79–81]. The presented chips have channels with diameters in the range of 250 – 500 μm, though freestanding elements such as pillars are not realizable. With FFF-prints, reduced transparency due to surface roughness and tightness under perfusion remain as drawbacks. Stereolithography printing does not have these issues with tightness, can achieve a high transparency and can be adapted to ensure cytocompatibility, which has been shown for microfluidic chips with finely resolved structures[59,73,74,76,82–87].

Derived research motivation:

Stereolithography-based 3D-printing could be a valuable tool in the development of microfluidic chips in this work. The required adaptations to the print process, the selection of suitable materials as well as the evaluation of the printed microfluidic chips regarding their compatibility with 3D-bioprinting are researched and presented in **Section 4.2** and in detail in a publication[2] (→ Publication II).

2.4. Towards Automatization in Organ-on-a-Chip Fabrication

Today, most OOCs are fabricated using a long series of manual steps, including chip fabrication via PDMS molding, tissue model formation via manual pipetting as well as manual media exchange and imaging. Especially manual pipetting of the bioink is a tedious and slow process with low scalability, high handling variation and lacking resolution to spatially place different cell types in the small volume. Therefore, there is a need for advanced methods to place cells and biomaterials on chip in a non-harming, ensuring a high cell viability. Automation is also essential to minimize handling errors and streamline the process from a digital sketch to the final OOC within a short timeframe[88,89].

Modern 3D-bioprinting technologies are a promising tool here, though the combination of bioprinting with OOCs is just at the beginning[1,89,90]. Vastly different types of bioprinters exist that can overtake the placing of cells and biomaterials inside the chip, with their specific advantages and disadvantages (→**Section 3.6**). Bioprinters today have achieved resolutions of down to 10 μm and can process even sensitive cells without impacting viability or cell function[91,92]. They can also simultaneously place different cells and materials side by side in complex spatial arrangements and therefore more closely mimic human tissues[32,89,93]. Regardless of the chosen printer, the right combination of printer and material is the key to maintaining cell viability, high print resolution and to complex cell arrangements. The material has to be selected so that it can support the print process in terms of resolution, handling and crosslinking, while also offering a cell-friendly environment that can stimulate cell function and growth[31,94]. The print process itself as well as the material have to ensure that the process parameters such as shear stress, potential UV exposure, drop impact and more are controlled to maintain cell viability and function[95–97]. At times, these factors are contradictory and become even more challenging if multiple cell types are printed with spatial patterning, when a certain biofunctionality of the material is required to obtain self-assembled microvascular networks or by the restricted space available on chip.

While there are published works available that employ 3D-bioprinting to obtain vascularized OOCs[98–101], they often remain at lower complexity levels and use the bioprinter to print open channels instead of opting for self-assembled μVN[1,102].

Derived research motivation:

3D-Bioprinting is a key technology to advance automation in OOCs. For a multi-material, multi-cellular and vascularized model, different bioinks and print strategies are developed to achieve high control over cellular placement while maintaining cell function. First, a study on possible matrix materials and print parameters for HepG2 cells using a Drop-on-Demand (DoD) bioprinter is conducted[3] (→ Publication III) as presented in section 4.3. Next, a multi-material print process resulting in a vascularized liver carcinoma model is developed as presented in **Section 4.4**. and in detail in a publication[4] (→ Publication IV).

To further establish vascularized OOCs as a standard tool in industrial pharmaceutical research, an upscaled and automated fabrication process is required[29]. There is little research yet done on this topic with a focus on OOCs, but there are already different tools and concepts available that could boost the technology readiness of OOCs[27,28,103,104]. Aspects that can profit from automatization reach from chip fabrication, chip handling and preparation, filling of the chip with the tissue model to pump systems, imaging and read-outs. Apart from the tissue model printing, there are already some works available on fluidic units and automated sample taking[105,106] as well as automated continuous imaging and incubator systems[107–109].

Derived research motivation:

Three aspects of automation are addressed in this work – a mass-producible microfluidic chip compatible with 3D-bioprinting is developed, the chip is filled with a complex and vascularized tissue model using a DoD 3D-bioprinter, and the surrounding handling and storage of the chip is conducted by a robotic unit as presented in **Section 4.4** and in a publication bioprinter[4] (→ Publication IV).

3. Theoretical Background

This section explains certain key aspects regarding cell biology, 3D-printing and 3D-bioprinting to give a short introduction to these topics and to create a basic understanding of this work. In-depth literature references regarding these topics are given for readers for further studies.

3.1. 3D-DLP-Printing

The terms additive manufacturing and 3D-printing describe fabrication technologies that produce three-dimensional physical objects by depositing, solidifying or joining materials based on a 3D digital model. The advantage of 3D-printing over other fabrication technologies is that objects can be built directly from a digital model without the need for tools, reducing cost and time, which makes it an ideal technology for rapid prototyping. Furthermore, a higher freedom of design is given, as complex shapes that are impossible or hard to manufacture with conventional fabrication technologies can be produced with little additional effort.[110–113]

A large variety of different printer types exist that build an object either point-, line- or layer-wise. Similarly, many distinct material classes can be handled, from metals to polymers, ceramics and biological materials such as wood or hydrogels. Of all these printers, only few are suitable to fabricate transparent microfluidic chips for cell culture experiments[77,78] (→ **Section 2.3**). One of the suitable options are stereolithography (SL) printers, which generate objects out of photocurable liquids (resin) by photopolymerization. A variation of this group of printers are digital light processing (DLP) printers, where a projector chip of very small micromirrors representing the pixels in the projected image reflects the incident light beam either to or away from the resin. For the printer configuration used in this work, a build plate is lowered into the resin-containing vat, leaving a layer between its surface and the bottom of the vat that is exactly as high as the set layer height. The DLP then projects a layer of the digital model into the vat, which starts the polymerization reaction by exposing the resin for a certain exposure time with a set light intensity (**Figure 5** A). Afterwards, the build plate is raised, and lowered to the set slice thickness between the existing print and vat, and the process is repeated until the object is finished.[110–113] In this process, the resolution is directly dependent on the pixel size in the x-y-direction and the accuracy of the z-stepper motor in the z-direction, but also reduced by the optical absorbance and the radical diffusivity of the resin. For microfluidic devices, resolutions down to a few tens of micrometers have been reported[114–116].

Resin materials compatible with DLP-printers are liquid blends of reactive monomers such as epoxy resins or acrylic acids with side chains for crosslinking, and a photoinitiator that starts the polymerization reaction. Other chemicals such as photosensitizers, fillers, stabilizers or chemical modifiers can be included as well to improve print performance. The photoinitiator is tailored to the wavelength of the DLP-printer. When hit by a photon, chemical bonds within the initiator molecule split, forming a radical that initiates a radical polymerization chain reaction (**Figure 5** B). The reaction stops once two polymer radicals combine, when free radicals cancel each other out or when they become trapped inside a solidified polymer matrix.[113,117,118]

The photoinitiator does not only act as a reaction catalyst, but it also spatially restricts the polymerization process to the desired volume. For DLP printers, benzoyl peroxide derivatives are the most commonly used material class, as their absorption profile fits well with the conventional DLP light sources[118–120]. Photosensitizers are at times added to improve the spectral sensitivity, as they absorb light at wavelengths out of the absorption region of the initiator and transfer their excitation onto the photoinitiator[118,120,121].

As prints are not fully cured after printing and as an initiator or radical residues remain, the printed object is washed with isopropanol (IPA) and post-cured under UV light to remove or photobleach residual photoinitiators[110,113]. This is especially crucial for microfluidics for OOCs, as no toxic or reactive components can remain after printing[122,123]. For microfluidic chips for cell culture applications, common initiators are benzoyl peroxide derivatives such as phenylbis(acyl) phosphine oxide (BAPO), diphenyl(2,4,6-trimethylbenzoyl) phosphine oxide or Irgacure 2959, which are cytocompatible at low concentrations and crosslink at wavelengths around 365 nm. For light sources with 405 nm wavelength, lithium phenyl-2,4,6-trimethylbenzoylphosphinate (LAP), a water-soluble and cytocompatible molecule is often used.[120,121,123,124]

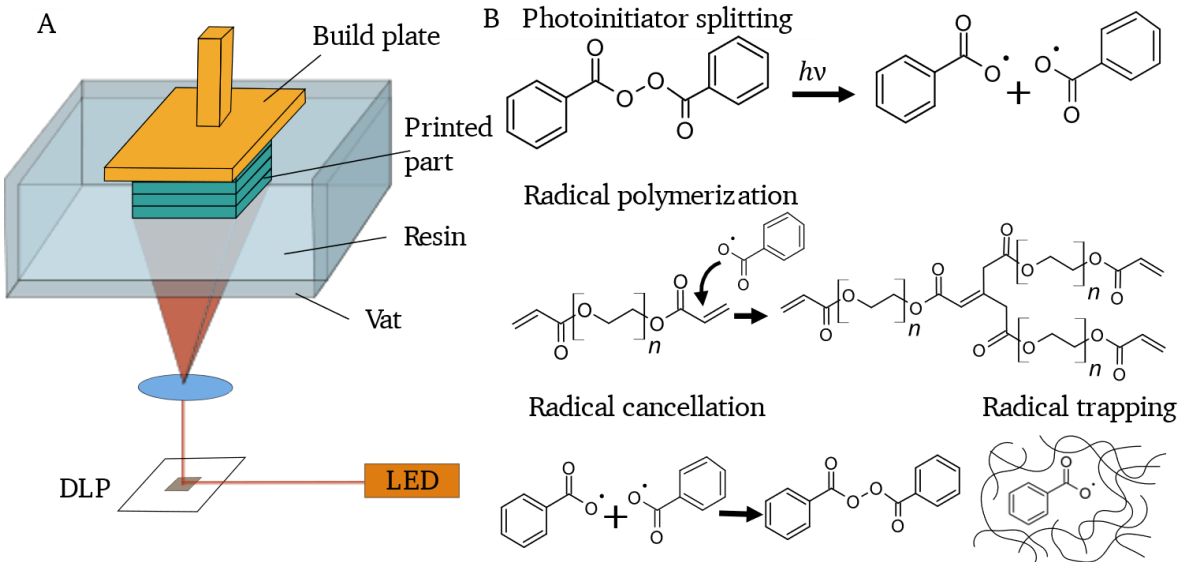

Figure 5: Schematic drawing of a DLP printer as used in this work (A). Photopolymerization reaction including the activation of a photoinitiator by UV photons (hv), radical polymerization creating a polymer network, and termination of the reaction by free radical cancellation or trapping of a radical inside the polymer network (B).

3.2. Cell Types and Sources

Various sources of mammalian cells are available to researchers in tissue engineering and general cell culture. Different cells do not only vary in the species they originate from, but also if they are primary cells taken directly from a human patient, or so-called cell lines. Cell lines are cell cultures that proliferate nearly indefinitely, which is why they are also called “immortalized”. This is in contrast to primary cells, which cease to grow in cell culture after a certain number of cell divisions, the so-called Hayflick limit. The abnormality of indefinite growth can happen spontaneously, especially in cancer cells, but is usually induced by specific genetic alterations via viral infection or modern genetic modification protocols. The advantage of cell lines is that they are easy to keep and have a stable genetic profile, but their genetic profile and behavior do not always correspond to the *in vivo* situation. Primary cells are therefore closer to the *in vivo* situation, but they are not easy to obtain as biopsies are required. They are also limited in their lifespan, are at times hard to maintain in culture and exhibit donor to donor variations.[125–130]

For the human vascularized liver carcinoma model created in this work, both primary cells and cell lines are used. The cells required for the vascular network – endothelial cells and

fibroblasts – are obtained from biopsies and kept as primary cells. The liver carcinoma cell line HepG2 is used for the carcinoma part of the model.

HepG2 is a hepatoblastoma cell line extracted from the cancer of a 15-year-old boy in 1975[131]. It is a robust and easy-to-keep cell line which offers most of the metabolic function of primary hepatocytes, making it a great candidate for *in vitro* cancer drug development studies[132–136]. Furthermore, most cases of liver cancer are hepatocellular carcinomas[137], which are the most common malignant variety of liver tumors in children[138]. In cell culture, HepG2 cells offer little cytosol around their nucleus with a compact rounded shape and a tendency to agglomerate in 2D culture.

The human vascular network is composed of different cells depending on the position in the body and the size of the vessel, but it always contains endothelial cells as the inner layer of the vessel. The most commonly used primary endothelial cell type, which is also used for this work, are human umbilical vein endothelial cells (HUVEC). They are isolated from the umbilical cord of newborns, making them easy to extract and abundantly available. In culture, they spread out and form a cobblestone morphology when reaching confluency.[139–141]

Fibroblasts are cells that build the connective tissue in the body and that can stabilize vessels in cell culture. In this work, primary human dermal fibroblasts (HDF) from foreskin biopsies are used. The advantages of dermal fibroblasts are their high availability, good cultivation behavior and moderate proliferation. In culture, they appear as large and spindle-shaped cells.[141,142]

3.3. Analysis Methods for Tissue Models

Many different measurement and observation techniques exist to characterize tissue samples. These include monitoring of cell numbers and confluency, staining of cell components with chemicals and antibody markers, measurement of the metabolic conversion of reagents, measurement of protein content expressed by cells and the quantification of gene expression. This work uses four methods to analyze the functionality of cell cultures. Specifically, the cellular morphology is monitored via (immuno-)fluorescence staining, live and dead cells are identified by their uptake of fluorophores, the metabolic activity and therefore proliferation is measured via the conversion of resazurin, and the production of a protein is quantified via an enzyme-linked immunosorbent assay.

The viability of cells is of interest to see how this is impacted during bioprinting, by the 3D-printing resins of the microfluidic chip or by a certain biomaterial in general. One of the most common and simplest methods is to double fluorescently stain cells with fluorescein diacetate (FDA) and propidium iodide (PI). FDA is a non-fluorescent molecule that can pass through the cell membrane and is only converted by live cells to highly fluorescent fluorescein. PI, on the contrary, cannot pass the membrane of healthy cells and only binds to the DNA of cells with a damaged membrane. With a fluorescent microscope, cells can therefore easily be identified as alive (green) or dead (red) (**Figure 6** A).[143–145]

An indirect method to measure cell viability is the measurement of the metabolic activity of cells via the conversion of resazurin. Resazurin is a non-fluorescent molecule, which can be metabolically converted by cells via mitochondrial reductase into strongly fluorescent resorufin. The amount of resorufin produced is measured by a fluorometric analysis, as the color changes from blue (resazurin) to pink (resorufin) (**Figure 6** B). After calibration, the fluorescence

intensity can be nearly linearly connected to its concentration and therefore to the number of cells or, more precisely, the metabolic activity of cells.[146–148]

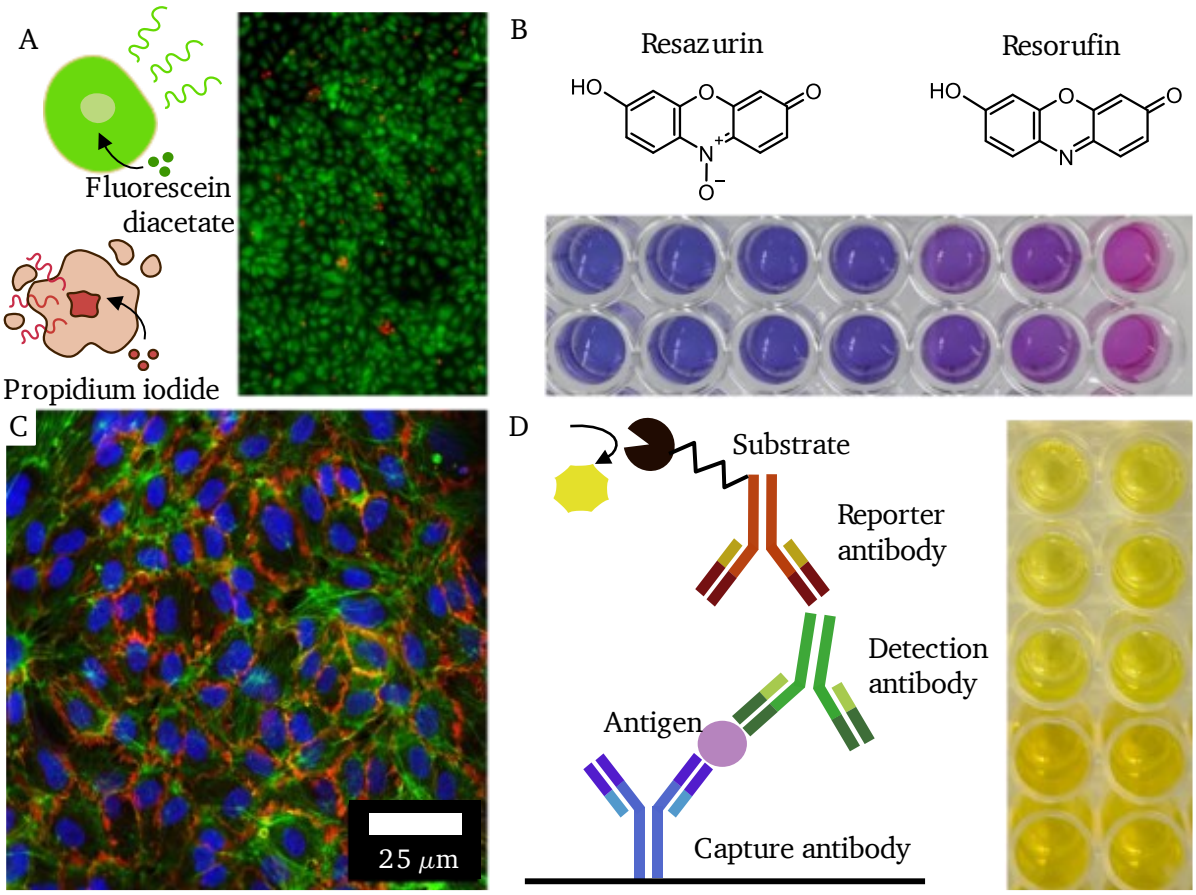

Figure 6: Cell assays used in this work include the staining of live cells with FDA (green) and dead cells with PI (red) (A), measurement of the metabolic conversion of blue resazurin into pink resorufin (B), fluorescence microscope image of HUVEC cells with nucleus stained with DAPI (blue), actin filaments stained with Alexa488-phalloidin (green) and anti-CD31 antibody coupled to Alexa594 (red) (C). Sketch of the components inside an enzyme-linked immunosorbent assay (ELISA) for the quantification of a detection protein, where the read-out is the intensity of a color change (D).

Apart from the indication of being alive and having a metabolism, the morphology of cells is also an indicator of their functionality. As cellular structures are difficult to distinguish under the microscope, fluorescent markers are employed that bind to specific cellular structures (**Figure 6** C). Three fluorescent markers are used in this work. Cell nuclei are stained with DAPI, a small fluorescent molecule that can pass through the cell membrane into the DNA and intercalate in the DNA strands. The actin filaments are stained by phalloidin, which is a toxin that binds and polymerizes with a high affinity to actin filaments. Phalloidin is in this work tagged with a green fluorescent marker. Endothelial cells are stained with an antibody against the cluster of differentiation 31 (CD-31), which is a cell adhesion protein expressed on the surface of endothelial cells, but not by fibroblasts or hepatic cells. In the next step, the primary antibody is labeled with a secondary antibody that contains a fluorescent marker.[149–151]

While immunofluorescence stainings can localize antigens of interest, other methods are required to quantitatively measure them. Enzyme-linked immunosorbent assays (ELISA) can quantify certain antigens, in this case, human serum albumin, though the demobilization of the antigen on a surface combined with a colorimetric signal. While there are different ways an ELISA can be conducted, the sandwich method is used in this work and presented here (**Figure**

6 D). In this type of ELISA, the antigen of interest is caught between a capture and detection antibody and immobilized on the surface of a well plate. In the indirect sandwich ELISA used here, the detection antibody is complexed with an enzyme-linked reporter antibody. The activity of this linked enzyme, in this case a biotin-streptavidin complex, is measured by incubating it with the enzyme's substrate. When the substrate binds to the enzyme, the reaction produces a signal, in most cases a color change that can be measured quantitatively by adsorption measurements. The intensity of color corresponds to the amount of antigen caught. While being more complex than direct ELISAs, sandwiching increases the sensitivity as two different antibodies bind to two different epitopes of the antigen.[152–154]

3.4. Biomaterials for 3D Tissue Culture

While cells have been grown on 2D surfaces since the beginning of cell culture, a transition into a 3D culture similar to the condition in the human body offers advantages for tissue models in research. In the body, most cells are anchored to an extracellular matrix (ECM) that provides physical support but also impacts cell differentiation, migration and gene expression. Mechanical properties such as elasticity, but also porosity and biofunctionality all play an important role in cellular behavior. These are in part intrinsic material properties, but are at times also tunable by varying the concentration of the material (**Figure 7** A).[155–159]

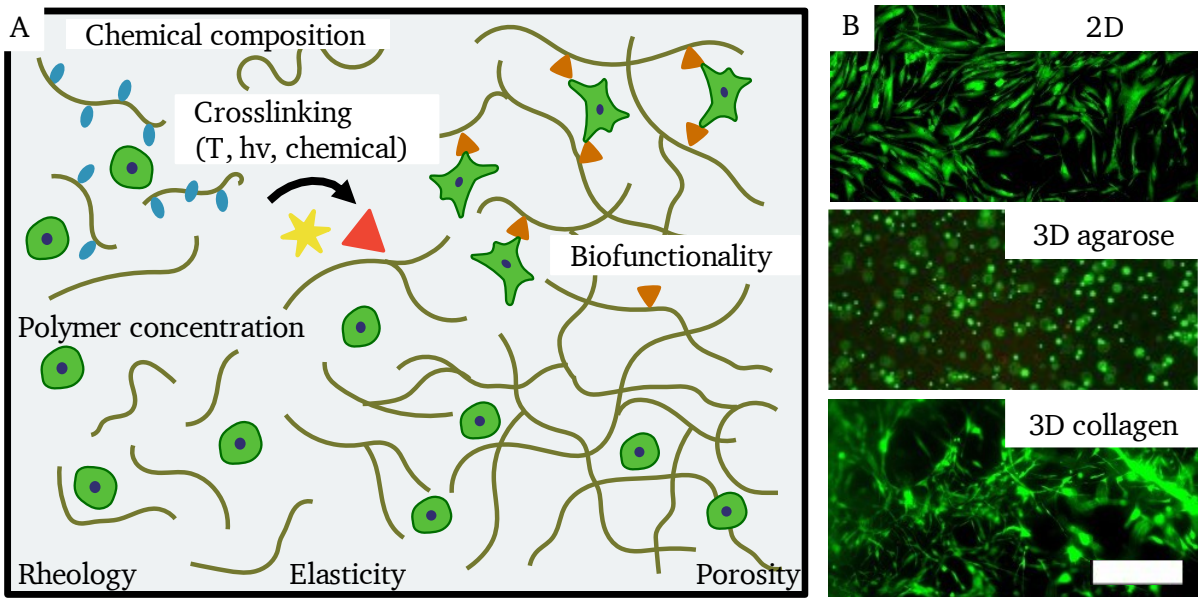

Figure 7: A variety of properties of a biomaterial govern its behavior in handling and cell culture (A). The morphology of cells greatly depends on the biofunctionality of the hydrogel or substrate, as seen for a 2D surface, an agarose hydrogel with no cell adhesion motifs and a collagen gel with cell adhesion motifs (B). Scale bar showing 500 µm and cells are stained green with FDA. Brown lines depict the polymer chains and green shapes depict cells. Chemical functional groups are represented as blue and orange shapes, while initiator and crosslinker systems are marked in yellow and red.

For *in vitro* cell culture, various material classes exist as an alternative to the ECM, but hydrogels are most commonly used as they closely mimic the aqueous ECM. Hydrogels are 3D-polymer networks that contain large amounts of water of up to 99.9 % of their weight, which is advantageous for cell culture and nutrient transport. They can be harvested naturally or be synthesized in the laboratory. Natural hydrogels again vary between animal- and plant-derived materials. The advantage of animal-derived hydrogels over plant-based hydrogels is that they

offer native cell-binding ligands for cells to attach to, making them intrinsically biofunctional and cytocompatible. However, their availability is limited, they are at times complex to handle and have batch-to-batch variations[50]. Synthetic materials offer a very high control over the structure and mechanical properties, are both reproducible and customizable, but are not intrinsically cytocompatible and might need the additional inclusion of cell-adhesion motifs.[50,160–164]

In this work, four natural hydrogels are the matrix for cell experiments. Those are the mammalian-derived fibrin, collagen and its derivative gelatin, and the plant-based agarose.
Collagen is the most abundant protein in the extracellular matrix in animals. There are different types of collagens, of which most are fibrillar, including the bovine collagen I type used in this work. Collagen polymerizes at neutral pH-values and temperatures around 37 °C into a triple-helix by hydrogen bonds and offers multiple cell adhesion sites, making it a popular scaffold material for tissue engineering. In 3D-bioprinting, however, its slow gelation kinetics can limit its application.[165–169]
A thermally and chemically degraded derivative of collagen is gelatin[161,169]. It contains the same chemical and biological active sites as collagen but is not stable under cell culture conditions when no chemical modifications are made. While this hinders its application as a stand-alone matrix material, it can be added to other hydrogels to increase their porosity or to tailor the rheology.[170–172]
Another natural hydrogel, in this case obtained from human blood, is fibrin. Fibrin takes part in human blood clot formation and is formed by crosslinking the fibrous glycoprotein fibrinogen with thrombin. Fibrin naturally contains pro-angiogenic factors, which makes it a popular material for vascularization experiments.[173–175]
Agarose is a plant-based polysaccharide gained from algae and seaweed. It is highly available, easy to handle and can be reversibly crosslinked by cooling it, therefore offering great processability with drop-based bioprinters and high cytocompatibility. However, it is rather inert to cells as it does not offer cell adhesion motifs (**Figure 7** B).[176–179]

3.5. Rheology of Hydrogels

The rheological properties of hydrogels are of great importance for 3D-bioprinted tissue models both in their liquid and gelled state. In the liquid state, the shear or dynamic viscosity η of the hydrogel impacts the printability and the cell viability (→ **Section 3.6**). It describes how a fluid reacts to an external shear force and is defined as the quotient of shear stress τ and shear rate $\dot{\gamma}$ (Equation 1).[180–183]

$$\eta\,(\dot{\gamma}) = \frac{\tau}{\dot{\gamma}} \qquad \text{(Equation 1)}$$

For Newtonian fluids such as water, no dependence of the viscosity on the shear rate is observed. In contrast, the shear viscosity of non-Newtonian fluids is dependent on the shear rate. If the viscosity increases with increasing shear rate, the material is classified as shear thickening, while it is a shear thinning material if the viscosity decreases. This dependence of the flow behavior can be described by the Power-law model or the Ostwald-de Waele relation, which links the shear stress and shear rate via a power law constant n and a consistency factor k (Equation 2).[180–183]

$$\tau = k\,\dot{\gamma}^{n} \qquad \text{(Equation 2)}$$

The dimensionless power law constant n describes the flow behavior, with n = 1 for Newtonian, n > 1 for shear thickening and n < 1 for shear thinning fluids. As water-based polymer solutions, hydrogels often exhibit a shear thinning behavior[184–186]. This behavior is desirable in bioprinting, as this implies low shear stress for cells during the print process (→ **Section 3.6**, Equation 7) and better printability while offering high shape fidelity post-printing[186,187]. Apart from the shear rate, the viscosity also depends on the temperature, which becomes especially predominant for thermally gelling hydrogels.[180,188]

In practice, the viscosity can be measured with a rotational rheometer by shearing the fluid between two plates with increasing shear rates and measuring the effective shear stress. The slope of the viscosity curve over the shear rate directly shows the difference between a Newtonian (material A) and a shear thinning hydrogel (materials B, C) (**Figure 8** A). The power law variables can be obtained by logarithmically plotting the viscosity over the shear rate (**Figure 8** B), which changes Equation 2 to

$$log_{10}(\eta) = (n-1)log_{10}(\dot{\gamma}) + log_{10}(k). \qquad \text{(Equation 3)}$$

The y-intersection of the linear fit can then be used to calculate the consistency factor k, and the slope of the viscosity versus the shear rate is equal to n – 1.

In contrast to pure solids like metals and ceramics, or pure liquids like water, hydrogels always exhibit both an elastic and plastic behavior under deformation, which is called viscoelasticity. This is caused by the breaking of crosslinks within the hydrogel, entanglement release or the unfolding of proteins even in the gelled state[189,190]. The viscoelasticity of hydrogels is described by the complex shear modulus G*, which is dependent on the elastic component G' and the viscous component G" (Equation 4).

$$G^{*} = G' + iG'' \qquad \text{(Equation 4)}$$

Both the elastic and the viscous component are linked by the phase angle δ (Equation 5).

$$\tan(\delta) = \frac{G''}{G'} \qquad \text{(Equation 5)}$$

For phase angles greater than 45°, the viscous component is greater and the material behaves predominantly as a liquid. The gelation of hydrogels can therefore be monitored with a rheometer by measuring the change in the viscous and elastic component of the shear modulus over time after crosslinking for materials such as fibrin and collagen, or over temperature for gelatin and agarose.[180–183]

In the experimental set-up, the hydrogel is between two parallel plates that apply oscillatory shear stress with a certain amplitude as well as frequency over a decreasing temperature (**Figure 8** C). The gelation point is indicated by the crossover point between G' and G", where the phase angle equals 45°. At even lower temperatures, the gelation is completed and the phase angle goes towards 0°, meaning the gel has a dominating elastic component.[184,185,188]

Once the hydrogel is fully crosslinked, the shear modulus becomes important for stability as well as for cellular behavior. The shear modulus for hydrogels is rather low and depends on the gel concentration as well as the type of crosslinking[184]. This ranges between pascal to kilopascal, which is similar to native soft tissue[186,189,191]. Hydrogels exhibit a linear viscoelastic region when

placed under strain up to a critical point (**Figure 8** D). This region also depends on the degree of crosslinking, as a higher crosslinking degree increases the length of the linear region as well as shifting it to higher moduli[184]. At higher strains, the modulus decreases and the materials either break (for highly elastic materials) or become liquid again (for more viscous materials)[184,185].

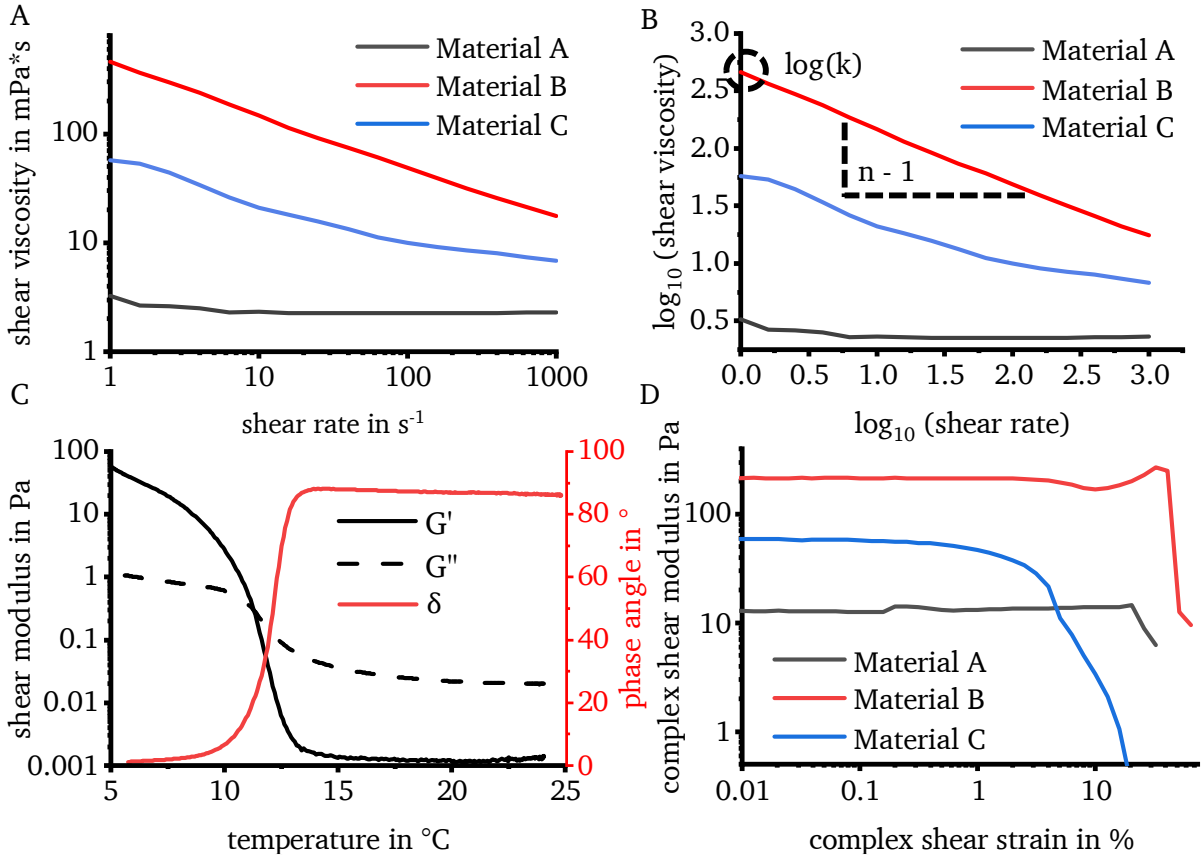

Figure 8: Shear viscosity plotted on a linear scale (A) and as a double-logarithmic plot with y-intersection marked for the calculation of the consistency factor k and the slope of the curve representing n – 1 for the determination of the flow exponent according to the power law (B). The measurement of the gelation of a thermally gelling hydrogel is shown for the measurement of the elastic modulus G', viscous modulus G'' and phase angle δ over a decreasing temperature (C). Different concentrations, but also types of polymers have different shear moduli and different maximum strains (D).

3.6. Drop-on-Demand Bioprinting

3D-bioprinting is defined as the additive manufacturing of living structures containing layers of living materials to generate functional tissues or organs[163,176]. Modern bioprinters can be categorized into extrusion-based, light-based, and drop-based technologies, which deposit material layer-wise, line-wise or point-wise[92,176,192]. While many bioprinters have the same working principle as conventional 3D-printers, they differ from conventional bioprinters because of the so-called bioink that is printed. A bioink is "a formulation of cells that is suitable to be processed by an automated biofabrication technology"[193]. It can therefore contain either only loose cells in suspension[194–196], cell agglomerates[197,198] or cells encapsulated in a matrix material[161,199]. To obtain more complex and structurally stable materials and to mimic the extracellular matrix of the human body, many users use a matrix material, which is usually a hydrogel (→ **Section 3.4**)[200,201]. Bioprinting makes high demands on the bioink properties: the

ink has to be adapted in rheology and crosslinking characteristics to the print system and be mechanically stable post-printing, while at the same time offering good cytocompatibility and biological properties for cells to grow in. This also implies that they can be handled at physiological temperatures and pH values with no cytotoxic solvents or components. The print process should also not harm the cells by high shear stress, UV light exposure or prolonged air exposure. These biological and technical aspects contradict each other at times.[161,171,192]

The most popular bioprinting technology is extrusion-based bioprinting, where the bioink is extruded in a continuous line through a dispensing head similar to conventional Fused Filament Fabrication. To enable extrusion and to prevent material from flowing out of the nozzle, rather viscous bioinks in the range of 20 – 9,000 mPas are required[92,202]. This viscosity results in a high shape fidelity post-printing and good resolution of $100 - 500\,\mu$m, but can also impact cell viability due to the high stress that cells experience during extrusion and the low porosity of the resulting matrix[91,96,203]. Light-based stereolithography printing is also available for bioprinting, with the same working principle as described in section 3.1. The advantages of light-based bioprinters are the large volumes that are structured in a short time as well as their high resolution of 25 - 50 μm in xy-direction, which can be reduced to the single micrometer range for Two-Photon-Polymerization[91,204,205]. However, material classes are limited to bioinks that can be crosslinked via light, which requires the addition of a photoinitiator, chemical modifications to natural hydrogels or synthesis of synthetic materials. Furthermore, the exposure of a focused laser light can impact the viability of cells[206–208]. The newly developed method of volumetric bioprinting reduces the exposure time to light in the near-UV spectrum and dramatically increases print times, though at the cost of resolution[209–211]. A rather diverse class of bioprinters are drop-based approaches, which can be based on inkjet technology, laser-induced forward transfer, acoustic bioprinting or microvalve-based bioprinting[212,213]. All of these methods require low viscous bioinks in the range of $1 - 300$ mPas[92,202], have high cell viabilities and a print resolution around $100 - 500\,\mu$m depending on the method and material[87,202,214].

All of the presented bioprinters have advantages and disadvantages and are not always suitable for a planned tissue model. On chip, laser-based bioprinting is not feasible, while Two-Photon-Polymerization would require too long to completely fill a tissue chamber[206]. Extrusion-based bioprinters are less suited for printing on microfluidic chips. As they deposit material in a continuous line, very small and discontinuous structures are hard to obtain. Furthermore, a very precise height control is required, as the tip of the extrusion system is very close to the substrate.

Drop-based approaches are however suitable, as they are contactless methods that move with a certain distance of various millimeters over the substrate. Of this class of printers, microvalve-based systems offer a good print resolution, a broader material variety than inkjet and a more stable process compared to acoustic-based bioprinting. For these reasons, the printer used in this work is a microvalve-based Drop-on-Demand (DoD) bioprinter. This printer dispenses single drops of a bioink via the opening of an electromagnetically controlled valve. The bioink is stored within a reservoir that can be heated and cooled. To dispense the drops, the reservoir is under pressurized air (**Figure 9** A)[95,212,215].

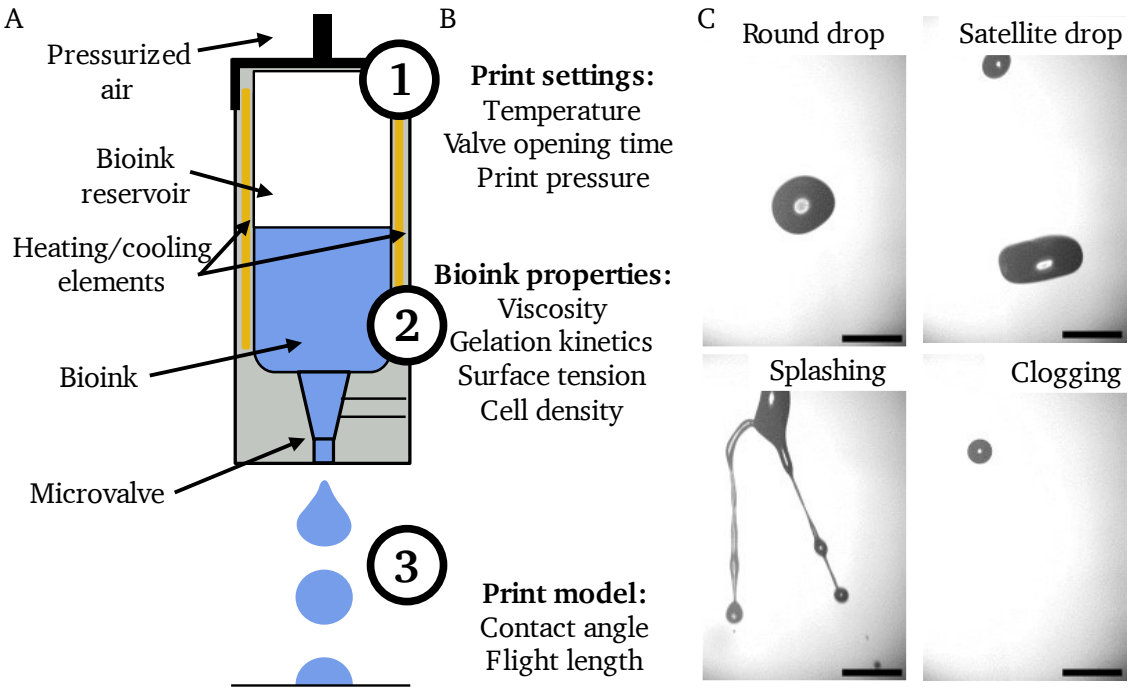

Figure 9: Sketch of the print head of a microvalve-based Drop-on-Demand bioprinter with critical components labeled (A). Parameters that affect the print resolution and performance include printer settings such as temperature, valve opening time and print pressure, the bioink properties such as rheology and surface tension, and the print model such as contact angle and flight length (B). The ideal drop shape in flight is round, though print mistakes like satellite drops, splashing or nozzle clogging can occur (C). Scale bar showing 500 µm.

Three classes of factors influence the printability and print resolution of this bioprinter: The print settings, the properties of the bioink and the print model (**Figure 9** B). By adjusting the opening time t_{valve} of the microvalve and the print pressure on the reservoir, the amount of bioink ejected can be directly controlled. With an increasing print pressure and valve opening time t_{valve}, more material is deposited, while a larger nozzle radius r also results in larger drops[215,216]. The set temperature impacts the result indirectly via the bioink, as the ink's shear viscosity η is affected by temperature (→ **Section 3.5**). The viscosity of the ink decides if the material is even printable, as a wrong viscosity can lead to nozzle clogging, satellite formation or splashing of the bioink (**Figure 9** C) and directly impacts the drop volume[217,218]. Together with the density ρ and the surface tension γ of the ink, which impacts drop formation and drop shape[219], the dimensionless number of printability Z can be defined as[218,220–222]

$$Z = \frac{(r\rho\gamma)^{1/2}}{\eta}. \qquad \text{(Equation 6)}$$

The higher limit of Z is given by the formation of satellite drops and is estimated to be around $14^{217} - 20^{218,223}$, while the lower limit of around $1^{224} - 4^{217}$ is governed by the maximum printable viscosity of the bioink. Apart from the hydrogel's properties, the printability is also impacted by the cell density inside the bioink[219]. With increasing print resolution, the average shear stress $\bar{\tau}$ that cells experience during the print increases as well. This shear stress depends on the biomaterial's rheology defined by the consistency factor k and the power law constant n (→ **Section 3.5**) and the print parameters that result in the drop volume V_{drop}[95,96,225] and can be approximated as

$$\bar{\tau} = \frac{1}{2} k \cdot \left[\frac{V_{drop}\left(\frac{1}{n}+3\right)}{r_{valve}^{3} \cdot \pi \cdot t_{valve}} \right]^{n}. \qquad \text{(Equation 7)}$$

As higher shear stresses of over a few kilopascals directly negatively affect cell viability and function[95,203,225], a balance between print accuracy and cell-friendly shear conditions has to be found.

In the last step, the print model settings have to be configured correctly. The slicing of the digital model has to correspond to the effective drop height and drop area. This drop volume and shape is dependent on both the bioink's viscosity and on the contact angle of the gel on the surface for the first layer, as well as on the wetting properties of the bioink on the already gelled layer below from the second layer onwards. A high contact angle leads to rounder drops and therefore higher lateral resolution, but can also promote drop rebound and drop fusion. During the slicing process, this drop behavior has to be taken into account. Finally, the distance between the nozzle and the substrate has to be set correctly as well. If the distance is too large, the drops accelerate too much and bouncing as well as splashing can occur during the impact on the surface, while a too small distance can lead to drop bridging.[218,226]

4. Results

4.1. Vascularization in Organs-on-a-Chip

Organs-on-a-Chip (OOCs) have gained significant popularity in biomedical research in recent years. As a further development, the inclusion of vasculature into these models has become a particular area of investigation. Such models would not only enable the study of organ-specific responses to drugs or impulses, but also offer insights into biomimetic drug pharmacokinetics, toxicology assessments, and disease mechanisms. Consequently, numerous researchers have dedicated substantial efforts to develop innovative approaches for the inclusion of functional vasculature within microfluidic chip-based organ models. To benefit from the existing knowledge about vascularized OOCs for this doctoral thesis, the first step was a comprehensive literature review of existing publications in this area to discern strategies, materials and methodologies explored in this context[1]. This entailed a thorough examination spanning fabrication approaches, biomaterial selection, and cell culture methods. From this overview, a targeted choice of approach for the planned 3D-bioprinted and vascularized OOC model should become possible.

In the first step of this review, three distinct types of approaches to vascularization could be identified and defined: Biosynthetic, biomimetic, and self-assembled vascular networks.
The developed definition of biosynthetic OOCs includes devices that employ synthetic materials in the form of membranes, layers or channels to spatially organize and separate distinct cell types. These synthetic materials remain in the tissue model throughout the entire culture time. They compartmentalize cell types, but at the same time allow for cell-cell contact via pores or gaps (**Figure 10** A). A major drawback of biosynthetic OOCs is the limited cell contact as well as the inclusion of synthetic materials, which strongly differ from the physiology of the human body. The restricted cell contact area might also result in undesired side effects as well as mechanical cues by the stiff synthetic material. In addition, cell type specific medium is often supplied directly onto each cell type in these models and not through the vasculature. While this approach carries practical advantages, especially when dealing with sensitive primary cell types, it fails to mimic the physiological nutrient and drug uptake through a tight endothelium[20,227,228].

Despite the mentioned drawbacks, biosynthetic OOCs have been used extensively and with wide success after their first presentation in 2010 by the group of Donald Ingber[229]. They presented a 2D-based approach, where a certain number of channels is separated by a porous membrane. A major advantage here is the possibility of mechanical stimulations e.g. for lung[229–231], intestine[232,233] or glomerulus[234] models, or the integration of sensors for on-chip readouts[235]. These OOCs were already successful at the correct prediction of the metabolic conversion of certain drugs[21,236] as well as in the identification of possible antivirals against SARS-CoV-2[237], highlighting the potential of OOCs for pharmaceutical studies.
The remaining limit of this approach is its confinement to a 2D environment as opposed to a 3D, extracellular matrix (ECM) mimicking environment. This is overcome by microfluidic systems which have an arrangement of parallel channels with gaps in the channel walls for an interface between these channels. These devices have various endothelialized channels under perfusion that mimic the blood flow, while other channels are filled with a hydrogel containing cells that resemble the tissue model. They have already been employed for studies on cancer cell invasion and endothelial barrier function[238–240] or in a complex blood-brain-barrier model[241].

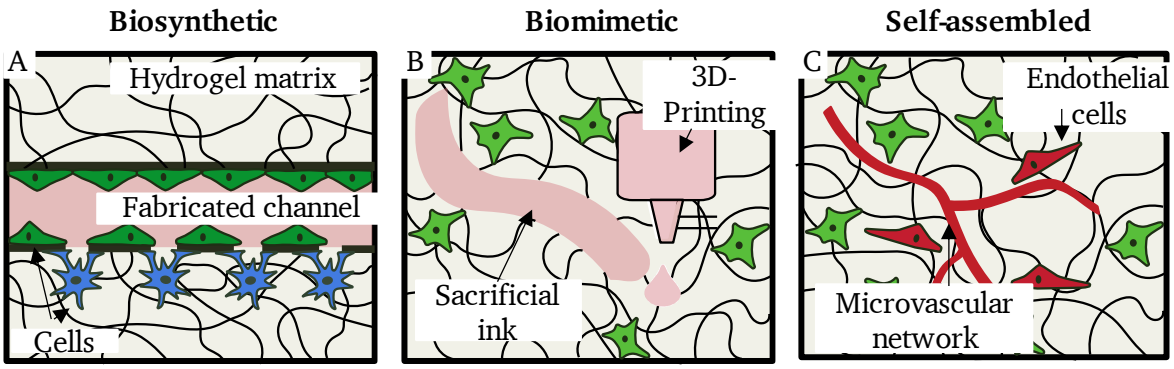

Figure 10: Classification of vascularized OOCs into biosynthetic (A), biomimetic (B) and self-assembled microvascular networks (C).

The second defined type of vasculature inclusion are biomimetic OOCs, which try to free themselves from synthetic elements and manufacture the open lumen of vasculature in a hydrogel matrix by different means of casting or printing (**Figure 10** B). These approaches are highly creative and include copying the tree leaf venation[242–244], casting of a hydrogel around melt-spun sugar fibers[245] or exploiting a typical print error (viscous fingering) in conventional printing[246]. Because of the variety of approaches, the shape of the resulting vasculature varies from round to rectangular and they range in size from a few micrometers up to millimeters.

The first attempts at biomimetic vascularized OOCs drew inspiration from established microfabrication techniques. These approaches involve the creation of master molds, which serve as templates for the casting of hydrogels[242,247–249]. While offering a superior resolution down to a few micrometers as well as high control over the resulting shape, this method is limited in speed and complexity, as manual stacking of the individually casted layers is required. An uncomplicated and fast method consists of simply casting the hydrogels around rods[250,251], wires[252] or even fishing lines[253]. By use of concentric needles, this extends to multilayered vessels that include the native tri-layer composition of larger vessels with fibroblasts, smooth muscle cells and endothelial cells[254]. However, the complexity of the vascular network is strongly limited by the subsequent removal of the rods. In more intricate configurations, networks can also be produced by 3D-printing of agarose, but the need for subsequent removal remains[255,256]. When sacrificial materials are however used for 3D-bioprinting, the printer can unfold its full potential and produce highly branched, complex designs, combine multiple materials and even achieve multi-cellular layered networks. Possible materials here are gelatin[33,56,257–260], Pluronic F-127[98–100,261] or carbohydrate glass[262]. Multi-layered vessels with distinct cellular distribution have been printed with coaxial nozzle extrusion printing[263,264] or by printing multiple layers in a drop-based approach[56,265]. In bioprinting of sacrificial materials, the resolution is a drawback, as the minimum vessel diameter starts at around 100 μm.
The appeal of these biomimetic approaches lies in the absence of any synthetic materials or limited cell-cell contacts. However, it's important to note that they often entail labor-intensive processes and fall short of achieving the fine resolution required for replicating capillaries.

In addition to the previously described engineering-based techniques, an alternative approach is to harness biological processes to create vascularized structures. This method leverages the self-organizing capabilities of cells and their natural behaviors to self-assemble into microvascular networks (μVN), mirroring the processes that occur *in vivo* (**Figure 10** C). By providing the right conditions and cues, such as appropriate culture media, co-culture cell types and extracellular matrix components, endothelial cells (ECs) can spontaneously organize into

capillary-like structures[53,266,267]. While this approach may not provide the same level of engineering control as some of the other methods, it excels in replicating the intricacies of natural vasculature with *in vivo*-like barrier function without manual work.

Translating this into OOCs, vascular networks can form when ECs are seeded in a suitable hydrogel lined by microfluidic channels on both sides. The hydrogel can have either a natural[66,67,75,268–274] or synthetic[275–277] origin. Similar to the previously presented approaches, different technologies and materials are employed for the fabrication of the channels. For example, parallel channels microfabricated in PDMS or other polymers[269,270,274,278–280] as well as 3D-printing of sacrificial materials has been presented[271–273,281]. These pre-fabricated channels can additionally be seeded by endothelial cells to connect to the μVN by anastomosis for their targeted perfusion. This process requires time though, as fully perfusable networks develop within 4 – 10 days depending on the size of the tissue model. In addition, a size limitation to several millimeters exists as necrosis would occur otherwise, with no control over the pathway of the vasculature.

These systems have been especially used to mimic the physiological function of the blood-brain-barrier[67,274,278] or tumor behavior[268–270,282]. Furthermore, the method of self-assembled μVN can also serve as a vascular platform for the combination with other cell types. In this case, microfluidic chips that have an open-top setup or that can be opened after the development of a robust vascular network are employed. Once this vascular network has matured, epithelial cells can for example be seeded either directly on top[280] or placed in a transwell configuration[75] to facilitate the fabrication of ocular retina or lung tissue, respectively. This method generally allows contacting of vascular beds with tissue-specific cell types for studies of barriers and interfaces of the stroma with parenchymal cells.

Interim conclusion and application of findings to this work:

Upon these findings of the literature review, the identified approaches were evaluated for their suitability considering the capabilities of the institute's existing printers and fabrication technology. In the first step, biosynthetic OOCs were discarded because of the unphysiological cell separation as well as the potential impact of the synthetic material. Biomimetic approaches are compatible with the existing printers, enable direct cell-cell contact in an ECM-like 3D-matrix and offer a high freedom of design. Nevertheless, a notable constraint emerges from the limited resolution of the available printers, which would result in relatively large vessels of several hundred micrometers. Considering the typical dimensions of microfluidic chambers, which typically range from 1 to 2 mm^1, the intention to print vascular networks would end in a single, considerably large channel with limited available space for the precise positioning of tissue-specific cells. Such an outcome would be neither practically advantageous nor scientifically compelling. Self-assembled μVN stand out as a more biologically authentic alternative, as they lead to fine and branched networks, which would provide a more realistic representation of physiological conditions. Furthermore, these networks can readily develop around printed structures comprised of tissue-specific cells and bioinks. Consequently, they emerged as the preferred choice of vascular network fabrication for this work.

With the design of the vasculature for a tissue model selected, the selection of cell types, especially of ECs as the basic cell type in vasculature, became a key question. Independently on

the chosen architecture for vascularized OOCs, a significant majority of studies (> 70 %) have chosen human umbilical vein endothelial cells (HUVEC) due to their availability. However, there are instances where researchers have opted for tissue-specific endothelial cells capable of mimicking the distinct morphological characteristics integral to the functionality of a specific organ[21,106,249,280]. Furthermore, the configuration of co-culture systems has demonstrated the great influence of additional cells on the formation and functionality of vascular networks. This influence stems from the secretion of bioactive factors by various cell types within the co-culture, which play a pivotal role in network formation[283–285]. As a result, a substantial portion of the analyzed studies, approximately half, have relied on co-culture methodologies to achieve their desired outcomes in the context of vascular network development.

Interim conclusion and application of findings to this work:

Considering these findings, HUVEC were chosen as endothelial cells for this project based on their availability as well as promising results regarding self-assembled μVN in literature. Human dermal fibroblasts (HDF) were selected as stabilizing co-culture cells.

In terms of material selection for the fabrication of microfluidic chips, the majority of approaches have traditionally utilized polydimethylsiloxane (PDMS) as the primary chip material. PDMS, however, has a high absorbance of small molecules, which could potentially affect the accuracy of metabolic assessments[286,287]. Only a small portion of the monitored studies has explored alternative materials such as polystyrene (PS)[66,67,268,282], which exhibits a reduced small molecule absorption. However, it's important to note that PS also has limitations, including lower gas diffusivity and challenges associated with manual processing in a laboratory setting[288–290]. A single study stands out for 3D-printing of the microfluidic chip in polycaprolactone, which has a significantly reduced protein absorption compared to PDMS[33].

Interim conclusion and application of findings to this work:

These observations underline the significance of both microfluidic chip fabrication and material selection, which have to be adapted to the specific requirements of the tissue model design. Given the cost-intensive nature of PDMS and soft-lithography, along with the need to design a microfluidic chip with a tissue chamber accessible to 3D-bioprinting that is sealable post-printing, an alternative approach had to be developed.

4.2. Prototyping of Microfluidic Chips via DLP-Printing

Designs of microfluidic chips for Organs-on-a-Chip are always tailored to the specific requirements of the tissue model. For the tissue model planned in this project, the chip design was a key aspect that would require many iterations to reach a final and suitable design for the envisioned process. To facilitate prototyping and not to rely on the costly and time-consuming process of soft-lithography, a 3D-DLP-print process of microfluidic chips had to be developed. This entailed the selection of a suitable printer, adaptations to the process as well as a selection of suitable materials[2].

The first step regarded the transparency of prints. To achieve transparency, diffuse light scattering from surface roughness or on bulk defects has to be reduced. This can be realized by

ensuring a very smooth build plate and a smooth surface of the resin vat, which makes changes to the hardware of a commercial DLP printer necessary. The printer's build plate was exchanged for a highly polished and hardened steel plate to ensure a nanometer-smooth surface on the bottom, and a coated glass plate replaced the resin vat. These two changes removed scattering defects in prints and led to fully transparent parts as seen in photographs of printed petri dishes and surface topography scans (**Figure 11**).

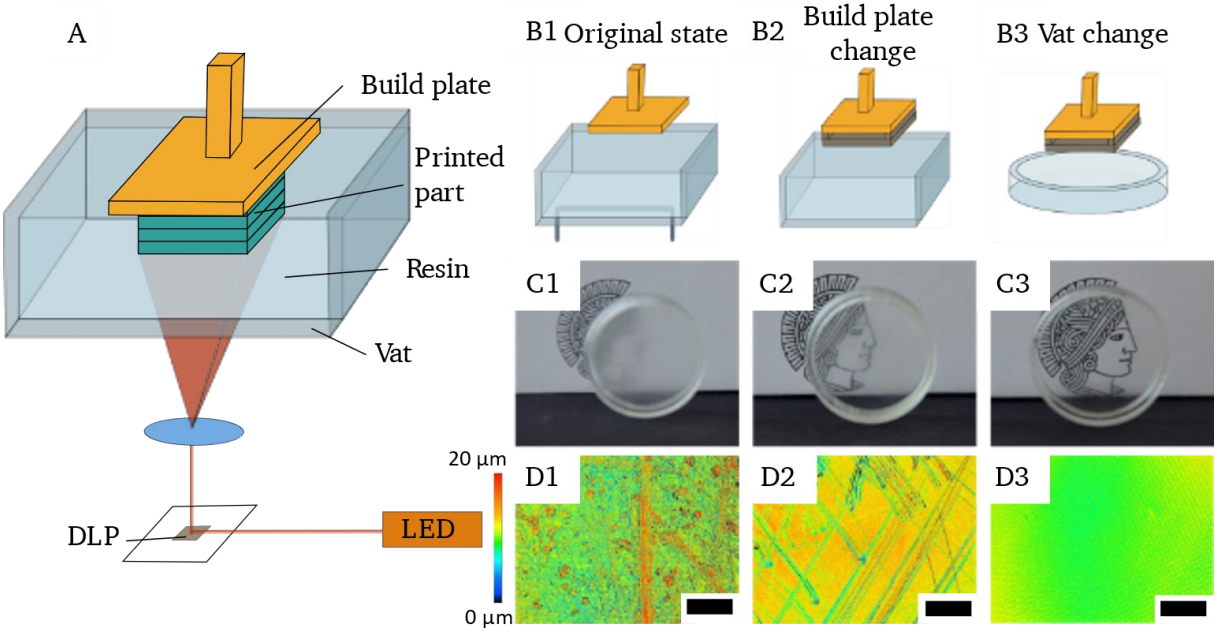

Figure 11: Hardware changes to the commercial DLP printer (A) reduce the present rough surfaces by replacing the build plate and resin vat with very smooth surfaces (B), which lead to transparency in prints (C). Confocal laser scanning images of the topography of the prints show a reduced number of scratches, defects and a generally lower height variation (D). Scale bar showing 500 µm. Figure adapted from Fritschen et al.[2].

The other main factor influencing both transparency and cytocompatibility is the choice of resin material. For this work, three materials were tested regarding their suitability for printing and cell culture applications. The first selection was a commercial material offered by the printer's manufacturer (PlasCLEAR), the second one a polyethylene glycol diacrylate mixed with a photoinitiator (PEG-1), and the third had an additional photosensitizer mixed in (PEG-2) for potentially better print resolution. The selection was based on previous studies that describe the general cytocompatibility and/or printability of the materials[76,84,291–294].

All three resins used in this work contain a photoinitiator that starts a radical polymerization process. As remaining free radicals, initiator residues or uncured monomer components impact both transparency and cytocompatibility, a post-printing treatment procedure had to be developed. To remove these residues, different solvents for an overnight solvent extraction (air, water, isopropanol) and different UV exposure times (0, 4 and 8 hours) after extraction were tested. The success of these steps regarding cellular response and transparency was monitored via a resazurin assay (**Figure 12** A), UV/VIS photospectroscopy (**Figure 12** B), morphology as well as fluorescence imaging of cells cultivated on prints (**Figure 12** C).

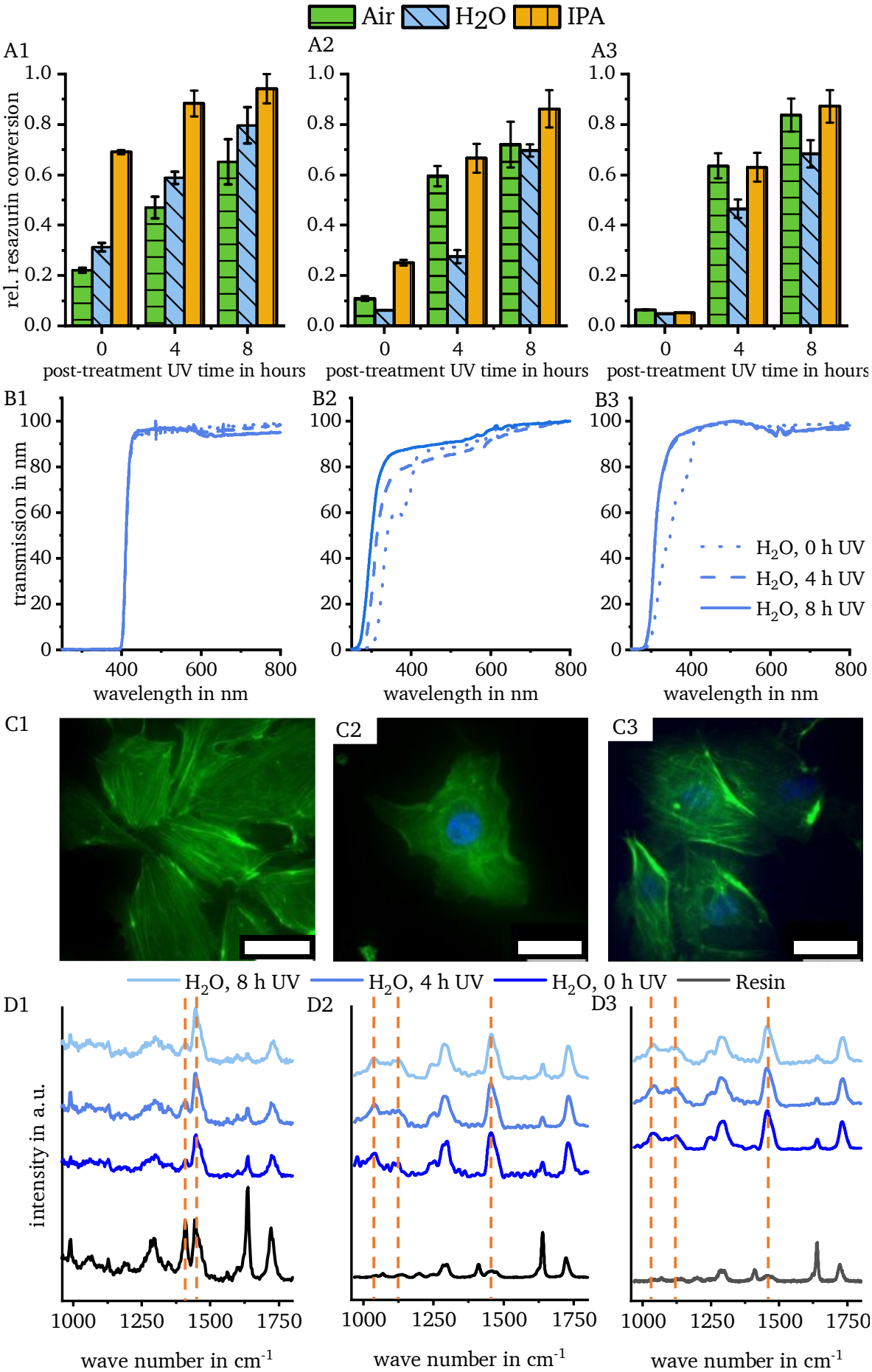
Air
H2O
IPA
A1
A2
A3
rel. resazurin conversion
post-treatment UV time in hours
B1
B2
B3
transmission in nm
wavelength in nm
H2O, 0 h UV
H2O, 4 h UV
H2O, 8 h UV
C1
C2
C3
H2O, 8 h UV
H2O, 4 h UV
H2O, 0 h UV
Resin
D1
D2
D3
intensity in a.u.
wave number in cm-1

Figure 12: Influence of post-treatment procedure on cytocompatibility as tested by resazurin conversion of L929 cells cultivated with prints (A). Transparency was measured by UV/VIS photospectroscopy of prints (B) and both cell morphology and imaging quality were determined by immunofluorescence microscopy of HUVEC cells cultured on prints, with nuclei stained in blue and actin filaments in green (C). Scale bar showing 50 µm. Raman spectroscopy on resins as well as prints with different post-treatment procedures with key peaks marked with orange lines (D). The peak at 1470 cm^{-1} corresponds to the -CH_2 deformation mode. The peak at 1410 cm^{-1} corresponds to the aliphatic C=C stretch, while the peaks at 1040 and 1140 cm^{-1} are the C-C stretching and various C-O-C modes. Graph data was determined for n = 3 showing the mean with error bars as the standard error of mean. For UV/VIS spectroscopy, 100 measurements per line and for Raman spectroscopy 3 measurements per sample were conducted for a total of 9 measurements per line. Figure adapted from Fritschen et al.[2].

For the commercial resin PlasCLEAR, the solvent was decisive for cytocompatibility, with isopropanol extraction leading to the highest cell metabolic activity. In addition, a prolonged UV exposure time of 8 hours further increased cell activity (**Figure 12** A1). The PEG-DA-based resins showed improved cytocompatibility as well as transparency for longer UV exposure times, too, but this was independent of the solvent type (**Figure 12** A2, A3). While PlasCLEAR parts do become cytocompatible through post-treatment and both cellular attachment as well as spreading can be observed, certain resin components remain that fully absorb light at wavelengths below 400 nm (**Figure 12** B1, C1). This is a disadvantage as blue fluorescence dyes with excitation wavelengths below 400 nm, such as DAPI, are no longer available for imaging. PEG-DA-based resins are an alternative here, as they become fully transparent after post-treatment with high cytocompatibility and good cell attachment (**Figure 12** B2, B3, C2, C3). But in the end, all three materials enable the highly resolved fluorescence microscopy that is required for the analysis of tissue models. For PlasCLEAR, the effect of the post-treatments can be correlated to a reduction of reactive C=C bonds at 1410 cm^{-1} compared to the predominantly constant signal of -CH_2 bonds of the cured acrylate backbone chain[295] (**Figure 12** D1). In the case of PEG-based polymers, an increase in C-C stretching vibrations as well as various C-O-C bond modes of the polymer chain at 1040 and 1140 cm^{-1} are taken as measures for an increasing degree of crosslinking compared to the constant -CH_2 signal[296,297] (**Figure 12** D2, D3).

With the suitability of DLP printing for cell applications proven, the next step was the fabrication of microfluidic chips. Since highly resolved features are required, a screening of print parameters was conducted to find correlations between printer settings and resolution as well as to identify significant parameters. As expected for photopolymerization, light intensity and exposure time at a certain slice thickness, and therefore the total energy input per volume, are decisive parameters. With appropriate parameters selected, all three resins performed well for positive features, and freestanding pillars with a high aspect ratio and only 50 μm in diameter were achieved (**Figure 13** A). However, overcuring occurs for negative features with PEG-1, which limits the resolution to only 370 μm. For the other materials, holes with a width of around 100 μm remain open (**Figure 13** B). All the same, there is always a trade-off in quality if both positive and negative features such as pillars and holes or channels are required in the same part. Positive features need a larger energy input to ensure their stability, while negative features need lower energy inputs to prevent overcuring. This has to be considered for chip printing and the settings optimized accordingly. With both PlasCLEAR and PEG-2, it was possible to print microfluidic chips with distinct pillars of round shape with a diameter of 250 μm within channels of 500 μm width and 300 μm height (**Figure 13** C – E). However, it was not possible to fabricate microfluidic chips with PEG-1 due to the lower printability, especially with regards to negative features.

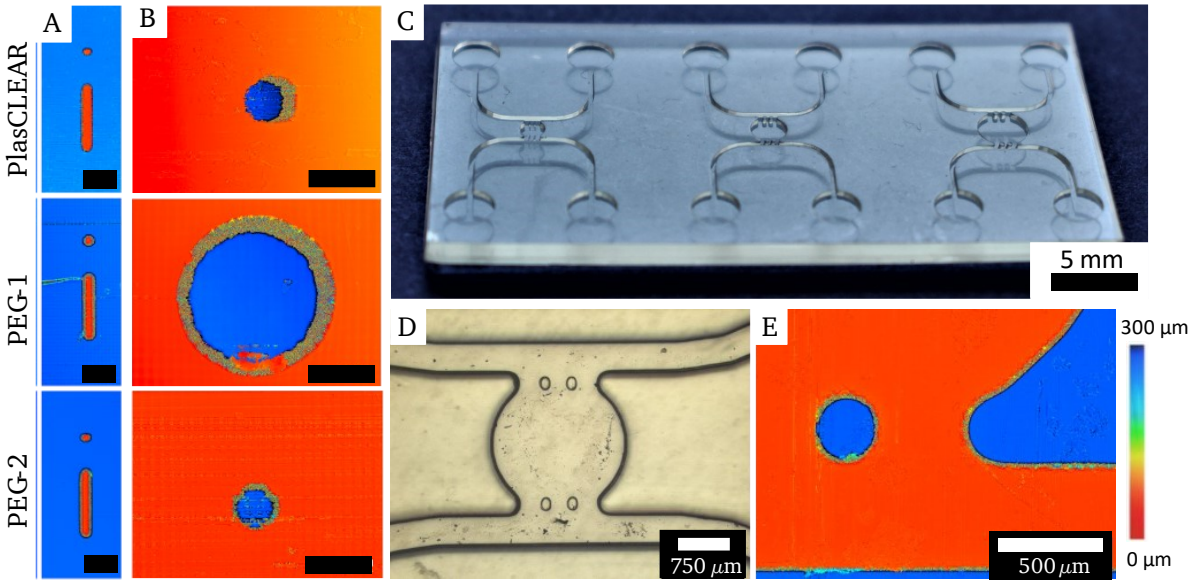

Figure 13: Height maps of freestanding positive (A) and negative (B) features show print resolution for all three resins. Scale bar showing 100 µm (A) and 200 µm (B). With PlasCLEAR, the print process is suitable for the fabrication of microfluidic chips containing microfluidic channels of 500 µm diameter, a tissue chamber as well as 250 µm wide pillars separating the tissue chamber from the channels (C, D). The edges are clearly visible and the height with 300 µm as designed (E). Height scale bar ranging from 0 µm (red) to 300 µm (blue) for all height maps. Figure adapted from Fritschen et al.[2].

Interim conclusion and application of findings to this work:

The printed microfluidic chips in both PlasCLEAR and PEG-2 demonstrate the feasibility of DLP-printing of transparent and cytocompatible microfluidic chip prototypes for the envisioned 3D-bioprinted OOC. Regarding the material selection, PlasCLEAR offers the advantage that it is easy to print, as its print characteristics are tailored to the printer. However, it lacks transparency in the lower wavelength regime and limits fluorescence microscopy colors. PEG-2 on the other hand is fully transparent at all wavelengths of interest but is more challenging in printing. For prototyping in this work, PlasCLEAR was therefore favored due to its ease of handling.

4.3. Bioink Selection for 3D-Bioprinted HepG2 Islands

With a working process for the microfluidic chip and a concept of the tissue model design, the next important step was the selection of the matrix material for the HepG2 cells. For the liver carcinoma model, HepG2 cells were selected because of their availability[136,298–300] and as they are the most commonly used hepatoblastoma cell line for printed tissue and cancer drug models[132,134,135,301–303]. For these cells to achieve their full proliferation and functional potential, a suitable bioink had to be found that could both fulfil the requirements of good printability as well as cellular behavior[3] (**Figure 14**).

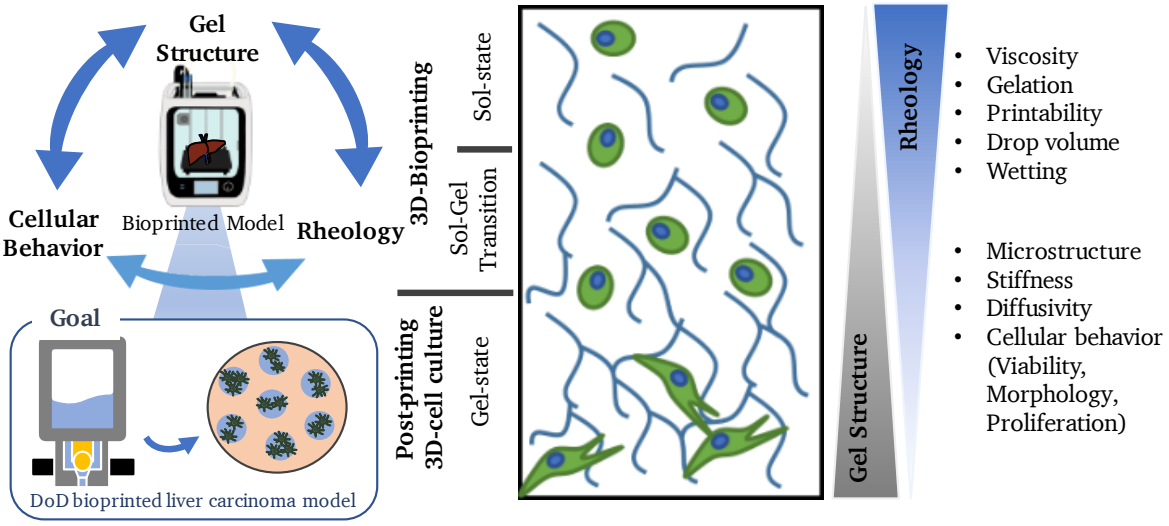

Figure 14: Relevant properties of possible bioinks for a DoD bioprinted liver carcinoma model for both the 3D-bioprint process as well as the post-printing 3D cell culture. Figure adapted from Fritschen et al.[3].

General physical, as well as chemical bioink properties such as microstructure, stiffness, diffusivity, and cell-matrix interaction sites impact the morphology, viability and functionality of cells. For a high-resolution Drop-on-Demand (DoD) bioprinting process, the rheology becomes important. These requirements are at times contradictory and limit the choice of materials. This choice was further limited to only thermally gelling bioinks, as crosslinking mechanisms that require the addition of a certain chemical are difficult to realize on chip. In addition, photocuring materials were excluded as both the exposure to near UV light and the photoinitiators themselves can impact cell viability[187]. In the end, three base materials – agarose, collagen and gelatin – as well as blends thereof were selected based on their proven processability by DoD bioprinters and suitability for cancer models[33,259,304–306].

Agarose (Ag) was selected as a simple, low-cost and very well-printable material even though it lacks cell adhesion motifs[163,171,176,304]. Collagen I (Col) has the advantage that it is the most abundant component in our extracellular matrix and highly cell compatible, but its slow gelation kinetics are a drawback in bioprinting[169,264,307–309]. While unstable under cell culture conditions, native gelatin (Gel) was chosen as an additive to improve both gelation kinetics and drop formation as well as to adjust the rheology[310,311]. The impact of different concentrations and blends of these hydrogels was studied for 7 variations that were selected after a pre-screening of 15 variations.

Shear viscosity measurements show that all selected hydrogels are generally suitable for DoD bioprinting[202,215] as they either have a low viscosity (1 – 5 mPa*s for agarose) or are shear thinning (**Figure 15** A). The shear-thinning behavior is caused by collagen[186,312], which has a

dynamic viscosity ranging from 10 to below 100 mPa*s at 2.5 mg/ml concentration. This effect is enhanced in combination with agarose. This is probably also due to the onset of collagen fibrillogenesis during printing caused by the neutralized pH and elevated temperature of 25 °C[186], which is visible in the increasing complex shear modulus for all blends (**Figure 15** B). As agarose and collagen have no temperature window in which they both remain liquid (**Figure 15** C), this effect cannot be prevented in blends. However, they remain processable if print times are kept short.

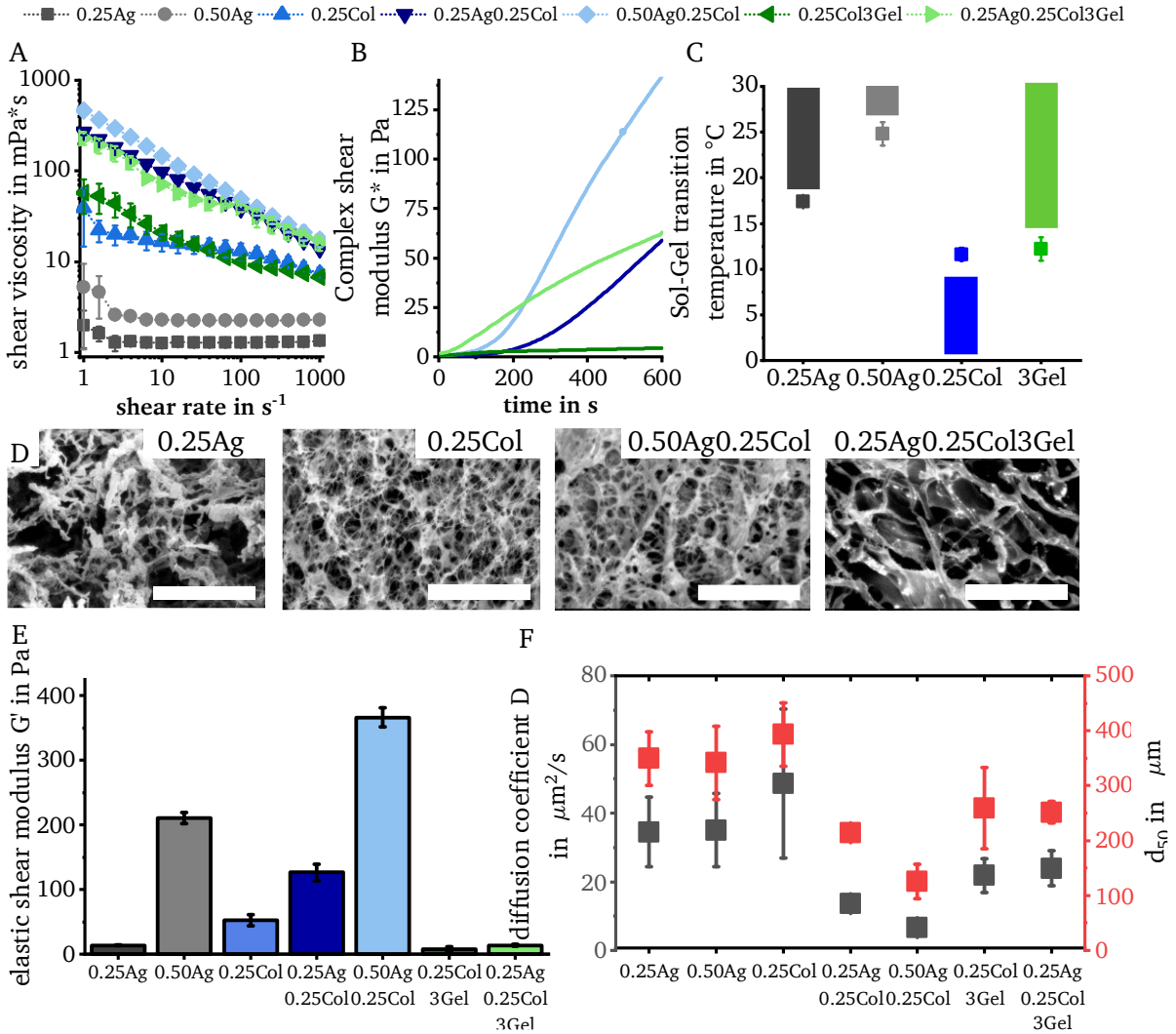

Figure 15: Shear-viscosity measurements of seven bioinks show a Newtonian character for agarose gels, while other hydrogels are shear-thinning (A). In blends, the complex shear modulus increases over time (B), as no common fabrication windows is visible in the sol-gel transition temperature measurements (C). Further analysis includes SEM images of the microstructure of four hydrogels (D), the elastic shear modulus (E) and the diffusion of FITC-labeled BSA (F). Scale bar showing 20 µm. The diffusion coefficient D was calculated using Fick's second law of diffusion and the distance of 50 % signal intensity d_{50} was obtained from microscopy images. Graph data was determined for n = 3 showing the mean with error bars as the standard error of the mean. Figure adapted from Fritschen et al.[3].

After printing and gelation, not all tested hydrogels remained stable for 14 days under culture conditions. For example, 0.25Ag and 0.25Ag0.25Col3Gel did not withstand in culture, probably due to their low elastic shear modulus of only around 13 Pa, which corresponds to the very porous microstructure (**Figure 15** D, E). While 0.25Col3Gel also exhibits a low shear modulus of 8 Pa, its stability increased over the course of days and it supported 14 days of culture. The blend of 0.50Ag0.25Col was discarded for further studies due to its low diffusion coefficient of FITC-BSA of only 6 $\mu m^2/s$, which is limited by the dense polymer network (**Figure 15** D, F).

Bovine serum albumin (BSA) is the most abundant component of cell culture media and relevant in nutrient transport[313] and therefore a good model protein for the general nutrient transport through the material. If its transport is hindered by the gel, the nutrient supply to cells is not secured, making such hydrogels unsuitable for on-chip tissue models. For the other blends, the diffusion coefficient is lower than for the individual components, which can most likely be attributed to the higher total polymer content and therefore denser network. This also corresponds to the higher shear modulus.

Next, cell experiments were conducted with the four promising candidates 0.50Ag, 0.25Col, 0.25Ag0.25Col and 0.25Col3Gel. In all hydrogels, HepG2 cells exhibit round shapes and tend to agglomerate, with little amounts of cytosol and actin filaments visible around the nucleus (**Figure 16** A). Cells embedded in agarose show a very round morphology due to a lack of cell adhesion motifs[176,177], which could not be compensated by the addition of collagen as seen for 0.25Ag0.25Col. For cells inside 0.25Col and 0.25Col3Gel, small protrusions and actin filaments become visible after three days of culture time, which increase to small networks and cell-cell contacts on day 14 as seen for cells with cytosol stained by CellTracker or fluorescein diacetate (FDA) (**Figure 16** B, C). While the collagen fibers are well distributed inside their respective matrix material as seen for the collagen-reflectance images, HepG2 cells seem to be only embedded in the fibers and do not interact strongly. From the cellular perspective, pure collagen is therefore the most promising material. However, its printability and general handling during the bioprint process is a key aspect of the final material choice.

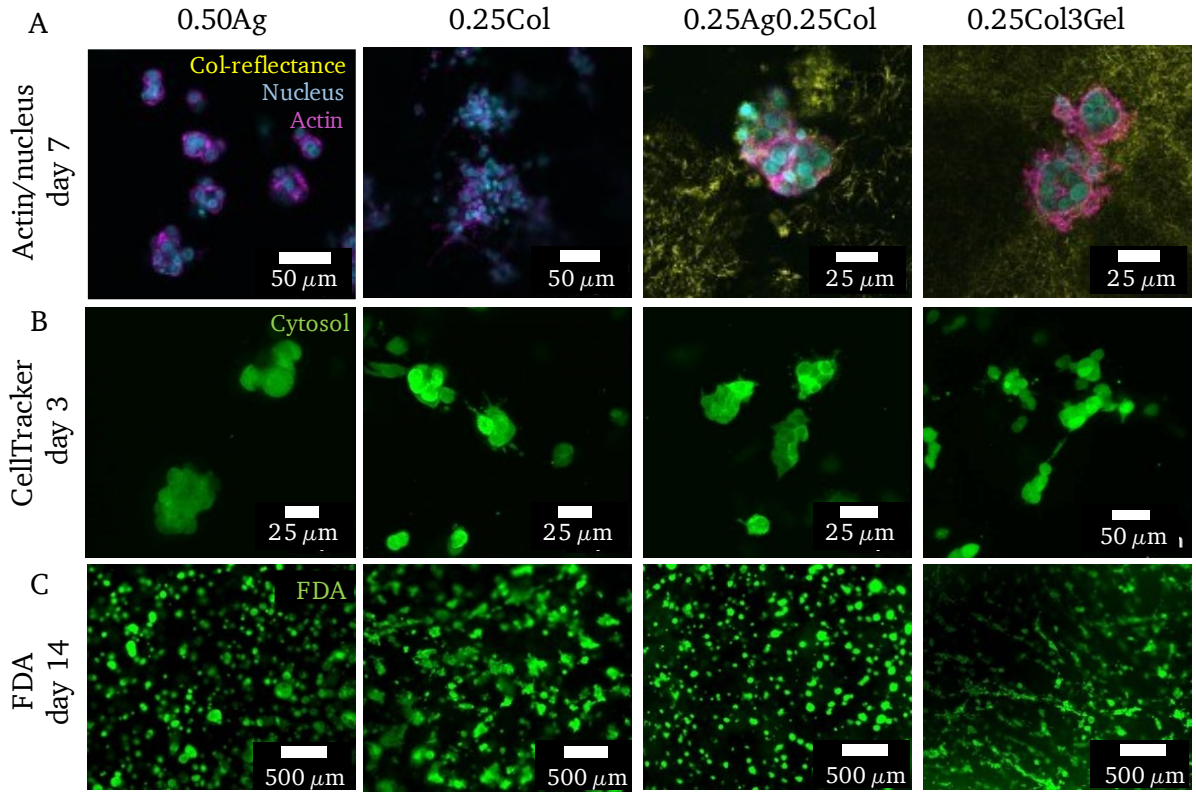

Figure 16: Study of cell behavior inside the hydrogels. CLSM of HepG2 with stained nuclei (blue), actin filaments (magenta) and collagen I fibers (yellow) on day 7 show embedding of HepG2 in collagen matrix as well as little cytosol for cells in all materials (A). Cells exhibit small protrusions and even small networks in 0.25Col and 0.25Col3Gel, while remaining round when cultured in agarose-containing gels (B, C). Figure adapted from Fritschen et al.[3].

For printability, three different properties are important – drop volume, the resulting drop diameter on the substrate as governed by the wettability and the general drop quality. These properties can be monitored both in flight as well as post-printing with different imaging technologies. As expected[95,215], the drop volume is directly impacted by the print pressure (**Figure 17** A). While most of the studied materials show a drop volume of around 200 nl when printed with a nozzle diameter of 300 μm, 0.25Col3Gel can achieve volumes of around 100 nl. When monitored on substrate, the lower drop volume of 0.25Col3Gel does not results in the lowest effective drop diameter, but quite the contrary, to a higher effective diameter than the other materials (**Figure 17** B). This is caused by its better wettability, which reduces the effective print resolution due to drop spreading. For all materials, the contact angle is as expected lower on glass than on PDMS, leading to a smaller drop diameter (**Figure 17** C, D). Overall, drop diameters of around 1000 μm are achievable on PDMS. However, the lowest printable print pressure is given by the limit where nozzle clogging or incomplete drop formation occurs. This minimum pressure is also dependent on the material's viscosity and surface tension[215,218] (→ **Section 3.6**), which is not exhausted in this work. Therefore, only print pressures where a reliable drop dispensing is achieved are shown. Apart from the drop diameter, the drop quality is also important for a tissue model on chip. The blend of agarose and collagen often ended in splashing and irregular drop shape, while pure agarose and collagen exhibited a very round and regular shape (**Figure 17** E, F). Again, this is most likely caused by the onset of collagen fibrillogenesis inside the nozzle during print time.

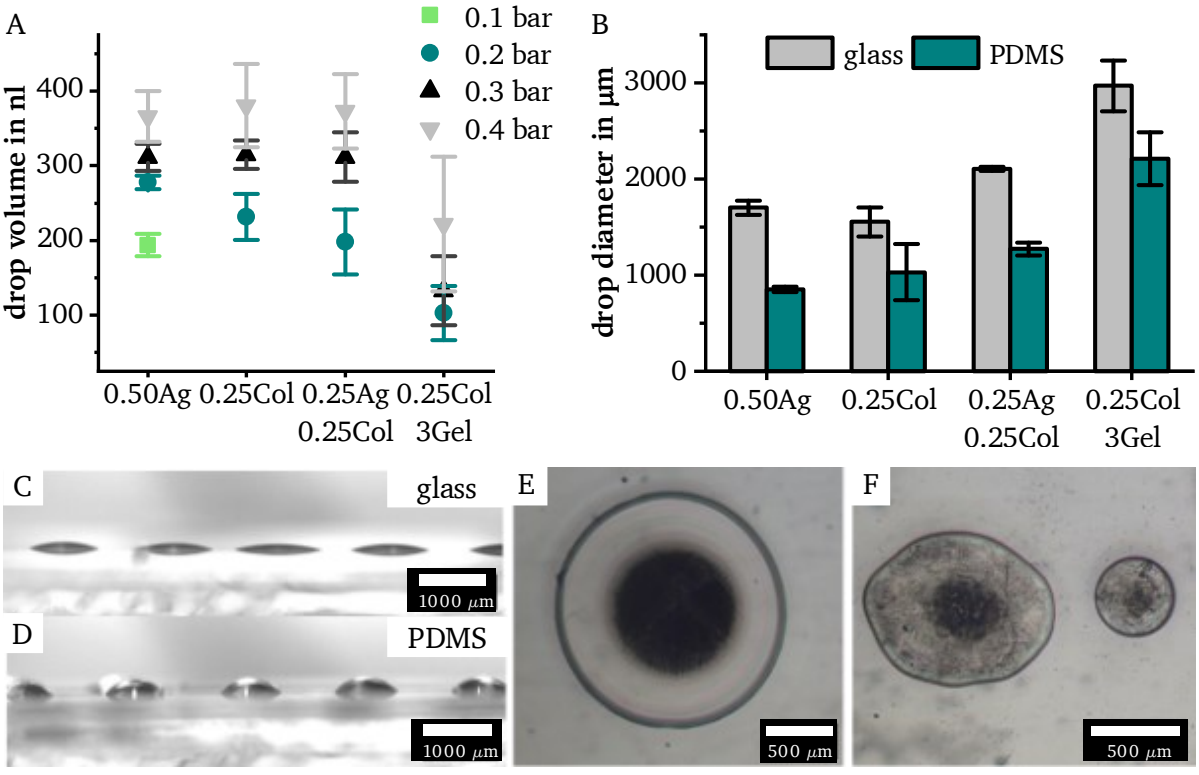

Figure 17: Monitoring of the materials' printability shows that the drop volume depends on the applied print pressure and material (A), while the effective drop diameter depends on the substrate and the wetting properties of the printed material (B - D). The drop quality post-printing as monitored by microscopy (E, F) also has an impact on the effective resolution. Graph data was determined for 500 drops for the drop volume and n = 10 for the drop diameter showing the mean with error bars as the standard error of the mean. Figure adapted from Fritschen et al.[3].

During bioprinting, cells exhibit shear stresses as well as waiting times and temperature gradients, which are often correlated to a loss in cell viability[96,225]. However, in the case of HepG2 cells in combination with our four materials, cell viability and proliferation are unaffected by the print process compared to a non-printed control group (**Figure 18** A, B). This is probably due to the very low average shear stresses of below 1 kPa experienced by cells in these materials (**Figure 18** C), which is much below the critical values reported in DoD bioprinting of 18 kPa for cancer cells[225] or of 2 – 5 kPa for primary mesenchymal stem cells[95]. The slight decrease in viability over the course of 14 days can be explained by the agglomeration of HepG2 cells over time, which leads to the formation of necrotic cores (**Figure 18** D).

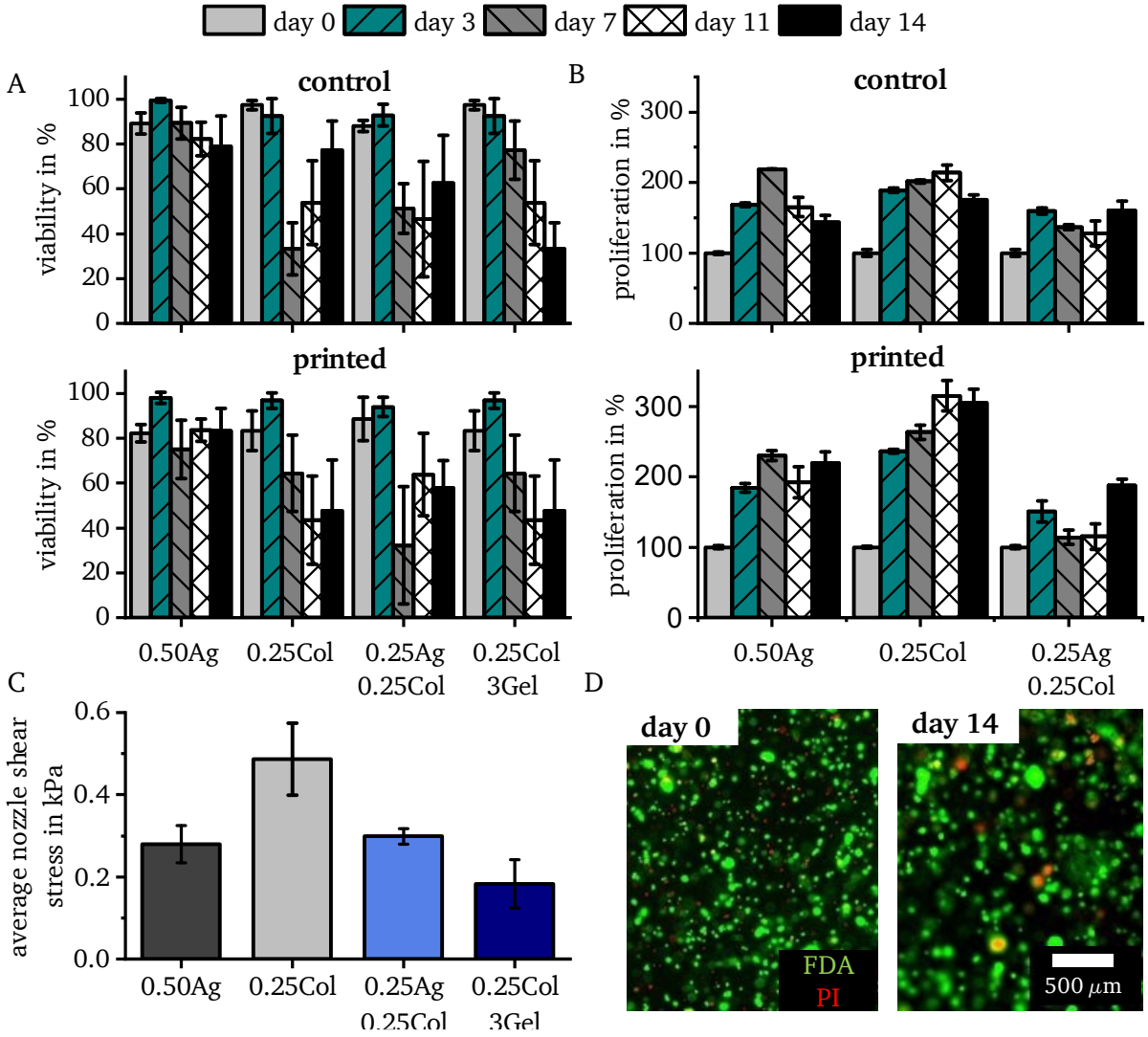

Figure 18: No significant effect of printing on cell viability (A) and proliferation (B) for HepG2 cells can be observed, as the average shear stress on cells within the printer's nozzle is negligible with below 0.6 kPa (C). Viability was determined by FDA/PI staining and image analysis, where the formation of agglomerates with necrotic cores can be observed in a 0.5Ag gel over the course of 14 days (D). Graph data was determined for n = 3 showing the mean with error bars as the standard error of the mean. The error bars for (D) were calculated through error propagation of the standard error of the mean of the variables contained in equation 7. Figure adapted from Fritschen et al.[3].

Interim conclusion and application of findings to this work:

Multiple materials have shown their potential as bioinks for a HepG2-based carcinoma OOC. Different materials and blends showed good printability, with no notable impact of the print process on cell viability of proliferation. For this work, agarose was chosen as a material for further studies, as it offers very good print resolution and quality combined with high cell viability and proliferation despite its lack of cell adhesion motifs. In addition, it is easy to handle and not too costly.

4.4. Automated Production of a Vascularized and 3D-Bioprinted OOC Model

The final phase of this work involved the integration of the preliminary work on vascularization, microfluidic chip printing and Drop-on-Demand (DoD) bioprinting into the development of a fully 3D-bioprinted and vascularized Carcinoma-on-a-Chip model. Furthermore, to enhance the efficiency and provide insights into a potential translation to industry, an automated handling of the microfluidic chip via a robotic system was introduced (**Figure 19**).

In the initial step, the design of the tissue model was considered with regard to the selection of cell types, cell combinations and biomaterials. Single carcinoma islets of HepG2 cells had to be precisely positioned within the chip's tissue chamber using DoD bioprinting (**Figure 19** A). As a matrix material, low-concentrated agarose was chosen because of its good printability as well as cellular behavior (→ **Section 4.3**,[3]). Based on the thorough literature review of possible vascularization strategies suitable for 3D-bioprinting on chip (→ **Section 4.1**,[1]), HUVEC and HDF were embedded in a fibrin matrix at a ratio of 10:1 to assemble into microvascular networks (μVN). With this approach, direct cell-cell contact was possible and nutrient supply is regulated through the μVN.

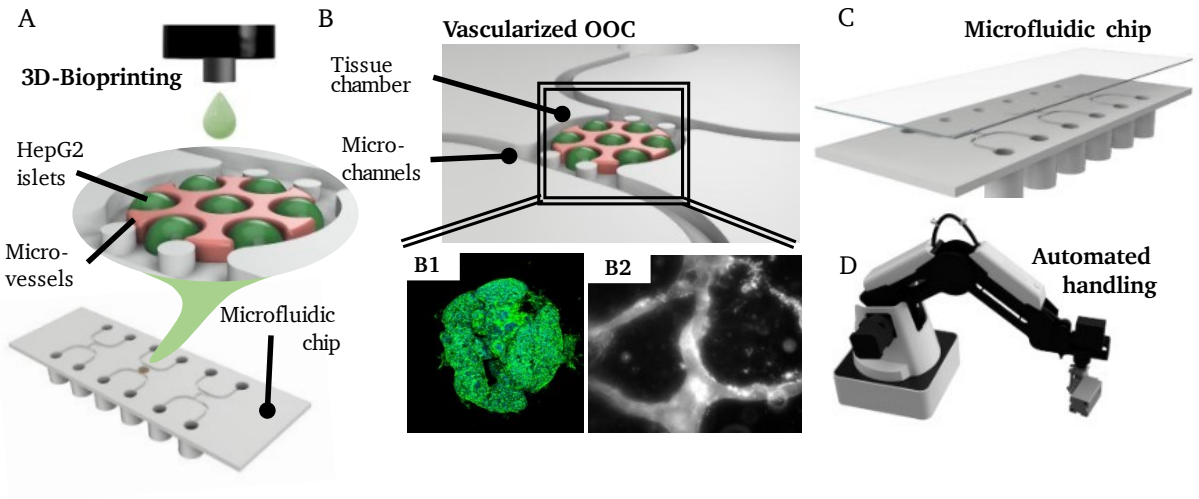

Figure 19: Envisioned 3D-bioprint process of HepG2 carcinoma islets surrounded by a microvascular network on a microfluidic chip (A). The tissue model is contained in a tissue chamber separated from the microchannels via pillars. Within the tissue chamber, HepG2 cells constituting carcinoma islets (B1) are embedded in a fibrin matrix, where a microvascular network is achieved during cultivation (B2). For this, a sealable microfluidic chip with a tissue chamber accessible by the bioprinter was developed (C). Handling of the microfluidic chip is automated via a robotic unit (D). Figure adapted from Fritschen et al.[4].

Next, a microfluidic chip suitable for the tissue model had to be designed and tested. In the prototyping phase, the presented 3D-DLP printing method was employed for chip fabrication (**Section 4.2**,[2]). Given the necessity for this chip to be filled via 3D-bioprinting, a design that contained an open central tissue chamber (**Figure 20** A) was devised. After bioprinting, this chip could be sealed tightly with a printed and transparent lid (**Figure 20** B).

The general chip design was iteratively adapted while always containing two microchannels that pass a central tissue chamber on both sides and that later enable perfusion of the chip. After testing different variations, the central chamber was designed with a diameter of 3 mm. This size offers space for several cell islets as well as some tolerance in print accuracy, while being small enough for μVN to fully develop and support the tissue model without necrotic core formation. The tissue chamber is separated from the microchannels by two pillars that retain the hydrogel and prevent it from leaking into the channels before gelation. Once the prototyping phase was finished, a final design was translated to an industrial scale with partners by injection molding of a cyclic olefin polymer (COP). This material is advantageous for microfluidic chips due to its supreme optical qualities, biological inertness and processability by injection molding in large quantities[314–316]. As the injection molding process is different to 3D-printing, several adaptations to the design were made. The industrial chip design features three microfluidic components on a chip with the dimensions of commercial objective slides, making it compatible with commercial microscope systems. For easy connection to a perfusion system, Luer adapters were added at the end of the channels. The chip base is covered with an adhesive tape layer and can be sealed post-printing with a thin polymer coverslip (**Figure 20** C). The coverslip's thickness of 170 μm is adapted to the standard microscopy slide thickness for high-resolution microscopy.

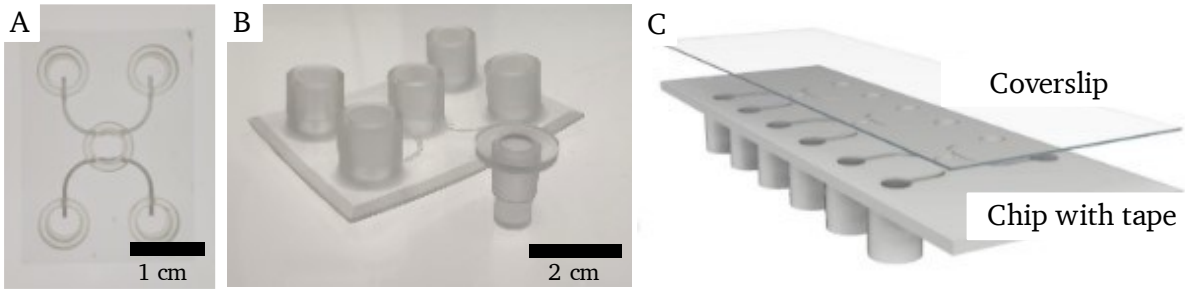

Figure 20: DLP prototype of a microfluidic chip with an open top that can be closed post-printing by a lid (A, B). Final chip design of the injection molded industrial chip that contains three tissue chambers on a microscopy slide format with Luer connectors. The chip is sealed post-printing by a thin coverslip with a double-sided adhesive tape (C). Figure adapted from Fritschen et al.[4].

With a microfluidic chip designed and fabricated, the focus shifted to the aspect of on-chip DoD bioprinting. To assess the feasibility of the process, factors such as the general bioink characteristics, print resolution and the potential impact on cellular behavior were studied. The rheological characterization revealed that both hydrogels are suitable for bioprinting at low print pressures based on their viscosity[202,215]. Low-concentrated agarose has an intrinsic low viscosity, while fibrinogen exhibited a strong shear-thinning behavior (**Figure 21** A) and becomes very liquid at higher shear rates as observed in literature, too[312]. Because of the low viscosity and resulting low print pressure, very small drops of just 27 nl could be printed with agarose when a small printer valve of 150 μm was used (**Figure 21** B). This low volume is required for high-resolution bioprinting on chip. The final drop diameter post-printing depends on the wettability of the substrate[215,218], and was around 850 μm for both the DLP-printed

prototypes as well as the COP molded chips (**Figure 21** C). This diameter is large compared to other diameters of down to 200 μm achieved in literature[87,215], which is most likely caused by the low viscosity of agarose, which reduces print resolution, and the good wettability of the substrate. However, the drop diameter, which governs the possible arrangement of the HepG2 islets, is still small enough to print up to seven drops into the tissue chamber when considering the theory of circle packing in a circle[317] and leaving a small tolerance of 15 %.

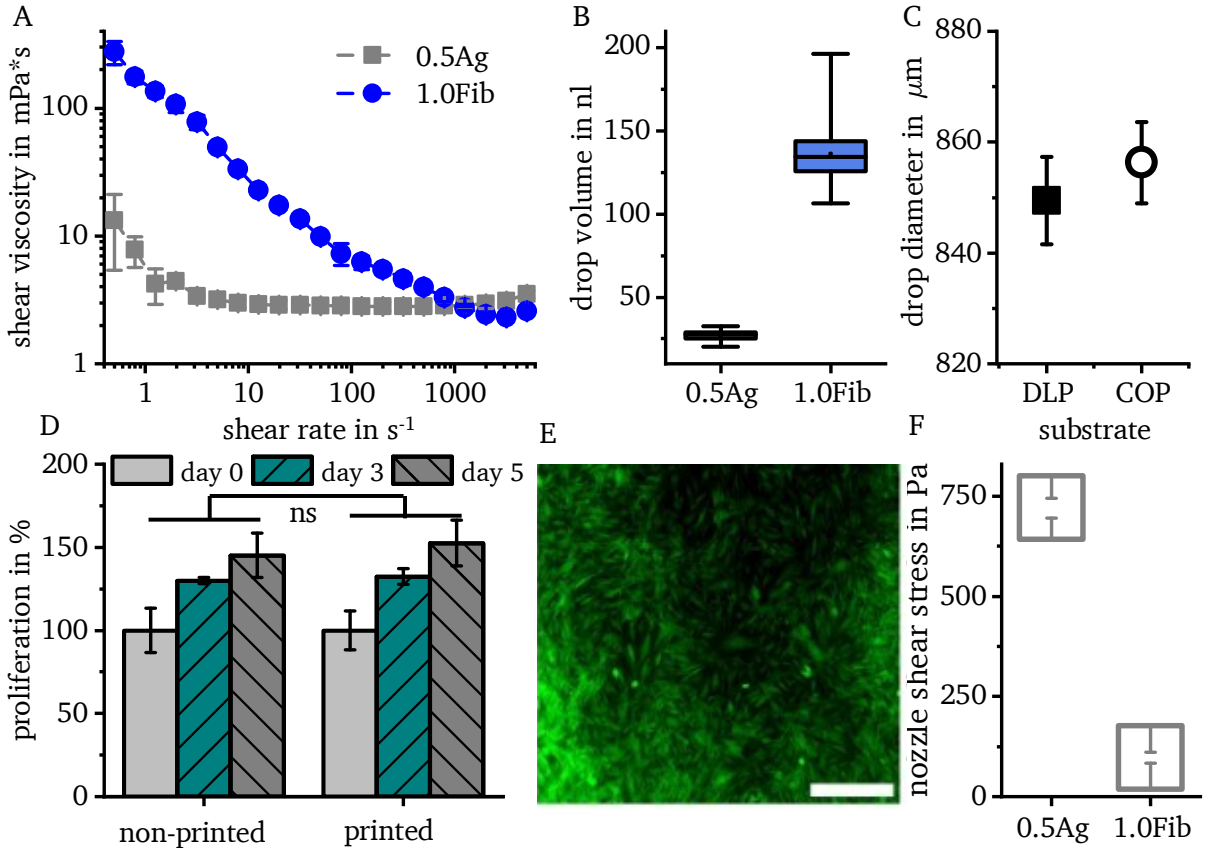

Figure 21: Shear viscosity measurements show a strong shear thinning behavior for fibrinogen and a low viscosity for agarose (A). The resulting drop volumes in flight (B) are much larger for fibrinogen than for agarose due to a larger nozzle. The resulting drop diameter of agarose depends on the substrate and has no significant (ns) difference between DLP-prints and COP (C). No significant (ns) impact of printing is observed for the proliferation of HUVEC (D). The viability of HDF 14 hours post-printing (live stained with FDA in green, dead with PI in red, scale bar showing 500 µm) is also high (E) due to the low average shear stress that cells exhibit in the nozzle (F). Graph data was determined for n = 3 (A, D, F), n = 40 for agarose and n = 150 for fibrinogen (B) and n = 20 (C) showing the mean with error bars as the standard error of the mean. Statistical significance was determined with a two-sample t-test. Figure adapted from Fritschen et al.[4].

The μVN-bioink of fibrinogen with HUVEC and HDF was processed with a larger microvalve of 300 μm diameter, as no precision is required to fill the space between the HepG2 islets. The larger valve in combination with a low print pressure of 0.2 bar was assumed to offer favorable conditions for the handling of sensitive primary cells. This assumption was confirmed, as the proliferation of HUVEC is not impacted compared to a non-printed control group (**Figure 21** D) and HDF also show a high post-printing viability (**Figure 21** E). This observation corresponds to the low nozzle shear stress that all cells experience inside the nozzle during printing, which is below 1 kPa and therefore far below reported critical values for primary cells[95,215] (**Figure 21** F).

To finally print the multi-material, multi-cellular tissue model on chip, two print heads were employed simultaneously. The HepG2 bioink is contained in a heated print head with the smaller microvalve, while the μVN bioink is cooled inside another print head with a larger nozzle. The microfluidic chip is placed on a temperature-controlled sample holder, which is necessary to initiate the gelation of agarose at temperatures below 20 °C (**Figure 22** A). First, seven distinct drops of the HepG2 bioink are printed (**Figure 22** B). Once gelation of agarose is achieved, the fibrinogen layer is applied on top. Crosslinking of fibrinogen is started by thrombin, which is contained in the previously printed drops of agarose. The print process is repeated three times to fill all three tissue chambers on chip before the chip is sealed and placed in the incubator for complete gelation (**Figure 22** C). The complete print process required less than a minute and could be scaled up for high-throughput assays by an array of multiple print heads.

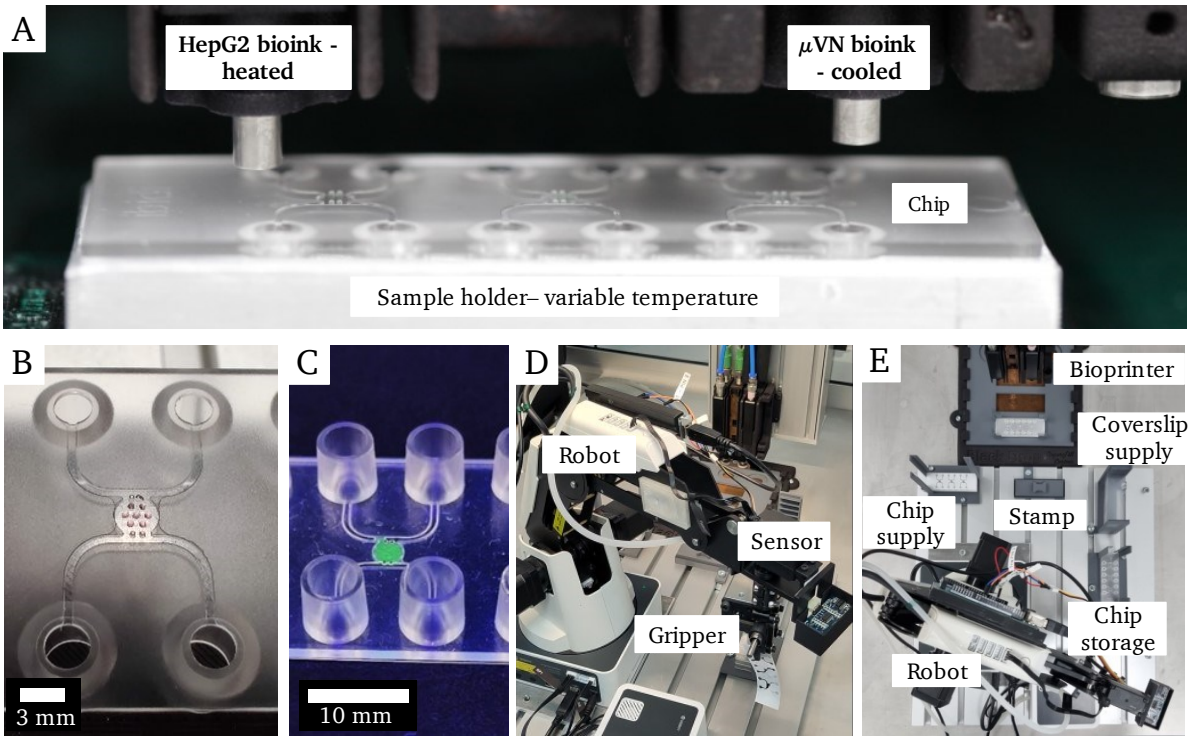

Figure 22: Printing of two bioinks is realized via two printheads that can be heated for the HepG2 bioink and cooled for the µVN bioink containing fibrinogen. The chip is placed on a temperature-controlled sample holder (A). Seven drops of the HepG2 bioink are printed first (B), followed by the µVN bioink. The chip is sealed afterwards (C). A robot equipped with a gripper (D) performs the manipulation and transport of the microfluidic chips (E). Figure adapted from Fritschen et al.[4].

Aside from the print process, the preparation and handling of the microfluidic chip was still a manual process. Recognizing the possible need for larger quantities of OOC systems, particularly for industrial or large-scale assay applications, this manual process is not only labor-intensive but also susceptible to errors. To address this challenge, an automated manipulation and transport system was devised. This system utilizes a robotic platform equipped with a gripper, automating the chip handling process and improving efficiency (**Figure 22** D). The robot system performs the chip delivery, lid removal, chip closure and chip storage. Different workstations were designed which contain the feed of fresh chips, a sample holder where the bioprinting takes place, a supply of the closing coverslip and a storage place for finished chips (**Figure 22** E). Integrated cameras and ultrasonic sensors monitor the success of placing the chip as well as the removal of a protective cover foil over the adhesive tape. The integration of

this automated system is a step towards the industrial translation of complex OOCs, as manual steps are reduced.

Having addressed the fundamental considerations related to printability and material selection, the remaining scientific question revolved around demonstrating the feasibility of self-assembled μVN using the selected materials, culture conditions and in particular the designed microfluidic chip. Immunofluorescence images show that branched μVN develop throughout the whole chip within 14 days of culture (**Figure 23** A).

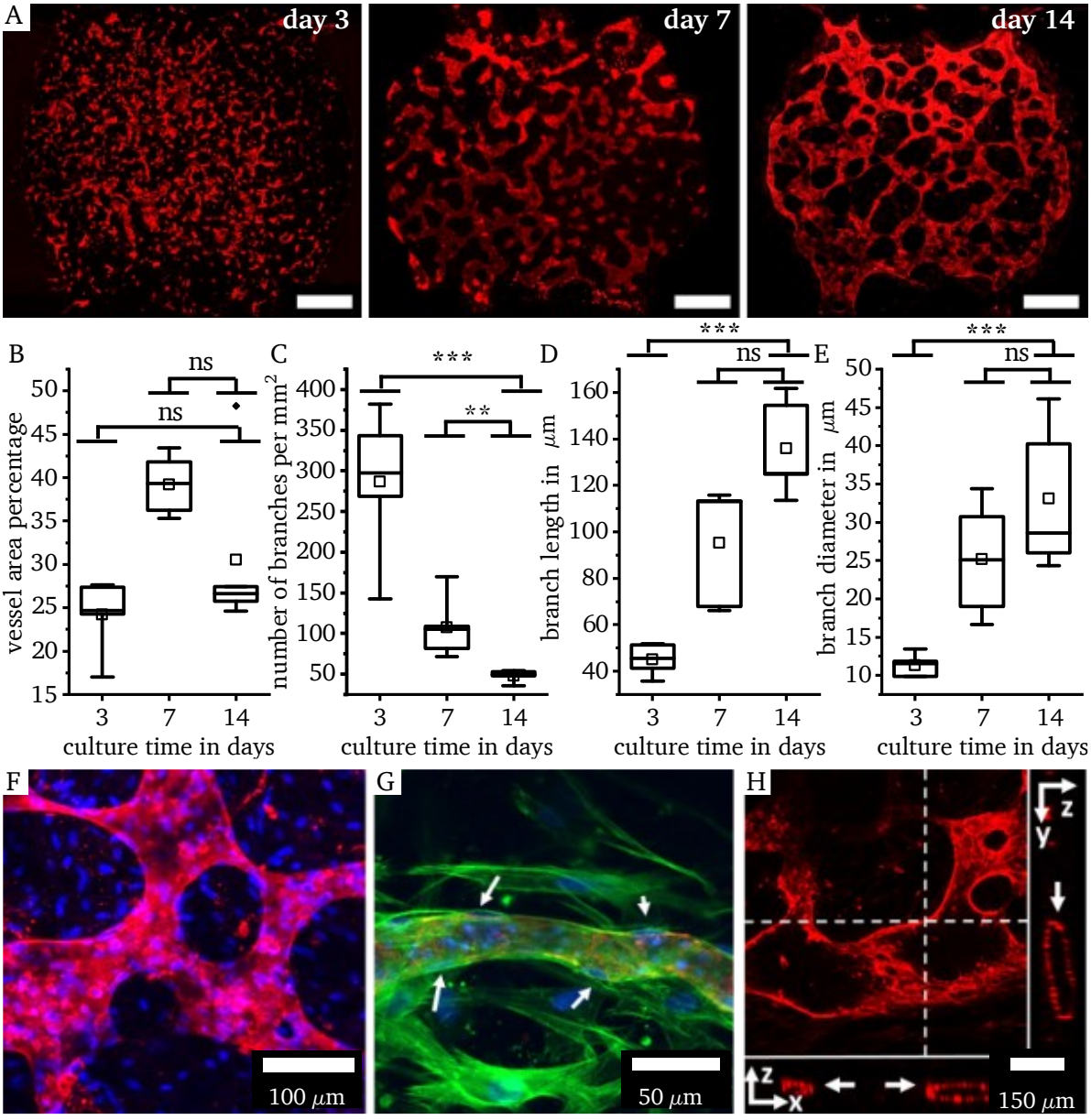

Figure 23: By culturing HUVEC and HDF in the fibrin bioink, finely branched microvascular networks self-assemble on-chip over the course of 14 days, with CD-31 stained red (A). Scale bar showing 500 µm. With a steady vessel area percentage (B), the number of branches decreases over culture time (C), while the branch length and diameter increase over time (D, E). Immunofluorescence microscopy images show the highly branched network with various diameters (F), with HDF lining the vessel walls as indicated by white arrows (G). The networks show open lumen (white arrows) as shown for a z-projection image of a cross-section confocal microscopy image with the slice direction shown in the x- and y-plane as indicated by white lines (H). Endothelial cells stained red for CD31, cell nuclei stained with DAPI in blue and actin filaments stained green with phalloidin. Graph data was determined for n = 5. Statistical significance was determined with a two-sample t-test. Differences between days are marked as ns for not significant, ** for $p < 0.01$, *** for $p < 0.001$. Figure adapted from Fritschen et al.[4].

While the total vessel area does not vary significantly over the time of culture (**Figure 23** B), the number of branches decreases to around 50 per mm^2 (**Figure 23** C), which corresponds to literature reports[280,318,319]. Similar to other reports on vasculogenesis in fibrin gels[280,320,321], the vessel length (**Figure 23** D) and diameter (**Figure 23** E) increase during the formation of the μVN. The formed networks are finely branched with ranging diameters (**Figure 23** F) and are supported by HDF lining the outside of the vessel walls (**Figure 23** G), demonstrating the need for supporting cell types and their functionality for maintaining the stability of networks for prolonged times as reported before[322–324]. Furthermore, the networks are hollow inside and a lumen is visible in cross-sections of confocal microscopy images (**Figure 23** H).

The final point of this study was the fabrication of a DoD-bioprinted, vascularized liver Carcinoma-on-a-Chip. Immunofluorescence images show that the HepG2 islets can be printed at a high quality in a circular arrangement of seven drops with an even distribution of HepG2 cells inside the drops (**Figure 24** A). Within the drops, HepG2 cells proliferate strongly and form spheroid-like agglomerates within 14 days of culture on chip (**Figure 24** B, C).

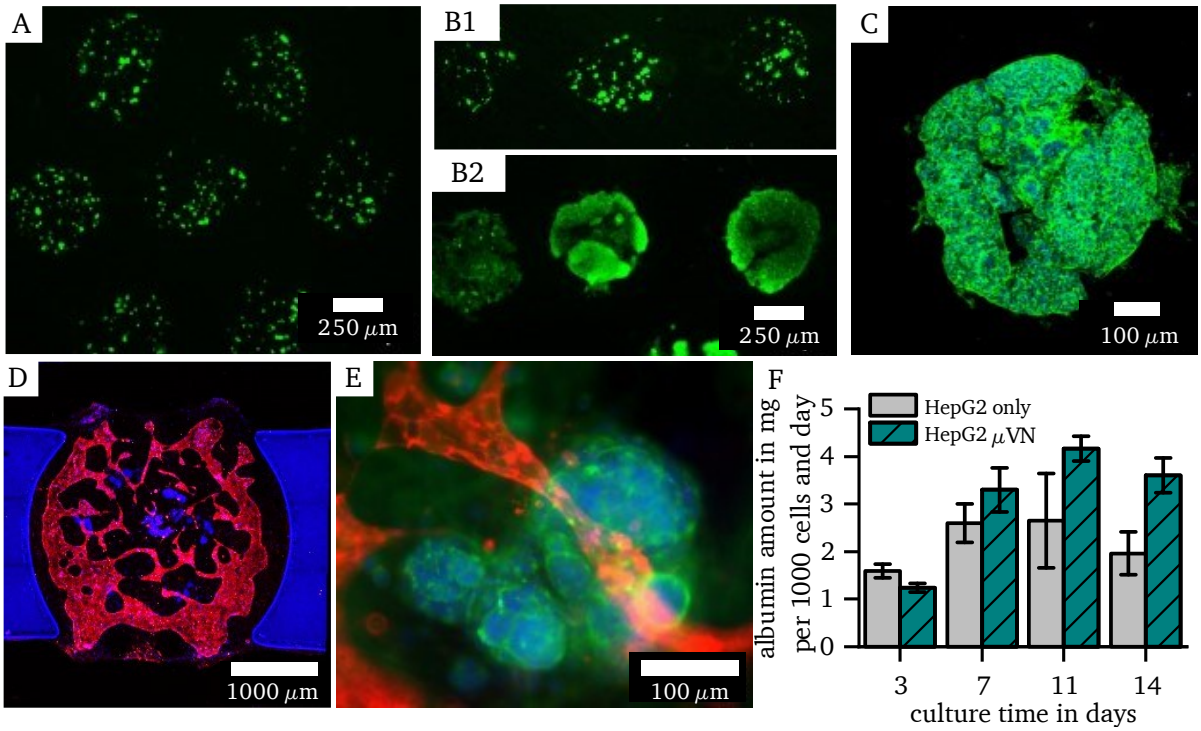

Figure 24: Immunofluorescence images show that DoD-bioprinting is successful at placing the HepG2 bioink in a circular arrangement of seven drops with a homogeneous distribution of HepG2 within the drops (A). HepG2 cells proliferate and agglomerate between day 0 (B1) and day 14 (B2) to form spheroid-like structures (C). In the tri-culture model, a vascular network forms throughout the chip around the HepG2 islets (D). The vascular networks grow above and around the HepG2 islets (E). Endothelial cells stained red for CD31, cell nuclei stained with DAPI in blue and actin filaments stained green with phalloidin. The production of human albumin is increased when HepG2 cells are cultured with a surrounding μVN network compared to non-vascularized samples (F). Graph data was determined for n = 3 showing the mean with error bars as the standard error of the mean. Statistical significance was determined with a two-sample t-test. Differences between days are marked as * for $p < 0.05$ and ** for $p < 0.01$. Figure adapted from Fritschen et al.[4].

This behavior is typical for HepG2 cells cultured in 3D[325,326] and has been reported for both cancerogenic and other hepatic cells, be it with hepatic cells alone[18,327–330], in combination with vascular channels[331–333] or with endothelia cells[334,335]. The HepG2 cells are retained within the drop of agarose, which is utilized in this work to form cell-spheroids directly on-chip instead of

placing pre-formed spheroids on-chip as is commonly done by other works[47,269,270,336–340]. This accelerates the fabrication process by removing the need to manually pre-fabricate spheroids.

In this tri-culture model, the vascular network develops throughout the chip and around the printed islets of HepG2 cells in agarose (**Figure 24** D). Furthermore, the vascular networks do not only pass around the agarose islets but also grow above the islets (**Figure 24** E). The addition of vasculature not only retains cell viability, but also leads to an increased production of human albumin by the cells compared to the non-vascularized control group, highlighting the improved functionality of cells when they are supported by μVN (**Figure 24** F), which corresponds to findings of previous studies[331,335].

Interim conclusion:

With this work, DoD bioprinting has demonstrated its capacity to generate complex OOCs that exhibit a multi-cellular and vascularized architecture enabled by the precise spatial arrangement of parenchymal and stromal cells. For the microfluidic chip development, DLP printing of prototypes served as a valuable method for testing and fine-tuning of designs. This iterative process ensured that the chips were tailored to the specific requirements of bioprinting technologies, facilitating a more precise integration of print heads and biomaterials. Furthermore, the successful formation of self-assembled μVN within a fibrin matrix provided the foundation for the integration of vasculature in the OOC, which can in turn support the growth and function of other cell types within the OOC. An exciting development was the spontaneous formation of spheroid-like structures by HepG2 cultured in nanoliter drops of agarose on chip. This eliminated the need to manually place pre-formed spheroids into the chip, simplifying the experimental workflow. In addition, the inclusion of vascular networks showed significant benefits in terms of enhancing cellular functions as shown for the production of human albumin.

Finally, the potential for upscaling OOC production was addressed through two approaches. First, the adaptation of a chip design for industrial-scale fabrication enabled the fabrication of microfluidic chips compatible with 3D-bioprinting at a large scale. Second, the integration of a robotic system reduced the need for manual steps, enhancing efficiency and repeatability, which are crucial for industrial translation. These collective advancements represent a major step forward in the field of OOC technology, enabling the creation of more sophisticated and biologically faithful *in vitro* models for both basic research and large-throughput pharmaceutical applications.

5. Conclusion and Outlook

This work addressed various aspects required to increase automation in the fabrication of vascularized Organs-on-a-Chip (OOC), which are required to translate these models into preclinical pharmaceutical research. Different aspects were studied individually and presented in four publications, concluding in a three-dimensional, vascularized and multicellular liver Carcinoma-on-a-Chip model which was fabricated using microvalve-based 3D-bioprinting and robotic handling. The objective was to determine whether 3D-bioprinting could enhance the fabrication process of OOCs with high complexity and vascularization without additional manual steps.

In the first step, existing approaches to incorporate vascularization in OOC models were reviewed in detail and evaluated for their compatibility with the available Drop-on-Demand (DoD) bioprinter as well as for their suitability for a multicellular tissue model. The use of the intrinsic capability of endothelial cells to spontaneously form microvascular networks (μVN) was found to be the most biomimetic and appropriate approach to obtain a fine vascular network that supports parenchymal cells, as this method is compatible with DoD-bioprinting and applicable to different tissue model designs. Based on successful literature reports, human umbilical vein endothelial cells (HUVEC) were selected as endothelial cells, while human dermal fibroblasts (HDF) were chosen as stabilizing co-culture cells.

Next, a fast and flexible method to fabricate microfluidic chip prototypes compatible with the DoD-bioprinting process was required. Based on promising literature reports on 3D-printed microfluidics, a commercial 3D-DLP-printer was modified and a print process as well as post-process procedure were developed, which resulted in transparent and biocompatible components. With these adaptations and protocols, even small features such as freestanding pillars of only 50 μm in diameter or small microfluidic channels were possible with the printer's resolution. These results demonstrate the suitability of DLP-printing for the prototyping of microfluidic chips that were required for this research.

With an available method to fabricate microfluidic chips and a strategy to include a vascular network, an example tissue on-chip was the next step. For demonstration purposes, a three-dimensional liver carcinoma model was selected based on the HepG2 cell line. To realize this model, a hydrogel that could be printed at high-resolution on-chip with the DoD-bioprinter had to be found, which would at the same time retain cellular function. A screening of three thermally gelling hydrogels (agarose, gelatin and collagen) and combinations thereof was performed and their suitability for the DoD-bioprinting process, compatibility with the selected cell line as well as their possible impact on cell viability or proliferation post-printing was assessed. While offering no cell adhesion motifs, agarose still supported cell growth and viability similar to collagen-containing blends and showed superior handling and printability. As it had no negative impact on the cells, it was preferred over blends containing collagen.

In the final step, a final microfluidic chip design obtained from the printed prototypes was translated to an industrial fabrication step using a thermoplastic polymer and injection molding. A multi-material DoD-bioprint process was developed, which enabled the printing of the HepG2-containing bioink as well as a vasculogenesis bioink made HUVEC and HDF in fibrin directly onto the chip in a single-step process. To reduce the number of manual steps in printing, a robotic manipulation and transport system was implemented that performs steps such as chip

delivery, chip closure and chip storage. The final vascularized Carcinoma-on-a-Chip model comprised seven drops of HepG2 cells in agarose, which were surrounded by the vasculogenesis bioink. Within 14 days of cultivation, finely branched μVN developed throughout the whole tissue chamber that were stabilized by HDF and exhibited open and perfusable lumen. HepG2 cells proliferated strongly inside their drops of agarose and formed spheroid-like structures. Their functionality was increased when supported by the μVN as seen in an increased protein level as shown for albumin.

The results of this work highlight that 3D-bioprinting, especially in combination with robotics, can play an important role in the translation of complex, vascularized OOCs into industry and that these automated systems are not limited to simple structures. Furthermore, it has been shown that conventional 3D-printing is a powerful tool in the development phase of OOCs, offering a high degree of flexibility with high precision.

The developed process has the potential to serve as a basis for further experiments and different research areas, as the whole platform – microfluidic chip and 3D-bioprinter – is adaptable to a variety of cell types, bioinks and even bioprinters. Due to its open top, the developed microfluidic chip is compatible with different non-contact bioprinters such as laser-induced forward transfer, acoustic or magnetic bioprinting[31,94], or with extrusion-based systems if a small enough nozzle or needle is used[87,89]. Together with the presented DoD bioprint process, a wide variety of bioinks can be processed and tailored to the tissue model of choice. Based on this platform, further in-depth biological research is possible, for example on tissue drug response, the interaction between parenchymal cells and the vasculature, cancer cell migration, barrier function of the microvasculature or even for patient-specific models. Since the presented DoD-bioprinting process is associated with a low shear stress and short handling times, even primary cell types or iPSC-derived cells can be incorporated, as has already been shown for various cell types[178,259,341,342]. Furthermore, the developed microfluidic chip offers the capability to interconnect three distinct tissues on a single chip, making it ideally suited for the development of Body-on-a-Chip models. This potential opens up exciting opportunities for the creation of more comprehensive and integrated *in vitro* systems that can mimic the complex interactions between various tissues within the human body. These models could also be employed to study important organ-to-organ interactions of drug metabolites that may reveal secondary toxicities[343–345].

The observed spontaneous agglomeration of HepG2 cells opens another field of study, as this could be a method to replace the manual placement of spheroids with an on-chip spheroid formation process. This will require experiments with other carcinoma cell types to determine whether this behavior is specific to HepG2 cells or is also characteristic of other carcinoma cells. In addition, this research could be advanced by working towards the development of pre-vascularized spheroids by mixing endothelial cells, carcinoma cells and potentially stabilizing co-culture cells within the islet bioink. By moving from agarose to a more bio-interactive material, it may be possible to monitor the formation of pre-vascularized spheroids, along with their angiogenesis and anastomosis with the μVN.

In the context of clinical applications and pharmaceutical research, the small sample volume of only 3 μl per tissue chamber offers significant advantages when working with patient biopsies or with tissue samples of limited availability such as primary human hepatocytes[346,347]. Such considerations are important for the development of personalized medicine or for monitoring the effects of anticancer drugs on cancer patients. This monitoring could extend beyond the

response of just the cancer cells to the vasculature and other tissues, providing a comprehensive assessment of potential side effects. By integrating 3D-bioprinting and robotic automation, the need for trained personnel in the preparation of these OOCs can be significantly reduced. By simplifying the handling of these complex, yet more manageable and vascularized OOCs, their potential incorporation into hospital settings and pharmaceutical trials comes closer. The results presented here therefore have the potential to streamline and enhance the translation of OOC technology into real-world clinical and research applications.

Bibliography

1. Fritschen, A. & Blaeser, A. Biosynthetic, biomimetic, and self-assembled vascularized Organ-on-a-Chip systems. *Biomaterials* **268**, 120556 (2020).
2. Fritschen, A., Bell, A. K., Königstein, I., Stark, R. W. & Blaeser, A. Investigation and comparison of resin materials in transparent DLP-printing for application in cell culture and organs-on-a-chip. *Biomater. Sci.* **10**, 1981–1994 (2022).
3. Fritschen, A., Acedo Mestre, M., Scholpp, S. & Blaeser, A. Influence of the physico-chemical bioink composition on the printability and cell biological properties in 3D-bioprinting of a liver tumor cell line. *Front. Bioeng. Biotechnol.* **11**, 1093101 (2023).
4. Fritschen, A. *et al.* High-Scale 3D-Bioprinting Platform for the Automated Production of Vascularized Organs-on-a-Chip. *Adv. Healthc. Mater.* **2304028**, 1–11 (2024).
5. Bonam, S. R. *et al.* Role of pharmaceutical sciences in future drug discovery. *Futur. Drug Discov.* **3**, (2021).
6. Meganck, R. M. & Baric, R. S. Developing therapeutic approaches for twenty-first-century emerging infectious viral diseases. *Nat. Med.* **27**, 401–410 (2021).
7. Han, Q. *et al.* Research advances in treatment methods and drug development for rare diseases. *Front. Pharmacol.* **13**, 1–9 (2022).
8. Esch, E. W., Bahinski, A. & Huh, D. Organs-on-chips at the frontiers of drug discovery. *Nat. Rev. Drug Discov.* **14**, 248–260 (2015).
9. Breslin, S. & O'Driscoll, L. Three-dimensional cell culture: The missing link in drug discovery. *Drug Discov. Today* **18**, 240–249 (2013).
10. Ingber, D. E. Human organs-on-chips for disease modelling, drug development and personalized medicine. *Nat. Rev.* **23**, 467–491 (2022).
11. Fetah, K. *et al.* The emergence of 3D bioprinting in organ-on-chip systems. *Prog. Biomed. Eng.* **1**, 012001 (2019).
12. Leung, C. M. *et al.* A guide to the organ-on-a-chip. *Nat. Rev. Methods Prim.* **2**, 33 (2022).
13. Zhao, Y., Wang, E. Y., Lai, B. F. L., Cheung, K. & Radisic, M. Organs-on-a-chip: a union of tissue engineering and microfabrication. *Trends Biotechnol.* **41**, 410–424 (2023).
14. Jang, K. J. *et al.* Reproducing human and cross-species drug toxicities using a Liver-Chip. *Sci. Transl. Med.* **11**, (2019).
15. Homan, K. A. *et al.* Flow-enhanced vascularization and maturation of kidney organoids in vitro. *Nat. Methods* **16**, 255–262 (2019).
16. Bhatia, S. N. & Ingber, D. E. Microfluidic organs-on-chips. *Nat. Biotechnol.* **32**, 760–772 (2014).
17. Barbosa, M. A. G., Xavier, C. P. R., Pereira, R. F., Petrikaité, V. & Vasconcelos, H. 3D Cell Culture Models as Recapitulators of the Tumor Microenvironment for the Screening of Anti-Cancer Drugs. *Cancers (Basel).* **14**, 190 (2021).
18. Ma, C., Peng, Y., Li, H. & Chen, W. Organ-on-a-Chip: A New Paradigm for Drug Development. *Trends Pharmacol. Sci.* **42**, 119–133 (2021).
19. Vunjak-Novakovic, G., Ronaldson-Bouchard, K. & Radisic, M. Organs-on-a-chip models for biological research. *Cell* **184**, 4597–4611 (2021).
20. Bhise, N. S. *et al.* Organ-on-a-chip platforms for studying drug delivery systems. *J. Control. Release* **190**, 82–93 (2014).
21. Herland, A. *et al.* Quantitative prediction of human pharmacokinetic responses to drugs via fluidically coupled vascularized organ chips. *Nat. Biomed. Eng.* **4**, 421–436 (2020).
22. Zhang, Y. S. *et al.* Multisensor-integrated organs-on-chips platform for automated and continual in situ monitoring of organoid behaviors. *Proc. Natl. Acad. Sci. U. S. A.* **114**, E2293–E2302 (2017).
23. Rogal, J., Schlünder, K. & Loskill, P. Developer's Guide to an Organ-on-Chip Model. *ACS Biomater. Sci. Eng.* **8**, 4643–4647 (2022).

24. Zhang, B. & Radisic, M. Organ-on-A-chip devices advance to market. *Lab Chip* **17**, 2395–2420 (2017).
25. Marx, U. *et al.* Biology-inspired microphysiological systems to advance patient benefit and animal welfare in drug development. *ALTEX* **37**, 365–394 (2020).
26. Moutinho, S. Researchers and regulators plan for a future without lab animals. *Nat. Med.* **29**, 2151–2154 (2023).
27. Saharan, V. A. Robotic Automation of Pharmaceutical and Life Science Industries. in *Computer Aided Pharmaceutics and Drug Delivery* (ed. Saharan, V. A.) 381–414 (Springer Singapore, 2022).
28. Stasevych, M. & Zvarych, V. Innovative Robotic Technologies and Artificial Intelligence in Pharmacy and Medicine: Paving the Way for the Future of Health Care—A Review. *Big Data Cogn. Comput.* **7**, 147 (2023).
29. Allwardt, V. *et al.* Translational roadmap for the organs-on-a-chip industry toward broad adoption. *Bioengineering* **7**, 1–27 (2020).
30. Bishop, E. S. *et al.* 3-D bioprinting technologies in tissue engineering and regenerative medicine: Current and future trends. *Genes Dis.* **4**, 185–195 (2017).
31. Chliara, M. A., Elezoglou, S. & Zergioti, I. Bioprinting on Organ-on-Chip: Development and Applications. *Biosensors* **12**, (2022).
32. Rahmani Dabbagh, S. *et al.* 3D bioprinted organ-on-chips. *Aggregate* **4**, 1–26 (2023).
33. Lee, H. & Cho, D. W. One-step fabrication of an organ-on-a-chip with spatial heterogeneity using a 3D bioprinting technology. *Lab Chip* **16**, 2618–2625 (2016).
34. Lee, H. *et al.* Cell-printed 3D liver-on-a-chip possessing a liver microenvironment and biliary system. *Biofabrication* **11**, (2019).
35. Zhang, B. *et al.* Biodegradable scaffold with built-in vasculature for organ-on-a-chip engineering and direct surgical anastomosis. *Nat. Mater.* **15**, 669–678 (2016).
36. Zhang, Y. S. *et al.* Bioprinting 3D microfibrous scaffolds for engineering endothelialized myocardium and heart-on-a-chip. *Biomaterials* **110**, 45–59 (2016).
37. Silvani, G. *et al.* A 3D-Bioprinted Vascularized Glioblastoma-on-a-Chip for Studying the Impact of Simulated Microgravity as a Novel Pre-Clinical Approach in Brain Tumor Therapy. *Adv. Ther.* **4**, 1–14 (2021).
38. Yi, H. G. *et al.* A bioprinted human-glioblastoma-on-a-chip for the identification of patient-specific responses to chemoradiotherapy. *Nat. Biomed. Eng.* **3**, 509–519 (2019).
39. Cao, X. *et al.* A Tumor-on-a-Chip System with Bioprinted Blood and Lymphatic Vessel Pair. *Adv. Funct. Mater.* **29**, 1–13 (2019).
40. Park, D. Y., Lee, J., Chung, J. J., Jung, Y. & Kim, S. H. Integrating Organs-on-Chips: Multiplexing, Scaling, Vascularization, and Innervation. *Trends Biotechnol.* **38**, 99–112 (2020).
41. Osaki, T., Sivathanu, V. & Kamm, R. D. Vascularized microfluidic organ-chips for drug screening, disease models and tissue engineering. *Curr. Opin. Biotechnol.* **52**, 116–123 (2018).
42. Kim, S., Kim, W., Lim, S. & Jeon, J. S. Vasculature-on-a-chip for in vitro disease models. *Bioengineering* **4**, (2017).
43. Rademakers, T., Horvath, J. M., van Blitterswijk, C. A. & LaPointe, V. L. S. Oxygen and nutrient delivery in tissue engineering: Approaches to graft vascularization. *J. Tissue Eng. Regen. Med.* **13**, 1815–1829 (2019).
44. Poisson, J. *et al.* Liver sinusoidal endothelial cells: Physiology and role in liver diseases. *J. Hepatol.* **66**, 212–227 (2017).
45. Low, L., Mummery, C., Berridge, B. R., Austin, C. P. & Tagle, D. A. Organs-on-chips: into the next decade. *Nat. Rev. Drug Discov.* **20**, 345–361 (2020).
46. Mandrycky, C. J., Howard, C. C., Rayner, S. G., Shin, Y. J. & Zheng, Y. Organ-on-a-chip systems for vascular biology. *J. Mol. Cell. Cardiol.* **159**, 1–13 (2021).
47. Wang, E., Andrade, M. J. & Smith, Q. Vascularized liver-on-a-chip model to investigate nicotine-induced dysfunction. *Biomicrofluidics* **17**, (2023).

48. Strelez, C., Jiang, H. Y. & Mumenthaler, S. M. Organs-on-chips: a decade of innovation. *Trends Biotechnol.* **41**, 278–280 (2023).
49. Bahnemann, J., Enders, A. & Winkler, S. Microfluidic Systems and Organ (Human) on a Chip. in *Basic Concepts on 3D Cell Culture. Learning Materials in Biosciences* (eds. Kaspers, C., Egger, D. & Lavrentieva, A.) 176–197 (Springer, 2021).
50. Terrell, J. A., Jones, C. G., Kabandana, G. K. M. & Chen, C. From cells-on-a-chip to organs-on-a-chip: Scaffolding materials for 3D cell culture in microfluidics. *J. Mater. Chem. B* **8**, 6667–6685 (2020).
51. Ronaldson-Bouchard, K. & Vunjak-Novakovic, G. Organs-on-a-Chip: A Fast Track for Engineered Human Tissues in Drug Development. *Cell Stem Cell* **22**, 310–324 (2018).
52. Fuchs, S. *et al.* In-line analysis of organ-on-chip systems with sensors: Integration, fabrication, challenges, and potential. *ACS Biomater. Sci. Eng.* **7**, 2926–2948 (2021).
53. Fleischer, S., Tavakol, D. N. & Vunjak-Novakovic, G. From Arteries to Capillaries: Approaches to Engineering Human Vasculature. *Adv. Funct. Mater.* **30**, 1–23 (2020).
54. Blache, U., Guerrero, J., Güven, S., Klar, A. S. & Scherberich, A. Microvascular Networks and Models: In Vitro Formation. in *Vascularization for Tissue Engineering and Regenerative Medicine. Reference Series in Biomedical Engineering* (eds. Holnthoner, W., Banfi, W., Kirkpatrick, J. & Redl, H.) 345–383 (Springer, 2021).
55. Bogorad, M. I. *et al.* Review: In vitro microvessel models. *Lab Chip* **15**, 4242–4255 (2015).
56. Schöneberg, J. *et al.* Engineering biofunctional in vitro vessel models using a multilayer bioprinting technique. *Sci. Rep.* **8**, 1–13 (2018).
57. Tomasina, C., Bodet, T., Mota, C., Moroni, L. & Camarero-espinosa, S. Bioprinting Vasculature: Materials, Cells and Emergent Techniques. *Materials (Basel).* **12**, 2701 (2019).
58. Perry, L., Ben-Shaul, S., Landau, S. & Levenberg, S. Co-culture Systems for Vasculogenesis. in *Vascularization for Tissue Engineering and Regenerative Medicine. Reference Series in Biomedical Engineering* (eds. Holnthoner, W., Banfi, W., Kirkpatrick, J. & Redl, H.) 385–413 (Springer, 2021).
59. Milton, L. A., Viglione, M. S., Ong, L. J. Y., Nordin, G. P. & Toh, Y. C. Vat photopolymerization 3D printed microfluidic devices for organ-on-a-chip applications. *Lab Chip* **23**, 3537–3560 (2023).
60. Shuchat, S., Yossifon, G. & Huleihel, M. Perfusion in Organ-on-Chip Models and Its Applicability to the Replication of Spermatogenesis In Vitro. *Int. J. Mol. Sci.* **23**, 1–24 (2022).
61. Nahak, B. K., Mishra, A., Preetam, S. & Tiwari, A. Advances in Organ-on-a-Chip Materials and Devices. *ACS Appl. Bio Mater.* **5**, 3576–3607 (2022).
62. Campbell, S. B. *et al.* Beyond Polydimethylsiloxane: Alternative Materials for Fabrication of Organ-on-a-Chip Devices and Microphysiological Systems. *ACS Biomater. Sci. Eng.* **7**, 2880–2899 (2021).
63. Van Midwoud, P. M., Verpoorte, E. & Groothuis, G. M. M. Microfluidic devices for in vitro studies on liver drug metabolism and toxicity. *Integr. Biol.* **3**, 509–521 (2011).
64. Bilican, I. & Tahsin Guler, M. Assessment of PMMA and polystyrene based microfluidic chips fabricated using CO2 laser machining. *Appl. Surf. Sci.* **534**, 147642 (2020).
65. Kojic, S. P., Stojanovic, G. M. & Radonic, V. Novel cost-effective microfluidic chip based on hybrid fabrication and its comprehensive characterization. *Sensors* **19**, 1719 (2019).
66. Ko, J., Lee, Y., Lee, S., Lee, S. & Jeon, N. L. Human Ocular Angiogenesis-Inspired Vascular Models on an Injection-Molded Microfluidic Chip. *Adv. Healthc. Mater.* **1900328**, 1–10 (2019).
67. Lee, S. R. *et al.* Modeling neural circuit, blood-brain barrier, and myelination on a microfluidic 96 well plate. *Biofabrication* **11**, (2019).
68. Kaden, T. *et al.* Evaluation of drug-induced liver toxicity of trovafloxacin and levofloxacin in a human microphysiological liver model. *Sci. Rep.* **13**, 13338 (2023).

69. Ma, X. *et al.* Injection molding and characterization of PMMA-based microfluidic devices. *Microsyst. Technol.* **26**, 1317–1324 (2020).
70. Nguyen, T., Vinayaka, A. C., Bang, D. D. & Wolff, A. A complete protocol for rapid and low-cost fabrication of polymer microfluidic chips containing three-dimensional microstructures used in point-of-care devices. *Micromachines* **10**, 624 (2019).
71. Lai, B. F. L. *et al.* A well plate–based multiplexed platform for incorporation of organoids into an organ-on-a-chip system with a perfusable vasculature. *Nat. Protoc.* **16**, 2158–2189 (2021).
72. Goldstein, Y. *et al.* Breaking the third wall: Implementing 3d-printing technics to expand the complexity and abilities of multi-organ-on-a-chip devices. *Micromachines* **12**, (2021).
73. Ho, C. M. B., Ng, S. H., Li, K. H. H. & Yoon, Y. J. 3D printed microfluidics for biological applications. *Lab Chip* **15**, 3627–3637 (2015).
74. Au, A. K., Huynh, W., Horowitz, L. F. & Folch, A. 3D-Printed Microfluidics. *Angew. Chemie - Int. Ed.* **55**, 3862–3881 (2016).
75. Park, J. Y. *et al.* Development of a functional airway-on-a-chip by 3D cell printing. *Biofabrication* **11**, 015002 (2019).
76. Urrios, A. *et al.* 3D-printing of transparent bio-microfluidic devices in PEG-DA. *Lab Chip* **16**, 2287–2294 (2016).
77. Macdonald, N. P. *et al.* Comparing Microfluidic Performance of Three-Dimensional (3D) Printing Platforms. *Anal. Chem.* **89**, 3858–3866 (2017).
78. Su, R., Wang, F. & McAlpine, M. C. 3D printed microfluidics: advances in strategies, integration, and applications. *Lab Chip* **23**, 1279–1299 (2023).
79. Salentijn, G. I. J., Oomen, P. E., Grajewski, M. & Verpoorte, E. Fused Deposition Modeling 3D Printing for (Bio)analytical Device Fabrication: Procedures, Materials, and Applications. *Anal. Chem.* **89**, 7053–7061 (2017).
80. Romanov, V. *et al.* FDM 3D Printing of High-Pressure, Heat-Resistant, Transparent Microfluidic Devices. *Anal. Chem.* **90**, 10450–10456 (2018).
81. Bressan, L. P., Adamo, C. B., Quero, R. F., De Jesus, D. P. & Da Silva, J. A. F. A simple procedure to produce FDM-based 3D-printed microfluidic devices with an integrated PMMA optical window. *Anal. Methods* **11**, 1014–1020 (2019).
82. Gross, B. C., Erkal, J. L., Lockwood, S. Y., Chen, C. & Spence, D. M. Evaluation of 3D printing and its potential impact on biotechnology and the chemical sciences. *Anal. Chem.* **86**, 3240–3253 (2014).
83. Bhattacharjee, N., Urrios, A., Kang, S. & Folch, A. The upcoming 3D-printing revolution in microfluidics. *Lab Chip* **16**, 1720–1742 (2016).
84. Kuo, A. P. *et al.* High-Precision Stereolithography of Biomicrofluidic Devices. *Adv. Mater. Technol.* **4**, 1–11 (2019).
85. Gong, H., Bickham, B. P., Woolley, A. T. & Nordin, G. P. Custom 3D printer and resin for 18 μm × 20 μm microfluidic flow channels. *Lab Chip* **17**, 2899–2909 (2017).
86. Bhattacharjee, N., Parra-Cabrera, C., Kim, Y. T., Kuo, A. P. & Folch, A. Desktop-Stereolithography 3D-Printing of a Poly(dimethylsiloxane)-Based Material with Sylgard-184 Properties. *Adv. Mater.* **30**, (2018).
87. Matai, I., Kaur, G., Seyedsalehi, A., McClinton, A. & Laurencin, C. T. Progress in 3D bioprinting technology for tissue/organ regenerative engineering. *Biomaterials* **226**, 119536 (2020).
88. Miri, A. K. *et al.* Bioprinters for organs-on-chips. *Biofabrication* **11**, 042002 (2019).
89. Rothbauer, M. *et al.* Recent Advances in Additive Manufacturing and 3D Bioprinting for Organs-On-A-Chip and Microphysiological Systems. *Front. Bioeng. Biotechnol.* **10**, 1–14 (2022).
90. Carvalho, V. *et al.* 3d printing techniques and their applications to organ-on-a-chip platforms: A systematic review. *Sensors* **21**, (2021).
91. Miri, A. K. *et al.* Effective bioprinting resolution in tissue model fabrication. *Lab Chip*

19, 2019–2037 (2019).
92. Blaeser, A., Duarte Campos, D. F. & Fischer, H. 3D bioprinting of cell-laden hydrogels for advanced tissue engineering. *Curr. Opin. Biomed. Eng.* **2**, 58–66 (2017).
93. Dikyol, C., Altunbek, M., Bartolo, P. & Koc, B. Multimaterial bioprinting approaches and their implementations for vascular and vascularized tissues. *Bioprinting* **24**, e00159 (2021).
94. Park, J. Y., Jang, J. & Kang, H. W. 3D Bioprinting and its application to organ-on-a-chip. *Microelectron. Eng.* **200**, 1–11 (2018).
95. Blaeser, A. *et al.* Controlling Shear Stress in 3D Bioprinting is a Key Factor to Balance Printing Resolution and Stem Cell Integrity. *Adv. Healthc. Mater.* **5**, 326–333 (2016).
96. Xu, H. Q., Liu, J. C., Zhang, Z. Y. & Xu, C. X. A review on cell damage, viability, and functionality during 3D bioprinting. *Mil. Med. Res.* **9**, 1–15 (2022).
97. Adhikari, J. *et al.* Effects of Processing Parameters of 3D Bioprinting on the Cellular Activity of Bioinks. *Macromol. Biosci.* **21**, (2021).
98. Kolesky, D. B. *et al.* 3D bioprinting of vascularized, heterogeneous cell-laden tissue constructs. *Adv. Mater.* **26**, 3124–3130 (2014).
99. Homan, K. A. *et al.* Bioprinting of 3D Convoluted Renal Proximal Tubules on Perfusable Chips. *Sci. Rep.* **6**, 1–13 (2016).
100. Lin, N. Y. C. *et al.* Renal reabsorption in 3D vascularized proximal tubule models. *Proc. Natl. Acad. Sci. U. S. A.* **116**, 5399–5404 (2019).
101. Nothdurfter, D. *et al.* 3D bioprinted, vascularized neuroblastoma tumor environment in fluidic chip devices for precision medicine drug testing. *Biofabrication* **14**, (2022).
102. Hwang, D. G., Choi, Y. M. & Jang, J. 3D Bioprinting-Based Vascularized Tissue Models Mimicking Tissue-Specific Architecture and Pathophysiology for in vitro Studies. *Front. Bioeng. Biotechnol.* **9**, 1–16 (2021).
103. Lindner, N. & Blaeser, A. Scalable Biofabrication : A Perspective on the Current State and Future Potentials of Process Automation in 3D-Bioprinting Applications. *Front. Bioeng. Biotechnol.* **10**, 1–8 (2022).
104. Santoni, S., Gugliandolo, S. G., Sponchioni, M., Moscatelli, D. & Colosimo, B. M. 3D bioprinting: current status and trends—a guide to the literature and industrial practice. *Bio-Design Manuf.* **5**, 14–42 (2022).
105. Azizgolshani, H. *et al.* High-throughput organ-on-chip platform with integrated programmable fluid flow and real-time sensing for complex tissue models in drug development workflows. *Lab Chip* **21**, 1454–1474 (2021).
106. Novak, R. *et al.* Robotic fluidic coupling and interrogation of multiple vascularized organ chips. *Nat. Biomed. Eng.* 1–14 (2020).
107. Peel, S. *et al.* Introducing an automated high content confocal imaging approach for Organs-on-Chips. *Lab Chip* **19**, 410–421 (2019).
108. Konishi, S., Hashimoto, T., Nakabuchi, T., Ozeki, T. & Kajita, H. Cell and tissue system capable of automated culture, stimulation, and monitor with the aim of feedback control of organs-on-a-chip. *Sci. Rep.* **11**, 1–14 (2021).
109. Peel, S. & Jackman, M. Imaging microphysiological systems: A review. *Am. J. Physiol. - Cell Physiol.* **320**, C669–C680 (2021).
110. Gebhardt, A. & Jan-Steffen Hötter. *Additive Manufacturing : 3D Printing for Prototyping and Manufacturing*. (Carl Hanser Verlag GmbH & Co KG, 2016).
111. Chua, C. K. & Leong, K. F. *3D printing and additive manufacturing: principles and application*. (World Scientific, 2015).
112. Srivatsan, T. S. & Sudarshan, T. S. *Additive manufacturing: innovations, advances and applications*. (CRC Press, 2016).
113. Gibson, I., Rosen, D. & Stucker, B. *Additive Manufacturing Technologies: 3D Printing, Rapid Prototyping, and Direct Digital Manufacturing*. (Springer New York, 2015).
114. Luo, Z. *et al.* Digital light processing 3D printing for microfluidic chips with enhanced

resolution via dosing- and zoning-controlled vat photopolymerization. *Microsystems Nanoeng.* **9**, (2023).
115. Amini, A., Guijt, R. M., Themelis, T., De Vos, J. & Eeltink, S. Recent developments in digital light processing 3D-printing techniques for microfluidic analytical devices. *J. Chromatogr. A* **1692**, (2023).
116. Sanchez Noriega, J. L. *et al.* Spatially and optically tailored 3D printing for highly miniaturized and integrated microfluidics. *Nat. Commun.* **12**, (2021).
117. Yu, C. *et al.* Photopolymerizable Biomaterials and Light-Based 3D Printing Strategies for Biomedical Applications. *Chem. Rev.* **120**, 10695–10743 (2020).
118. Fouassier, J. P., Allonas, X. & Burget, D. Photopolymerization reactions under visible lights: Principle, mechanisms and examples of applications. *Prog. Org. Coatings* **47**, 16–36 (2003).
119. Ligon-Auer, S. C., Schwentenwein, M., Gorsche, C., Stampfl, J. & Liska, R. Toughening of photo-curable polymer networks: A review. *Polym. Chem.* **7**, 257–286 (2016).
120. Bao, Y. Recent Trends in Advanced Photoinitiators for Vat Photopolymerization 3D Printing. *Macromol. Rapid Commun.* **43**, 1–15 (2022).
121. Huh, J. T. *et al.* Combinations of photoinitiator and UV absorber for cell-based digital light processing (DLP) bioprinting. *Biofabrication* **13**, (2021).
122. Oskui, S. M. *et al.* Assessing and Reducing the Toxicity of 3D-Printed Parts. *Environ. Sci. Technol. Lett.* **3**, 1–6 (2016).
123. Zeng, B. *et al.* Cytotoxic and cytocompatible comparison among seven photoinitiators-triggered polymers in different tissue cells. *Toxicol. Vitr.* **72**, (2021).
124. Xu, H., Casillas, J., Krishnamoorthy, S. & Xu, C. Effects of Irgacure 2959 and lithium phenyl-2,4,6-trimethylbenzoylphosphinate on cell viability, physical properties, and microstructure in 3D bioprinting of vascular-like constructs. *Biomed. Mater.* **15**, (2020).
125. Richter, M. *et al.* From Donor to the Lab: A Fascinating Journey of Primary Cell Lines. *Front. Cell Dev. Biol.* **9**, 1–11 (2021).
126. Pan, C., Kumar, C., Bohl, S., Klingmueller, U. & Mann, M. Comparative proteomic phenotyping of cell lines and primary cells to assess preservation of cell type-specific functions. *Mol. Cell. Proteomics* **8**, 443–450 (2009).
127. Schmitz, S. Zellkulturen, Zelllinien und Primärkultur. in *Der Experimentator: Zellkultur* 95–125 (Springer Spektrum, 2020).
128. Kaur, G. & Dufour, J. M. Cell lines. *Spermatogenesis* **2**, 1–5 (2012).
129. Castan, A., Schulz, P., Wenger, T. & Fischer, S. *Cell Line Development*. *Biopharmaceutical Processing: Development, Design, and Implementation of Manufacturing Processes* (Elsevier Ltd., 2018).
130. Ruben, A. J. & Biology, E. Hayflick model. *Nat. Rev. Mol. Cell Biol.* **1**, 72–76 (2000).
131. Aden, D. P., Fogel, A., Plotkin, S., Damjanov, I. & Knowles, B. B. Controlled synthesis of HBsAg in a differentiated human liver carcinoma-derived cell line. *Nature* **282**, 615–616 (1979).
132. Arzumanian, V. A., Kiseleva, O. I. & Poverennaya, E. V. The curious case of the HepG2 cell line: 40 years of expertise. *Int. J. Mol. Sci.* **22**, (2021).
133. Donato, M. T., Tolosa, L. & Gómez-Lechón, M. J. Culture and Functional Characterization of Human Hepatoma HepG2 Cells. *Protoc. Vitr. Hepatocyte Res.* **1250**, 1–390 (2015).
134. Sun, L. *et al.* Application of a 3D Bioprinted Hepatocellular Carcinoma Cell Model in Antitumor Drug Research. *Front. Oncol.* **10**, 1–12 (2020).
135. Maloney, E. *et al.* Immersion bioprinting of tumor organoids in multi-well plates for increasing chemotherapy screening throughput. *Micromachines* **11**, (2020).
136. Kammerer, S. Three-dimensional liver culture systems to maintain primary hepatic properties for toxicological analysis in vitro. *Int. J. Mol. Sci.* **22**, (2021).
137. Ringelhan, M., Pfister, D., O'Connor, T., Pikarsky, E. & Heikenwalder, M. The immunology of hepatocellular carcinoma. *Nat. Immunol.* **19**, 222–232 (2018).

138. Angelico, R., Grimaldi, C., Saffioti, M. C., Castellano, A. & Spada, M. Hepatocellular carcinoma in children: Hepatic resection and liver transplantation. *Transl. Gastroenterol. Hepatol.* **3**, 1–10 (2018).
139. Jaffe, E. A., Nachman, R. L., Becker, C. G. & Minick, C. R. Culture of human endothelial cells derived from umbilical veins. Identification by morphologic and immunologic criteria. *J. Clin. Invest.* **52**, 2745–2756 (1973).
140. Nachman, R. L. & Jaffe, E. A. Endothelial cell culture: Beginnings of modern vascular biology. *J. Clin. Invest.* **114**, 1037–1040 (2004).
141. Alberts, B. *et al. Molecular Biology of the Cell*. *Garland Science* (Garland Science, 2002).
142. Plikus, M. V. *et al.* Fibroblasts: Origins, definitions, and functions in health and disease. *Cell* **184**, 3852–3872 (2021).
143. Jones, K. H. & Senft, J. A. An improved method to determine cell viability by simultaneous staining with fluorescein diacetate-propidium iodide. *J. Histochem. Cytochem.* **33**, 77–79 (1985).
144. Riccardi, C. & Nicoletti, I. Analysis of apoptosis by propidium iodide staining and flow cytometry. *Nat. Protoc.* **1**, 1458–1461 (2006).
145. Persidsky, M. D. & Baillie, G. S. Fluorometric test of cell membrane integrity. *Cryobiology* **14**, 322–331 (1977).
146. Riss, T. L. *et al.* Cell Viability Assays. *Assay Guid. Man.* 1–25 (2004).
147. O'Brien, J., Wilson, I., Orton, T. & Pognan, F. Investigation of the Alamar Blue (resazurin) fluorescent dye for the assessment of mammalian cell cytotoxicity. *Eur. J. Biochem.* **267**, 5421–5426 (2000).
148. Voytik-Harbin, S. L., Waisner, A. O. B. B., Lamar, C. H., Stephen, D. & Badylak, E. Applications and Evaluation of the AlamarBlue Assay for Cell Growth and Survival of Fibroblasts. *Vitr. Cell. Dev. Biol. - Anim.* **34**, 239–246 (1998).
149. Kapuscinski, J. DAPI: a DNA-Specific Fluorescent Probe. *Biotech. Histochem.* **70**, 220–233 (1995).
150. Li, K., Pu, K. Y., Cai, L. & Liu, B. Phalloidin-functionalized hyperbranched conjugated polyelectrolyte for filamentous actin imaging in living Hela cells. *Chem. Mater.* **23**, 2113–2119 (2011).
151. Im, K., Mareninov, S., Diaz, M. F. P. & Yong, W. H. An Introduction to Performing Immunofluorescence Staining. in *Biobanking. Methods in Molecular Biology* (ed. Yong, W. H.) vol. 1897 299–311 (Humana Press, 2019).
152. Engvall, E. & Perlmann, P. Enzyme-linked immunosorbent assay (ELISA) quantitative assay of immunoglobulin G. *Immunochemistry* **8**, 871–874 (1971).
153. Lin, A. V. Indirect ELISA. in *ELISA. Methods in Molecular Biology Methods in Molecular Biology* (ed. Hnasko, R.) vol. 1318 51–59 (Humana Press, New York, NY, 2015).
154. Stanker, L. H. & Hnasko, R. M. A Double-Sandwich ELISA for Identification of Monoclonal Antibodies Suitable for Sandwich Immunoassays. in *ELISA. Methods in Molecular Biology* (ed. Hnasko, R.) vol. 1318 69–78 (Humana Press, 2015).
155. Discher, D. E., Janmey, P. & Wang, Y. L. Tissue cells feel and respond to the stiffness of their substrate. *Science* vol. 310 1139–1143 (2005).
156. Engler, A. J., Sen, S., Sweeney, H. L. & Discher, D. E. Matrix Elasticity Directs Stem Cell Lineage Specification. *Cell* **126**, 677–689 (2006).
157. Langhans, S. A. Three-dimensional in vitro cell culture models in drug discovery and drug repositioning. *Front. Pharmacol.* **9**, 1–14 (2018).
158. Skardal, A., Mack, D., Atala, A. & Sokern, S. Substrate elasticity controls cell proliferation, surface marker expression and motile phenotype in amniotic fluid-derived stem cells. *J. Mech. Behav. Biomed. Mater.* **17**, 307–316 (2013).
159. Jensen, C. & Teng, Y. Is It Time to Start Transitioning From 2D to 3D Cell Culture? *Front. Mol. Biosci.* **7**, 1–15 (2020).
160. Lavrentina, A. & Spencer-Fry, J. Hydrogels for 3D Cell Culture. in *Basic Concepts on 3D Cell Culture. Learning Materials in Biosciences* (eds. Kasper, C., Egger, D. & Lavrentina,

A.) 201–232 (Springer, 2021).
161. Unagolla, J. M. & Jayasuriya, A. C. Hydrogel-based 3D bioprinting: A comprehensive review on cell-laden hydrogels, bioink formulations, and future perspectives. *Appl. Mater. Today* 100479 (2019).
162. Parak, A. *et al.* Functionalizing bioinks for 3D bioprinting applications. *Drug Discov. Today* **24**, 198–205 (2019).
163. Decante, G. *et al.* Engineering bioinks for 3D bioprinting. *Biofabrication* **13**, (2021).
164. Hoffman, A. S. Hydrogels for biomedical applications. *Adv. Drug Deliv. Rev.* **64**, 18–23 (2012).
165. Bella, J. Collagen structure: New tricks from a very old dog. *Biochem. J.* **473**, 1001–1025 (2016).
166. Darvish, D. M. Collagen fibril formation in vitro: From origin to opportunities. *Mater. Today Bio* **15**, 100322 (2022).
167. Parenteau-Bareil, R., Gauvin, R. & Berthod, F. Collagen-based biomaterials for tissue engineering applications. *Materials (Basel)*. **3**, 1863–1887 (2010).
168. Holder, A. J. *et al.* Control of collagen gel mechanical properties through manipulation of gelation conditions near the sol-gel transition. *This J. is Cite this Soft Matter* **14**, 574 (2018).
169. Das, S. & Basu, B. An Overview of Hydrogel-Based Bioinks for 3D Bioprinting of Soft Tissues. *J. Indian Inst. Sci.* **99**, 405–428 (2019).
170. Haug, I. J. & Draget, K. I. Gelatin. in *Handbook of Food Proteins* 92–115 (2011).
171. Valot, L., Martinez, J., Mehdi, A. & Subra, G. Chemical insights into bioinks for 3D printing. *Chem. Soc. Rev.* **48**, 4049–4086 (2019).
172. Donderwinkel, I., Van Hest, J. C. M. & Cameron, N. R. Bio-inks for 3D bioprinting: Recent advances and future prospects. *Polym. Chem.* **8**, 4451–4471 (2017).
173. Shpichka, A. *et al.* Fibrin-based bioinks: New tricks from an old dog. *Int. J. Bioprinting* **6**, 1–14 (2020).
174. Weisel, J. W. & Litvinov, R. I. Mechanisms of fibrin polymerization and clinical implications. *Blood* **121**, 1712–1719 (2013).
175. Brown, A. C. & Barker, T. H. Fibrin-based biomaterials: Modulation of macroscopic properties through rational design at the molecular level. *Acta Biomater.* **10**, 1502–1514 (2014).
176. Gopinathan, J. & Noh, I. Recent trends in bioinks for 3D printing. *Biomaterials Research* vol. 22 (2018).
177. Hospodiuk, M., Dey, M., Sosnoski, D. & Ozbolat, I. T. The bioink: A comprehensive review on bioprintable materials. *Biotechnol. Adv.* **35**, 217–239 (2017).
178. Forget, A. *et al.* Mechanically Tunable Bioink for 3D Bioprinting of Human Cells. *Adv. Healthc. Mater.* **6**, 1–7 (2017).
179. Normand, V., Lootens, D. L., Amici, E., Plucknett, K. P. & Aymard, P. New Insight into Agarose Gel Mechanical Properties. *Biomacromolecules* **1**, 730–738 (2000).
180. Mezger, T. C. *The rheology handbook: for users of rotational and oscillatory theometers*. (Vincentz Network, 2014).
181. Osswald, T. & Rudolph, N. *Polymer rheology: fundamentals and applications*. (Hanser, 2015).
182. Shaw, M. *Introduction to polymer rheology*. (Wiley, 2012).
183. Deshpande, A. P., Krishnan, J. M. & Kumar, P. B. S. *Rheology of complex fluids*. (Springer, 2010).
184. Stojkov, G., Niyazov, Z., Picchioni, F. & Bose, R. K. Relationship between structure and rheology of hydrogels for various applications. *Gels* **7**, (2021).
185. Chen, M. H. *et al.* Methods to Assess Shear-Thinning Hydrogels for Application As Injectable Biomaterials. *ACS Biomater. Sci. Eng.* **3**, 3146–3160 (2017).
186. Lan, X., Adesida, A. & Boluk, Y. Rheological and viscoelastic properties of collagens and their role in bioprinting by micro-extrusion. *Biomed. Mater.* **17**, (2022).

187. Malda, J. *et al.* 25th anniversary article: Engineering hydrogels for biofabrication. *Advanced Materials* vol. 25 5011–5028 (2013).
188. Herrada-Manchón, H., Fernández, M. A. & Aguilar, E. Essential Guide to Hydrogel Rheology in Extrusion 3D Printing: How to Measure It and Why It Matters? *Gels* **9**, (2023).
189. Chaudhuri, O., Cooper-White, J., Janmey, P. A., Mooney, D. J. & Shenoy, V. B. Effects of extracellular matrix viscoelasticity on cellular behaviour. *Nature* **584**, 535–546 (2020).
190. Ma, Y. *et al.* Viscoelastic Cell Microenvironment: Hydrogel-Based Strategy for Recapitulating Dynamic ECM Mechanics. *Adv. Funct. Mater.* **31**, 1–26 (2021).
191. Liu, C. *et al.* Engineering the viscoelasticity of gelatin methacryloyl (GelMA) hydrogels via small “dynamic bridges” to regulate BMSC behaviors for osteochondral regeneration. *Bioact. Mater.* **25**, 445–459 (2023).
192. Ji, S. & Guvendiren, M. Recent Advances in Bioink Design for 3D Bioprinting of Tissues and Organs. *Front. Bioeng. Biotechnol.* **5**, 1–8 (2017).
193. Groll, J. *et al.* A definition of bioinks and their distinction from biomaterial inks. *Biofabrication* **11**, 013001 (2018).
194. Yu, Y. *et al.* Three-dimensional bioprinting using self-Assembling scalable scaffold-free ‘tissue strands’ as a new bioink. *Sci. Rep.* **6**, 1–11 (2016).
195. Khoshnood, N. & Zamanian, A. A comprehensive review on scaffold-free bioinks for bioprinting. *Bioprinting* **19**, e00088 (2020).
196. Ozbolat, I. T. Scaffold-Based or Scaffold-Free Bioprinting: Competing or Complementing Approaches? *J. Nanotechnol. Eng. Med.* **6**, 1–6 (2015).
197. Moldovan, N. I., Hibino, N. & Nakayama, K. Principles of the kenzan method for robotic cell spheroid-based three-dimensional bioprinting. *Tissue Eng. - Part B Rev.* **23**, 237–244 (2017).
198. Murata, D., Arai, K. & Nakayama, K. Scaffold-Free Bio-3D Printing Using Spheroids as “Bio-Inks” for Tissue (Re-)Construction and Drug Response Tests. *Adv. Healthc. Mater.* **9**, 1–18 (2020).
199. Zhang, J., Wehrle, E., Rubert, M. & Müller, R. 3d bioprinting of human tissues: Biofabrication, bioinks and bioreactors. *Int. J. Mol. Sci.* **22**, (2021).
200. Mancha Sánchez, E. *et al.* Hydrogels for Bioprinting: A Systematic Review of Hydrogels Synthesis, Bioprinting Parameters, and Bioprinted Structures Behavior. *Front. Bioeng. Biotechnol.* **8**, (2020).
201. Wang, H. *et al.* An Overview of Extracellular Matrix-Based Bioinks for 3D Bioprinting. *Front. Bioeng. Biotechnol.* **10**, 1–17 (2022).
202. Hölzl, K. *et al.* Bioink properties before, during and after 3D bioprinting. *Biofabrication* **8**, (2016).
203. Boularaoui, S., Al Hussein, G., Khan, K. A., Christoforou, N. & Stefanini, C. An overview of extrusion-based bioprinting with a focus on induced shear stress and its effect on cell viability. *Bioprinting* **20**, e00093 (2020).
204. Dobos, A. *et al.* On-chip high-definition bioprinting of microvascular structures. *Biofabrication* **13**, (2020).
205. Tytgat, L. *et al.* High-Resolution 3D Bioprinting of Photo-Cross-linkable Recombinant Collagen to Serve Tissue Engineering Applications. *Biomacromolecules* **21**, 3997–4007 (2020).
206. Zandrini, T., Florczak, S., Levato, R. & Ovsianikov, A. Breaking the resolution limits of 3D bioprinting: future opportunities and present challenges. *Trends Biotechnol.* **41**, 604–614 (2023).
207. Zuev, D. M., Nguyen, A. K., Putlyaev, V. I. & Narayan, R. J. 3D printing and bioprinting using multiphoton lithography. *Bioprinting* **20**, e00090 (2020).
208. Nieto, D., Marchal Corrales, J. A., Jorge De Mora, A. & Moroni, L. Fundamentals of light-cell-polymer interactions in photo-cross-linking based bioprinting. *APL Bioeng.* **4**,

(2020).
209. Bernal, P. N. *et al.* Volumetric Bioprinting of Complex Living-Tissue Constructs within Seconds. *Adv. Mater.* **31**, (2019).
210. Rizzo, R., Ruetsche, D., Liu, H. & Zenobi-Wong, M. Optimized Photoclick (Bio)Resins for Fast Volumetric Bioprinting. *Adv. Mater.* **33**, (2021).
211. Bernal, P. N. *et al.* Volumetric Bioprinting of Organoids and Optically Tuned Hydrogels to Build Liver-Like Metabolic Biofactories. *Adv. Mater.* **34**, (2022).
212. Gudapati, H., Dey, M. & Ozbolat, I. A comprehensive review on droplet-based bioprinting: Past, present and future. *Biomaterials* **102**, 20–42 (2016).
213. Ashammakhi, N. *et al.* Bioinks and bioprinting technologies to make heterogeneous and biomimetic tissue constructs. *Mater. Today Bio* **1**, 100008 (2019).
214. Duarte Campos, D. F. & Blaeser, A. 3D-Bioprinting. in *Basic Concepts on 3D Cell Culture. Learning Materials in Biosciences* (eds. Kasper, C., Egger, D. & Lavrentieva, A.) 201–232 (Springer, 2021).
215. Ng, W. L., Lee, J. M., Yeong, W. Y. & Win Naing, M. Microvalve-based bioprinting-process, bio-inks and applications. *Biomater. Sci.* **5**, 632–647 (2017).
216. Sun, J. *et al.* Comparison of micro-dispensing performance between micro-valve and piezoelectric printhead. *Microsyst. Technol.* **15**, 1437–1448 (2009).
217. Jang, D., Kim, D. & Moon, J. Influence of fluid physical properties on ink-jet printability. *Langmuir* **25**, 2629–2635 (2009).
218. Chen, X., O'Mahony, A. P. & Barber, T. Experimental study of the stable droplet formation process during micro-valve-based three-dimensional bioprinting. *Phys. Fluids* **35**, (2023).
219. Chen, X., OMahony, A. P. & Barber, T. The assessment of average cell number inside in-flight 3D printed droplets in microvalve-based bioprinting. *J. Appl. Phys.* **131**, (2022).
220. Zhang, Z. *et al.* Evaluation of bioink printability for bioprinting applications. *Appl. Phys. Rev.* **5**, (2018).
221. Liu, H. *et al.* Advances in Hydrogels in Organoids and Organs-on-a-Chip. *Adv. Mater.* **31**, 1–28 (2019).
222. Fromm, J. E. Numerical Calculation of the Fluid Dynamics of Drop-on-Demand Jets. *IBM J. Res. Dev.* **28**, 322–333 (1984).
223. Liu, Y. & Derby, B. Experimental study of the parameters for stable drop-on-demand inkjet performance. *Phys. Fluids* **31**, (2019).
224. Derby, B. Inkjet printing ceramics: From drops to solid. *J. Eur. Ceram. Soc.* **31**, 2543–2550 (2011).
225. Shi, J. *et al.* Shear stress analysis and its effects on cell viability and cell proliferation in drop-on-demand bioprinting. *Biomed. Phys. Eng. Express* **4**, (2018).
226. Mao, T., Kuhn, D. C. S. & Tran, H. Spread and Rebound of Liquid Droplets upon Impact on Flat Surfaces. *AIChE J.* **43**, 2169–2179 (1997).
227. Caballero, D., Blackburn, S. M., De Pablo, M., Samitier, J. & Albertazzi, L. Tumour-vessel-on-a-chip models for drug delivery. *Lab Chip* **17**, 3760–3771 (2017).
228. Tabatabaei Rezaei, N. *et al.* Recent Advances in Organ-on-Chips Integrated with Bioprinting Technologies for Drug Screening. *Adv. Healthc. Mater.* **12**, 1–22 (2023).
229. Huh, D. *et al.* Reconstituting Organ-Level Lung Functions on a Chip. *Science (80-.).* **328**, 1662–1668 (2010).
230. Douville, N. J. *et al.* Combination of fluid and solid mechanical stresses contribute to cell death and detachment in a microfluidic alveolar model. *Lab Chip* **11**, 609–619 (2011).
231. Plebani, R. *et al.* Modeling pulmonary cystic fibrosis in a human lung airway-on-a-chip. *J. Cyst. Fibros.* **21**, 606–615 (2022).
232. Bein, A. *et al.* Nutritional deficiency in an intestine-on-a-chip recapitulates injury hallmarks associated with environmental enteric dysfunction. *Nat. Biomed. Eng.* **6**, 1236–1247 (2022).

233. Bein, A. *et al.* Enteric Coronavirus Infection and Treatment Modeled With an Immunocompetent Human Intestine-On-A-Chip. *Front. Pharmacol.* **12**, 1–11 (2021).
234. Zhou, M. *et al.* Development of a Functional Glomerulus at the Organ Level on a Chip to Mimic Hypertensive Nephropathy. *Sci. Rep.* **6**, 1–13 (2016).
235. Douville, N. J. *et al.* Fabrication of Two-Layered Channel System with Embedded Electrodes to Measure Resistance Across Epithelial and Endothelial Barriers. *Anal. Chem.* **82**, 2505–2511 (2010).
236. Ewart, L. *et al.* Performance assessment and economic analysis of a human Liver-Chip for predictive toxicology. *Commun. Med.* **2**, 1–16 (2022).
237. Si, L., Bai, H., Rodas, M. & Ingber, D. E. A human-airway-on-a-chip for the rapid identification of candidate antiviral therapeutics and prophylactics. *Nat. Biomed. Eng.* **5**, 815–829 (2021).
238. Bersini, S. *et al.* A microfluidic 3D in vitro model for specificity of breast cancer metastasis to bone. *Biomaterials* **35**, 2454–2461 (2014).
239. Du, B., Tsui, O. K. C., Zhang, Q. & He, T. Study of elastic modulus and yield strength of polymer thin films using atomic force microscopy. *Langmuir* **17**, 3286–3291 (2001).
240. Zervantonakis, I. K., Hughes-alford, S. K., Charest, J. L. & Condeelis, J. S. Three-dimensional microfluidic model for tumor cell intravasation and endothelial barrier function. *Proc. Natl. Acad. Sci. U. S. A.* **109**, 03515–13520 (2012).
241. Adriani, G., Ma, D., Pavesi, A., Kamm, R. D. & Goh, E. L. K. A 3D neurovascular microfluidic model consisting of neurons, astrocytes and cerebral endothelial cells as a blood–brain barrier. *Lab Chip* **17**, 448–459 (2017).
242. He, J. *et al.* Fabrication of nature-inspired microfluidic network for perfusable tissue constructs. *Adv. Healthc. Mater.* **2**, 1108–1113 (2013).
243. Mao, M. *et al.* Leaf-templated, microwell-integrated microfluidic chips for high-throughput cell experiments. *Biofabrication* **10**, 25008 (2018).
244. Mao, M. *et al.* Human-on-Leaf-Chip: A Biomimetic Vascular System Integrated with Chamber-Specific Organs. *Small* **16**, 1–11 (2020).
245. Bellan, L. M. *et al.* Fabrication of an artificial 3-dimensional vascular network using sacrificial sugar structures. *Soft Matter* **5**, 1354–1357 (2009).
246. Brumm, P., Fritschen, A., Dob, L., Dorsam, E. & Blaeser, A. Fabrication of biomimetic networks using viscous fingering in flexographic printing. *Biomed. Mater.* **17**, (2022).
247. Ling, Y. *et al.* A cell-laden microfluidic hydrogel. *Lab Chip* **7**, 756–762 (2007).
248. Zheng, Y. *et al.* In vitro microvessels for the study of angiogenesis and thrombosis. *Proc. Natl. Acad. Sci. U. S. A.* **109**, 9342–9347 (2012).
249. Golden, A. P. & Tien, J. Fabrication of microfluidic hydrogels using molded gelatin as a sacrificial element. *Lab Chip* **7**, 720–725 (2007).
250. Rein, J. L. *et al.* Effect of luminal flow on doming of mpkCCD cells in a 3D perfusable kidney cortical collecting duct model. *Am. J. Physiol. - Cell Physiol.* **318**, C136–C147 (2020).
251. Chrobak, K. M., Potter, D. R. & Tien, J. Formation of perfused, functional microvascular tubes in vitro. *Microvasc. Res.* **71**, 185–196 (2006).
252. Carracedo, M. *et al.* 3D vascularised proximal tubules-on-a-multiplexed chip model for enhanced cell phenotypes. *Lab Chip* **23**, 3226–3237 (2023).
253. Aceves, J. O. *et al.* 3D proximal tubule-on-chip model derived from kidney organoids with improved drug uptake. *Sci. Rep.* **12**, 1–14 (2022).
254. Hasan, A., Paul, A., Memic, A. & Khademhosseini, A. A multilayered microfluidic blood vessel-like structure. *Biomed. Microdevices* **17**, 1–13 (2015).
255. Bertassoni, L. *et al.* Hydrogel bioprinted microchannel networks for vascularization of tissue engineering constructs. *Lab Chip* **14**, 2202–2211 (2014).
256. Massa, S. *et al.* Bioprinted 3D vascularized tissue model for drug toxicity analysis. *Biomicrofluidics* **11**, (2017).

257. Duarte Campos, D. F. *et al.* Bioprinting Cell- and Spheroid-Laden Protein-Engineered Hydrogels as Tissue-on-Chip Platforms. *Front. Bioeng. Biotechnol.* **8**, 1–13 (2020).
258. Noor, N. *et al.* 3D Printing of Personalized Thick and Perfusable Cardiac Patches and Hearts. *Adv. Sci.* **6**, (2019).
259. Campos, D. F. D. *et al.* Synchronized Dual Bioprinting of Bioinks and Biomaterial Inks as a Translational Strategy for Cartilage Tissue Engineering. *3D Print. Addit. Manuf.* **6**, 63–71 (2019).
260. Skylar-Scott, M. A. *et al.* Biomanufacturing of organ-specific tissues with high cellular density and embedded vascular channels. *Sci. Adv.* **5**, (2019).
261. Kolesky, D. B., Homan, K. A., Skylar-Scott, M. A. & Lewis, J. A. Three-dimensional bioprinting of thick vascularized tissues. *Proc. Natl. Acad. Sci. U. S. A.* **113**, 3179–3184 (2016).
262. Miller, J. S. *et al.* Rapid casting of patterned vascular networks for perfusable engineered three-dimensional tissues. *Nat. Mater.* **11**, 768–774 (2012).
263. Pi, Q. *et al.* Digitally Tunable Microfluidic Bioprinting of Multilayered Cannular Tissues. *Adv. Mater.* **30**, 1–10 (2018).
264. Jia, W. *et al.* Direct 3D bioprinting of perfusable vascular constructs using a blend bioink. *Biomaterials* **106**, 58–68 (2016).
265. Blaeser, A. *et al.* Laser-based in situ embedding of metal nanoparticles into bioextruded alginate hydrogel tubes enhances human endothelial cell adhesion. *Nano Res.* **9**, 3407–3427 (2016).
266. Wang, X., Sun, Q. & Pei, J. Microfluidic-based 3D engineered microvascular networks and their applications in vascularized microtumor models. *Micromachines* **9**, 1–26 (2018).
267. Tronolone, J. J. & Jain, A. Engineering New Microvascular Networks On-Chip: Ingredients, Assembly, and Best Practices. *Adv. Funct. Mater.* **31**, 1–19 (2021).
268. Lee, Y. *et al.* Microfluidics within a well: An injection-molded plastic array 3D culture platform. *Lab Chip* **18**, 2433–2440 (2018).
269. Phan, D. T. T. *et al.* A vascularized and perfused organ-on-a-chip platform for large-scale drug screening applications. *Lab Chip* **17**, 511–520 (2017).
270. Sobrino, A. *et al.* 3D microtumors in vitro supported by perfused vascular networks. *Sci. Rep.* **6**, 1–11 (2016).
271. Lee, V. K. *et al.* Creating perfused functional vascular channels using 3D bio-printing technology. *Biomaterials* **35**, 8092–8102 (2014).
272. Lee, V. K. *et al.* Generation of multi-scale vascular network system within 3D hydrogel using 3D bio-printing technology. *Cell. Mol. Bioeng.* **7**, 460–472 (2014).
273. Lee, W. *et al.* On-demand three-dimensional freeform fabrication of multi-layered hydrogel scaffold with fluidic channels. *Biotechnol. Bioeng.* **105**, 1178–1186 (2010).
274. Bang, S., Lee, S., Ko, J., Son, K. & Tahk, D. A Low Permeability Microfluidic Blood-Brain Barrier Platform with Direct Contact between Perfusable Vascular Network and Astrocytes. *Sci. Rep.* **7**, 8083 (2017).
275. Cuchiara, M. P., Gould, D. J., McHale, M. K., Dickinson, M. E. & West, J. L. Integration of self-assembled microvascular networks with microfabricated PEG-based hydrogels. *Adv. Funct. Mater.* **22**, 4511–4518 (2012).
276. Chen, Y. C. *et al.* Functional human vascular network generated in photocrosslinkable gelatin methacrylate hydrogels. *Adv. Funct. Mater.* **22**, 2027–2039 (2012).
277. Chiu, L. L. Y., Montgomery, M., Liang, Y., Liu, H. & Radisic, M. Perfusable branching microvessel bed for vascularization of engineered tissues. *Proc. Natl. Acad. Sci. U. S. A.* **109**, (2012).
278. Campisi, M. *et al.* 3D self-organized microvascular model of the human blood-brain barrier with endothelial cells, pericytes and astrocytes. *Biomaterials* **180**, 117–129 (2018).

279. Wang, X. *et al.* Engineering anastomosis between living capillary networks and endothelial cell-lined microfluidic channels. *Lab Chip* **16**, 282–290 (2016).
280. Paek, J. *et al.* Microphysiological Engineering of Self-Assembled and Perfusable Microvascular Beds for the Production of Vascularized Three-Dimensional Human Microtissues. *ACS Nano* **13**, 7627–7643 (2019).
281. Zhao, L., Lee, V. K., Yoo, S. S., Dai, G. & Intes, X. The integration of 3-D cell printing and mesoscopic fluorescence molecular tomography of vascular constructs within thick hydrogel scaffolds. *Biomaterials* **33**, 5325–5332 (2012).
282. Ko, J. *et al.* Tumor spheroid-on-a-chip: A standardized microfluidic culture platform for investigating tumor angiogenesis. *Lab Chip* **19**, 2822–2833 (2019).
283. Kosyakova, N. *et al.* Differential functional roles of fibroblasts and pericytes in the formation of tissue-engineered microvascular networks in vitro. *npj Regen. Med.* **5**, (2020).
284. Mayer, H. *et al.* Vascular endothelial growth factor (VEGF-A) expression in human mesenchymal stem cells: Autocrine and paracrine role on osteoblastic and endothelial differentiation. *J. Cell. Biochem.* **95**, 827–839 (2005).
285. Caplan, A. I. Mesenchymal stem cells: Time to change the name! *Stem Cells Transl. Med.* **6**, 1445–1451 (2017).
286. Wang, J. D., Douville, N. J., Takayama, S. & Elsayed, M. Quantitative analysis of molecular absorption into PDMS microfluidic channels. *Ann. Biomed. Eng.* **40**, 1862–1873 (2012).
287. Toepke, M. W. & Beebe, D. J. PDMS absorption of small molecules and consequences in microfluidic applications. *Lab Chip* **6**, 1484–1486 (2006).
288. van Meer, B. J. *et al.* Small molecule absorption by PDMS in the context of drug response bioassays. *Biochem. Biophys. Res. Commun.* **482**, 323–328 (2017).
289. Li, L. *et al.* X-ray microscopy studies of protein adsorption on a phase-segregated polystyrene/polymethyl methacrylate surface. 1. Concentration and exposure-time dependence for albumin adsorption. *J. Phys. Chem. B* **110**, 16763–16773 (2006).
290. Li, N., Schwartz, M. & Ionescu-Zanetti, C. PDMS compound adsorption in context. *J. Biomol. Screen.* **14**, 194–202 (2009).
291. Warr, C. *et al.* Biocompatible PEGDA Resin for 3D Printing. *ACS Appl. Bio Mater.* **3**, 2239–2244 (2020).
292. Gong, H., Beauchamp, M., Perry, S., Woolley, A. T. & Nordin, G. P. Optical approach to resin formulation for 3D printed microfluidics. *RSC Adv.* **5**, 106621–106632 (2015).
293. Beckwith, A. L., Borenstein, J. T. & Velasquez-Garcia, L. F. Monolithic, 3D-Printed microfluidic platform for recapitulation of dynamic tumor microenvironments. *J. Microelectromechanical Syst.* **27**, 1009–1022 (2018).
294. Takenaga, S. *et al.* Fabrication of biocompatible lab-on-chip devices for biomedical applications by means of a 3D-printing process. *Phys. Status Solidi Appl. Mater. Sci.* **212**, 1347–1352 (2015).
295. Bäckström, S. *et al.* Tailoring Properties of Biocompatible PEG-DMA Hydrogels with UV Light. *Mater. Sci. Appl.* **03**, 425–431 (2012).
296. De Veij, M., Vandenabeele, P., De Beer, T., Remon, J. P. & Moens, L. Reference database of Raman spectra of pharmaceutical excipients. *J. Raman Spectrosc.* **40**, 297–307 (2009).
297. Lambert, J. B., Gronert, S., Shurvell, H. F. & Lightner, D. A. *Spektroskopie - Strukturaufklärung in der Organischen Chemie*. (Pearson, 2012).
298. Štampar, M., Breznik, B., Filipič, M. & Žegura, B. Characterization of In Vitro 3D Cell Model Developed from Human Hepatocellular Carcinoma (HepG2) Cell Line. *Cells* **9**, (2020).
299. Lv, W. *et al.* Constructing biomimetic liver models through biomaterials and vasculature engineering. *Regen. Biomater.* **9**, (2022).
300. Müsch, A. & Arias, I. M. Hepatocyte Surface Polarity. in *The Liver. Biology and*

Pathobiology (eds. Rias, I. M. et al.) 36–49 (John Wiley & Sons, Ltd, 2020).
301. Donato, M., Jover, R. & Gómez-Lechón, M. Hepatic Cell Lines for Drug Hepatotoxicity Testing: Limitations and Strategies to Upgrade their Metabolic Competence by Gene Engineering. *Curr. Drug Metab.* **14**, 946–968 (2013).
302. Ma, X. *et al.* Rapid 3D bioprinting of decellularized extracellular matrix with regionally varied mechanical properties and biomimetic microarchitecture. *Biomaterials* **185**, 310–321 (2018).
303. Zhu, W. *et al.* Direct 3D bioprinting of prevascularized tissue constructs with complex microarchitecture. *Biomaterials* **124**, 106–115 (2018).
304. Köpf, M., Campos, D. F. D., Blaeser, A., Sen, K. S. & Fischer, H. A tailored three-dimensionally printable agarose-collagen blend allows encapsulation, spreading, and attachment of human umbilical artery smooth muscle cells. *Biofabrication* **8**, 1–15 (2016).
305. Kreimendahl, F. *et al.* Three-Dimensional Printing and Angiogenesis: Tailored Agarose-Type i Collagen Blends Comprise Three-Dimensional Printability and Angiogenesis Potential for Tissue-Engineered Substitutes. *Tissue Eng. - Part C Methods* **23**, 604–615 (2017).
306. Lake, S. P., Hald, E. S. & Barocas, V. H. Collagen-agarose co-gels as a model for collagen–matrix interaction in soft tissues subjected to indentation. *J. Biomed. Mater. Res. Part A* **99A**, 507–515 (2011).
307. Duarte Campos, D. F. *et al.* Bioprinting Organotypic Hydrogels with Improved Mesenchymal Stem Cell Remodeling and Mineralization Properties for Bone Tissue Engineering. *Adv. Healthc. Mater.* **5**, 1336–1345 (2016).
308. Patterson, J., Martino, M. M. & Hubbell, J. A. Biomimetic materials in tissue engineering. *Mater. Today* **13**, 14–22 (2010).
309. Gungor-Ozkerim, P. S., Inci, I., Zhang, Y. S., Khademhosseini, A. & Dokmeci, M. R. Bioinks for 3D bioprinting: An overview. *Biomater. Sci.* **6**, 915–946 (2018).
310. Erkoc, P. *et al.* 3D Printing of Cytocompatible Gelatin-Cellulose-Alginate Blend Hydrogels. *Macromol. Biosci.* **20**, 1–15 (2020).
311. Piluso, S. *et al.* 3D bioprinting of molecularly engineered PEG-based hydrogels utilizing gelatin fragments. *Biofabrication* **13**, (2021).
312. Gudapati, H., Parisi, D., Colby, R. H. & Ozbolat, I. T. Rheological investigation of collagen, fibrinogen, and thrombin solutions for drop-on-demand 3D bioprinting. *Soft Matter* **16**, 10506–10517 (2020).
313. Francis, G. L. Albumin and mammalian cell culture: Implications for biotechnology applications. *Cytotechnology* **62**, 1–16 (2010).
314. Aghvami, S. A. *et al.* Rapid prototyping of cyclic olefin copolymer (COC) microfluidic devices. *Sensors Actuators, B Chem.* **247**, 940–949 (2017).
315. Agha, A. *et al.* A Review of Cyclic Olefin Copolymer Applications in Microfluidics and Microdevices. *Macromol. Mater. Eng.* **307**, 2200053 (2022).
316. Bruijns, B., Veciana, A., Tiggelaar, R. & Gardeniers, H. Cyclic olefin copolymer microfluidic devices for forensic applications. *Biosensors* **9**, 1–14 (2019).
317. Pirl, U. Der Mindestabstand von n in der Einheitskreisscheibe gelegenen Punkten. *Math. Nachrichten* **40**, 111–124 (1967).
318. Wan, H. Y. *et al.* Stabilization and improved functionality of three-dimensional perfusable microvascular networks in microfluidic devices under macromolecular crowding. *Biomater. Res.* **27**, 1–16 (2023).
319. Yue, T. *et al.* A modular microfluidic system based on a multilayered configuration to generate large-scale perfusable microvascular networks. *Microsystems Nanoeng.* **7**, (2021).
320. Rambøl, M. H., Han, E. & Niklason, L. E. Microvessel Network Formation and Interactions with Pancreatic Islets in Three-Dimensional Chip Cultures. *Tissue Eng. - Part A* **26**, 556–568 (2020).

321. Zhang, K. *et al.* Long-term cultured microvascular networks on chip for tumor vascularization research and drug testing. *Biomicrofluidics* **16**, 1–11 (2022).
322. Morin, K. T. & Tranquillo, R. T. In vitro models of angiogenesis and vasculogenesis in fibrin gel. *Exp. Cell Res.* **319**, 2409–2417 (2013).
323. Kosyakova, N. *et al.* Differential functional roles of fibroblasts and pericytes in the formation of tissue-engineered microvascular networks in vitro. *NPJ Regen. Med.* **5**, 1 (2020).
324. Newman, A. C. *et al.* Analysis of stromal cell secretomes reveals a critical role for stromal cell-derived hepatocyte growth factor and fibronectin in angiogenesis. *Arterioscler. Thromb. Vasc. Biol.* **33**, 513–522 (2013).
325. Luckert, C. *et al.* Comparative analysis of 3D culture methods on human HepG2 cells. *Arch. Toxicol.* **91**, 393–406 (2017).
326. Chen, L., Ma, H., Li, K., Song, X. & Zeng, X. Liver extracellular matrix hydrogel-based three-dimensional culture system of HepG2 cells to enhance cancer stem cell properties. *Mater. Sci. Eng. C* **126**, 112119 (2021).
327. Cui, J. *et al.* Fabrication of perfusable 3D hepatic lobule-like constructs through assembly of multiple cell type laden hydrogel microstructures. *Biofabrication* **11**, (2019).
328. Li, Y. *et al.* 3D bioprinting of hepatoma cells and application with microfluidics for pharmacodynamic test of Metuzumab. *Biofabrication* **11**, (2019).
329. Mao, S. *et al.* Bioprinting of patient-derived in vitro intrahepatic cholangiocarcinoma tumor model: Establishment, evaluation and anti-cancer drug testing. *Biofabrication* **12**, (2020).
330. Christoffersson, J. *et al.* Fabrication of modular hyaluronan-PEG hydrogels to support 3D cultures of hepatocytes in a perfused liver-on-a-chip device. *Biofabrication* **11**, (2019).
331. Taymour, R., Chicaiza-Cabezas, N. A., Gelinsky, M. & Lode, A. Core-shell bioprinting of vascularized in vitro liver sinusoid models. *Biofabrication* **14**, (2022).
332. Pimentel C., R. *et al.* Three-dimensional fabrication of thick and densely populated soft constructs with complex and actively perfused channel network. *Acta Biomater.* **65**, 174–184 (2018).
333. Taymour, R., Kilian, D., Ahlfeld, T., Gelinsky, M. & Lode, A. 3D bioprinting of hepatocytes: core–shell structured co-cultures with fibroblasts for enhanced functionality. *Sci. Rep.* **11**, 1–18 (2021).
334. Cuvellier, M. *et al.* 3D culture of HepaRG cells in GelMa and its application to bioprinting of a multicellular hepatic model. *Biomaterials* **269**, (2021).
335. Ma, X. *et al.* Deterministically patterned biomimetic human iPSC-derived hepatic model via rapid 3D bioprinting. *Proc. Natl. Acad. Sci. U. S. A.* **113**, 2206–2211 (2016).
336. Nashimoto, Y. *et al.* Vascularized cancer on a chip: The effect of perfusion on growth and drug delivery of tumor spheroid. *Biomaterials* **229**, 119547 (2020).
337. Hu, Z. *et al.* Vascularized Tumor Spheroid-on-a-Chip Model Verifies Synergistic Vasoprotective and Chemotherapeutic Effects. *ACS Biomater. Sci. Eng.* **8**, 1215–1225 (2022).
338. Li, Q., Niu, K., Wang, D., Xuan, L. & Wang, X. Low-cost rapid prototyping and assembly of an open microfluidic device for a 3D vascularized organ-on-a-chip. *Lab Chip* **22**, 2682–2694 (2021).
339. Wan, Z. *et al.* New Strategy for Promoting Vascularization in Tumor Spheroids in a Microfluidic Assay. *Adv. Healthc. Mater.* **12**, 1–12 (2023).
340. Tevlek, A., Kecili, S., Ozcelik, O. S., Kulah, H. & Tekin, H. C. Spheroid Engineering in Microfluidic Devices. *ACS Omega* **8**, 3630–3649 (2022).
341. Faulkner-Jones, A. *et al.* Bioprinting of human pluripotent stem cells and their directed differentiation into hepatocyte-like cells for the generation of mini-livers in 3D. *Biofabrication* **7**, (2015).

342. Duarte Campos, D. F. *et al.* Hand-held bioprinting for de novo vascular formation applicable to dental pulp regeneration. *Connect. Tissue Res.* **0**, 1–11 (2019).
343. Bhushan, A., Martucci, N. J., Usta, O. B. & Yarmush, M. L. New technologies in drug metabolism and toxicity screening: Organ-to-organ interaction. *Expert Opin. Drug Metab. Toxicol.* **12**, 475–477 (2016).
344. Oleaga, C. *et al.* Multi-Organ toxicity demonstration in a functional human in vitro system composed of four organs. *Sci. Rep.* **6**, 1–17 (2016).
345. Skardal, A., Shupe, T. & Atala, A. Organoid-on-a-chip and body-on-a-chip systems for drug screening and disease modeling. *Drug Discov. Today* **21**, 1399–1411 (2016).
346. Rose, S. *et al.* Generation of proliferating human adult hepatocytes using optimized 3D culture conditions. *Sci. Rep.* **11**, 1–16 (2021).
347. Levy, G. *et al.* Long-term culture and expansion of primary human hepatocytes. *Nat. Biotechnol.* **33**, 1264–1271 (2015).

Publication I

Biosynthetic, biomimetic, and self-assembled vascularized Organ-on-a-Chip systems

Fritschen, A., and Blaeser, A. (2021). *Biomaterials*, 268, 120556.

This article is published by Elsevier and available under
https://doi.org/10.1016/j.biomaterials.2020.120556

Publication II

Investigation and comparison of resin materials in transparent DLP-printing for application in cell culture and organs-on-a-chip

Fritschen, A., Bell, A. K., Königstein, I., Stühn, L., Stark, R. W. & Blaeser, A. (2022). *Biomaterials Science*, 10(8), 1981-1994.

Publication III

Influence of the physico-chemical bioink composition on the printability and cell biological properties in 3D-bioprinting of a liver tumor cell line

Fritschen, A., Acedo Mestre, M., Scholpp, S. & Blaeser, A. (2023). *Frontiers in Bioengineering and Biotechnology,* 11(2023): 1093101.

Publication IV

High-scale 3D-bioprinting platform for the automated production of vascularized Organs-on-a-Chip

Fritschen, A., Lindner, N., Scholpp, S., Richthof, P., Dietz, J., Linke, P., Guttenberg, Z. & Blaeser, A. (2024). *Advances Healthcare Materials*, 2304028 (2024): 1 – 11